University of Udine

Ph.D. Course in Biomedical Science and Biotechnology

XXXI° Cycle

Ph.D. Thesis

Characterization of pro-death activities and identification of molecular targets for small compound G5

Ph.D. Student:
Sonia Ciotti

Supervisor:
Prof. Claudio Brancolini

Academic year 2018/2019

TABLE OF CONTENTS

Abstract

The identification of alternative cell death pathways is an urgent necessity to overcome chemoresistance. In fact, the high prevalence of intrinsic and acquired apoptotic resistance, of cancer cells, to the pro-apoptotic drugs represents one of the main causes of chemotherapeutic failure. Among novel therapeutic targets, the deubiquitinating enzymes (DUBs) are intriguing and promising. Specifically, G5, a cell-permeable cross-conjugated unsaturated dienone, by inhibiting some DUBs, induces proteotoxic stress, and a peculiar largely unexplored necrotic response. In this context, to better dissect the components involved in the transducing G5-elicited cell death, two strategies have been followed: I) a proteomic approach to map the cellular targets using a G5-derivate (2c) for pull-down, and II) an unbiased genome screening to identify the key genes controlling G5-induced necrotic response.

Proteomic profiling was performed using a biotin-conjugated diaryldienone-derivative named 2c-Biotin, as a bait to purify the intracellular targets of this small molecule. The spectrum of proteins recognized by 2c-Biotin was quite large, showing a certain affinity for isopeptidases, but surprisingly, also for different proteins, such as Akt and Cofilin-1. The plethora of targets bound by G5 can elicit multiple stresses, thus explaining the efficient anti-tumor activity of these inhibitors observed *in vivo*. Moreover, a PEG-conjugated version of 2c was tested in leukemia cells to further study the transcriptional programs engaged by this inhibitor and to verify the possibility to use this inhibitor in clinic.

The short hairpin RNA screen strategy was used in U87MG glioblastoma cells, which were chosen for their apoptosis resistance and propensity to die by necrosis. The transduction of pooled library of 27500 shRNAs, and the selection of clones resistant to G5 treatment, allowed the identification of pro-death proteins. Among them, glycogen synthase kinase-3 β (GSK3β) was further investigated. U87MG cells knocked-out for GSK3β were generated by using the CRISPR/Cas9 system. The response of U87MG/GSK3β$^{-/-}$ cells to the treatment with two specific necrotic stressors, G5 and the redox cycling agent 2,3-Dimethoxy-1,4-naphthoquinone (DMNQ), showed that this kinase plays a main pro-death role in the ROS-induced necrosis generated by DMNQ, and a minor role during G5-induced necrosis. An early

and strong activation of GSK3β was reveled, upon DMNQ treatment, which in turn controls and modulates the integrity and functionality of mitochondria in the treated cells.

By a time lapse analysis, we demonstrated that GSK3β, in the U87MG/GSK3β$^{-/-}$ re-expressing GSK3β-GFP cells, translocates in the nucleus during the later steps of DMNQ treatment, but before $\Delta\psi_m$ collapse. Our results point out the essential role of GSK3β in the triggering the oxidative stress-dependent necrotic response. Nevertheless, further analysis are required to better investigate which substrates are involved in the GSK3β-mediated death/life balance control and which effects the kinase exerts in the nucleus.

1. Introduction

1.1 The ubiquitin-proteasome system (UPS)

1.1.1 The ubiquitylation process: components and cellular "meaning"

Cells have different strategies to control the protein status on the basis of the different extra- and intracellular signals. Alterations on transcriptome is a way to respond to the environmental changes, even if the post-translational modifications of the proteome provide a faster way to activate or to inhibit different signaling pathways. An alternative mechanism to regulate proteins levels is provided by their degradation, an irreversible strategy to switch off a particular pathway (Pickart, 2004; Wilkinson, 2004; Hershko et al., 2000).

In eukaryotic cells, one of the major responsible for the degradation of cellular proteins is the ubiquitin-proteasome system (UPS) (Chiechanover, 2005). The UPS-mediated protein degradation plays an essential role in a wide number of cellular processes, such as: cell-cycle progression, gene expression, differentiation and cell death. In fact, an abnormal regulation of this system can contribute to the onset of different pathological conditions, including tumor formation, autoimmunity and neurodegenerative diseases (Demarchi and Brancolini, 2005).

Generally, all cellular proteins are degraded to amino acids and replaced by newly synthesized proteins. The half-life of each protein is different, ranging from few minutes up to different days. A specific step for protein degradation is their labeling with a molecule called ubiquitin (Ub), through an energy-requiring process. The poly-ubiquitination represents the process by which this addressing signal is linked to target proteins for their digestion into smaller peptides through the proteolytic complex known as 26S proteasome. The importance of the UPS is testified by its involvement in the physiological protein turnover and in the protein quality-control. The UPS is critical to remove damaged or misfolded proteins that can interfere negatively with the cellular functions and viability (Goldberg and Dice, 1974; Sherman and Goldberg, 2001; Goldberg, 1972).

When a protein has to be degraded, it is marked with a chain of linked molecules of Ub. Ub is a small 76 amino acid polypeptide, highly conserved through the evolution, used to influence protein activities, interactions, stability and localization (Vijay-Kumar et al., 1987; Hershko et al., 1983). Generally, an isopeptide linkage (-CO-NH_2ε-) between a lysine residue of the protein target and the C-terminal glycine residue (G76) of Ub is involved in the conjugation process. This first Ub molecule can be next used to form a chain via additional linkages between one of the seven lysine residues present on itself and other Ub molecules. In this way, the target proteins can be mono-ubiquitylated, multi-monoubiquitylated or poly-ubiquitylated (**Fig.1**). Specifically, the Ub sequence presents the following lysine residues: K6, K11, K27, K29, K33, K48 and K63, which are available for the conjugation. The common Lys involved in protein degradation is the lysine-48 (K48). However, some findings reported that also homogenous poly-ubiquitin chains assembled through the lysine-63 (K63) are able to target the proteins to the proteasome (Saeki et al., 2009). In addition to the poly-ubiquitin chains, described as the minimal proteasomal targeting signal (Thrower et al., 2000), proteins conjugated with a single Ub moiety (mono-ubiquitylated) and multiple single moieties (multiple mono-ubiquitylated) can be recognized by the proteasome (Kim et al., 2007).

When an Ub-tagged protein is recognized by the proteasome, it is degraded into small peptides and Ub molecules are recycled (Chau et al., 1989; Gregori et al., 1990; Pickart, 2000). Furthermore, target proteins, linked by multiply branched ("forked") chains, in which two or more Ub molecules are linked to a single Ub molecule, cannot be processed by the proteasome, but they can play different roles in non-proteolytic regulatory processes, such as DNA repair, assembly of signaling complexes, endocytosis, intracellular trafficking and transcriptional regulation (Kim et al., 2007; Muratani and Tansey, 2003; Jesenberger and Jentsch, 2002; Jackson and Durocher, 2013). Not surprisingly, misregulation of the Ub system can be linked with severe pathological conditions, such as cancer, some types of mental retardation and neurodegenerative disorders (Parkinson's disease, Huntington's disease and Alzheimer's disease) (Schwartz and Chiechanover, 2009).

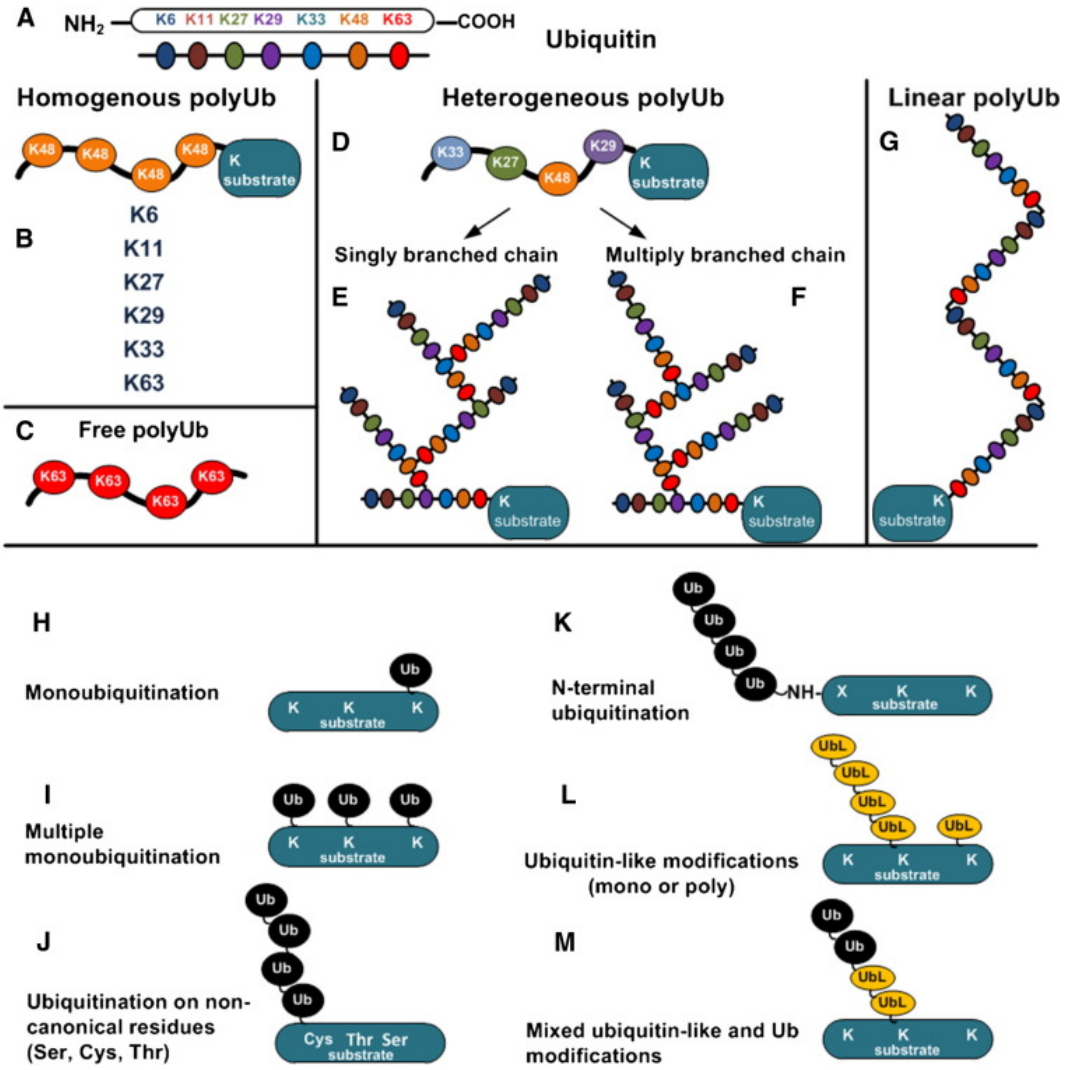

Fig.1: Complexity of Ub and UbL chains. (**A**) Seven lysine residues in a single Ub molecule. (**B**) Homogenous chains in which Ub moiety is linked to the next one through the same lys residue. (**C**) An example of free poly-ubiquitin chain. (**D**) Heterogeneous Ub chains in which the links between the Ub molecules involved different internal lysine residues. These chains can be singly branched (each Ub moiety is linked with a single Ub; **E**) or multiply branched (each Ub moiety is linked with two or more Ub moieties by different internal lysine residues; **F**). (**G**) An example of linear Ub chain. (**H**) Modification by a single Ub moiety. (**I**) Modification by multiple single Ub moieties. (**J**) Modification of "non -canonical" residues in the target protein. (**K**) N-terminal residue modification of the substrate. (**L**) Mono or poly-modification of the substrate by an UbL chain. (**M**) Modification of the substrate by a mixed chain of UbL and Ub molecules (Chiechanover and Stanhill, 2014).

Ub itself assumes a compact structure with a hydrophobic core given by 3 hydrophobic residues of α-helix and 11 hydrophobic residues of β-sheet (Vijay-Kumar et al., 1987). Sheet structure "grasps" around the α-helix, forming a β-grasp fold. Some areas of this structure represent the center of the most known interactions with the proteins containing Ub-binding domain (UBD) (Dikic et al., 2009). The formation of non-covalent interactions, between the

Ub hydrophobic area and the UBD of different interacting proteins, mediates the effects of the ubiquitylation process. Numerous UBDs have been found in some subunits of the proteasome. UBD containing proteins are also involved in DNA repair and endocytosis (Komander et al., 2009; Kodadek, 2010).

Similarly to Ub, Ub-like proteins (UbLs) are conjugated to various proteins or other molecules (**Fig.1**). Among these UbLs, the most studied are the interferon-stimulated gene product of 15 kDa ISG15 (Haas et al., 1987), the small ubiquitin-related modifier SUMO (Kerscher et al., 2006) and the neural precious cell-expressed developmentally downregulated protein 8 NEDD8.

Ub and UbLs conjugation process is provided by an enzymatic cascade involving E1 ubiquitin-activating enzymes (Schulman and Harper, 2009), E2 ubiquitin-conjugation enzymes (Ye and Rape, 2009) and E3 ubiquitin ligases (Buetow and Huang, 2016). The first class of enzymes hydrolyses ATP and adenylates the C-terminal Gly residue of a single Ub molecule, then this residue is linked to the active site of one E1 enzyme. Next, the thioester-linked Ub molecule is transferred to the cysteine residue of one E2 ubiquitin-conjugating enzyme through a thiol ester bond. Different enzymes are involved in the activation of UbL molecules: E1SUMO for SUMO, E1NEDD8 for NEDD8 and E1ISG15 for ISG15. These UbLs E1 enzymes are able to act on their respective E2 Ub-conjugating enzyme C9 (UBC9), UBC12 and UBC8 (Schwart and Hochstrasser, 2003).

E3 Ub ligases represent the most heterogeneous class of enzymes. In fact, the human genome contains two E1s, approximately 38 E2s and more than 600 E3s (Jin et al., 2007; Ye and Rape, 2009). The E3 enzymatic class can be subdivided in three subfamily (RING, HECT and RBR E3s) on the base of the containing enzymatic domains and of the mechanism by which the Ub is transferred (Morreale and Walden, 2016). Moreover, this last step confers specificity to the entire ubiquitylation process, defining in this way the final destination of each cellular protein. A comprehensive proteomic study reported tens-of-thousands ubiquitination sites detected on an equally number of proteins within a cell, demonstrating the strong impact of the Ub system on the cellular life (Peng et al., 2003; Kim et al., 2011).

Another component of UPS is represented by the 26S proteasome: a 2000 kDa multi-subunit cylindrical complex constituted by one 20S catalytic core (20S proteasome) capped on both the sides by 19S regulatory components (Adams, 2003). In details, in the 20S proteasomal core, 4 stacked rings exist: two outer α-rings and two internal β-rings. The last ones are composed by 7 subunits, responsible of the proteolysis thanks to three different enzymatic activities: trypsin-like, chymotrypsin-like and postglutamyl peptide hydrolase-like (or caspase-like) activities (Almond and Cohen, 2002; Adams, 2003).

In summary, the complete process is ensured by the initial ubiquitylation, and then the Ub-tagged proteins are recognized and bound by the 26S proteasome. However, for the transferring in the 20S core proteolytic chamber, the Ub signal should be previously removed from the target protein. This essential step is guaranteed and highly controlled by deubiquitinating enzymes (DUBs) (Komander et al., 2009) (**Fig.2**).

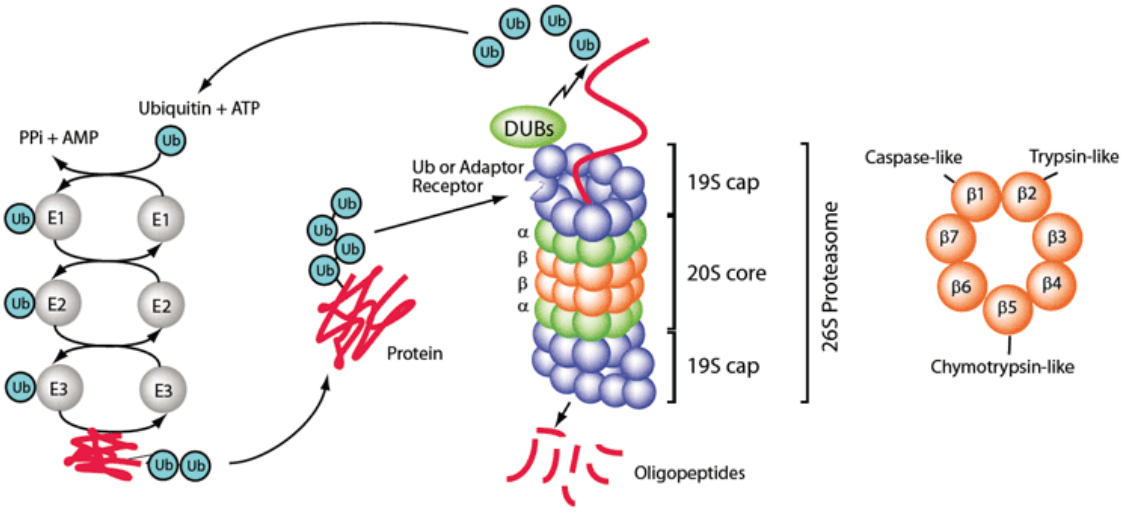

Fig.2: UPS: ubiquitylation process coupled with the 26S proteasome activity. The ubiquitylation process is an essential step to add the Ub-tag to the protein targets, recognized then by the 26S proteasome. The same tag is removed by DUBs activity for the protein transferring in the 20S proteasomal core, which is characterized by different proteolytic activities (biomol.com).

1.1.2 Deubiquitinating enzymes (DUBs): activity and specificity

The deubiquitination process is guaranteed by the enzymatic activity of the peptidases, named DUBs (Komander et al., 2009), which can catalyze:

- the Ub/UbLs monomers and chains removal from the tagged protein,
- the cleavage of the poly-ubiquitinylated chains,
- the generation of free Ub monomers ready to be recycled.

The DUBs control these reactions by hydrolyzing selectively the isopeptide or peptide bond present at the C-terminus of the Ub molecule (Komander, 2009).

Many aspects regarding the capability of the DUBs to select and to recognize, in a specific way, the modifier or the branching patterns of the poly-Ub chains remain to be clarified. Nevertheless, it is well know that the DUBs, to deubiquitinate the substrate, need their UBD, which is characterized by an Ub-interacting motif, a zinc finger Ub-specific protease (ZnF-UBP) domain and a Ub-associated (UBA) domain (Hurley et al., 2006). Some studies indicate that the specificity of the binding seems to be more attributable to the ZnF-UBP domain, ensuring a strictly regulation of the deubiquitination process (Komander, 2009).

The high number of DUBs reflects the complexity of UPS (Reyes-Turcu et al., 2009). They have been divided in six structurally distinct DUB families. In particular, five are cysteine proteases: ubiquitin-specific proteases (USPs, 54 members in human), ovarian tumor proteases (OTUs, 16 members), Ub C-terminal hydrolases (UCHs, 4 members), Josephin family (4 members) (Clague et al., 2013; Komander et al., 2009) and the motif interacting with Ub (MIU)-containing novel DUB family (MINDYs, 4 members) (Rehman et al., 2016). An other family exist: the Zn-dependent JAB1/MPN/MOV34 metalloproteases (JAMMs, 16 members). Regarding the UbL proteases, the sentrin/SUMO-specific proteases (SENPs), the deSUMOylating isopeptidases (DeSI) and the NEDD8-specific protease 1 (NEDP1, a SENP member) exist and they are all classified as ubiquitin-like proteases (ULPs) (Hickey et al., 2012; Shin et al., 2012).

Some DUBs are able to work individually, others as components of macromolecular machines. In particular, three DUBs are able to interact with the 26S proteasome: UCH37

(also known as UCH-L5), USP14 (Ubp6 in yeast), and the JAMM family DUB RPN11. These enzymes are involved in the engagement step of the Ub-tagged proteins on the cap of the proteasome with the help of the AAA+ ATPase ring (**Fig.3**).

In this context, UCH37 is recruited to the proteasome by RPN13 (also known as ADRM1), through the binding between the RPN13 C-terminal domain (RPN13CTD) and the C-terminal domain of UCH37 (UCH37CTD). The latter one is an autoinhibitory domain (Yao et al., 2006, 2008), which controls the N-terminal catalytic domain of UCH37 (UCH37UCH) (Burgie et al., 2012; Maiti et al., 2011; Nishio et al., 2009).

RPN11 is located directly on the entry channel of the 20S proteasome core and its activation occurs when the enzyme is incorporated in the proteasome by an energy-consuming process.

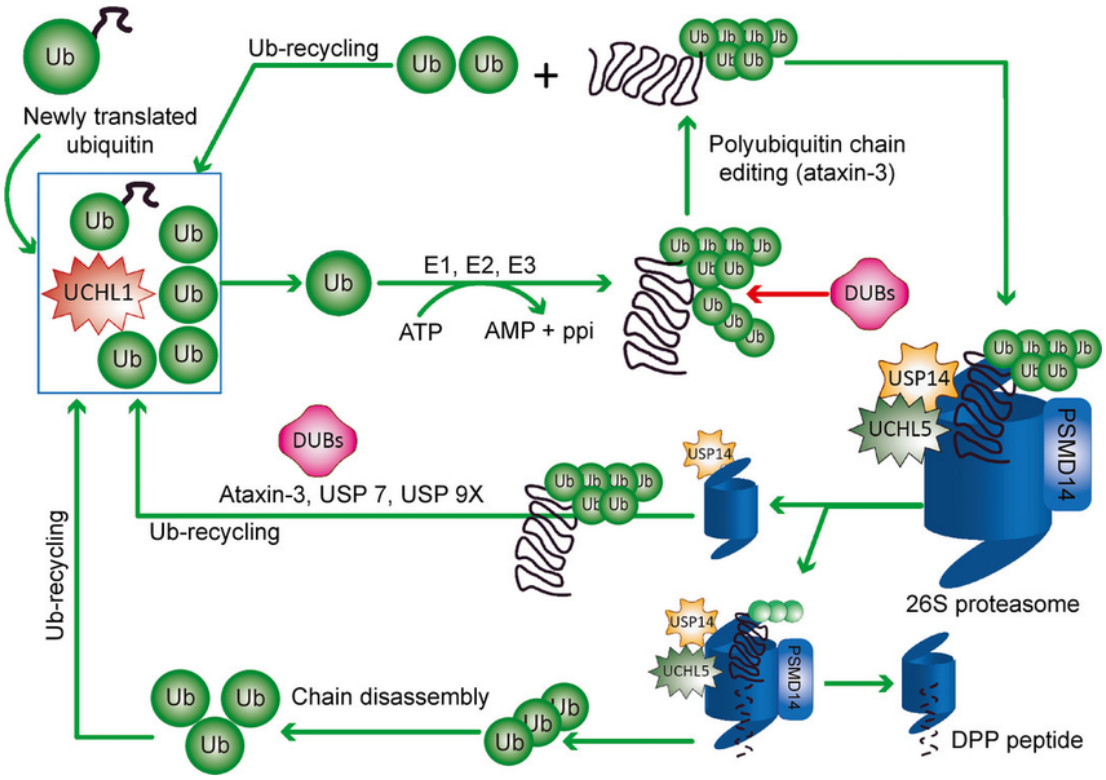

Fig.3: The DUBs-mediated deubiquitination process. Different DUBs are involved in the Ub and polyUb chains cleavage from the target proteins, and in the Ub-chains disassembling to maintain the mono-Ub pool. Some of them (USP14 and UCHL5) are also associated with the 26S proteasome to ensure the Ub removal from the tagged proteins before their entry in this proteolytic channel (Gadhave et al., 2016).

Once activated, RPN11 binds the proximal Ub of the target protein and removes the entire Ub chain (Verma et al., 2002; Yao and Cohen, 2002).

Similarly, USP14 is catalytically inactive, but when it binds the proteasome, an 800-fold activation occurs (Lee et al., 2010). This DUB plays a role in processing of incorrectly poly-ubiquitinated proteins loaded onto the proteasome (Lee et al., 2016).

The activity of these enzymes coupled with the UPS determine a timely-regulated degradation of the substrates and, a strong dysregulation of this system, can affect negatively the final fate of the cell. More specifically, the alteration of the DUB enzymatic activities has a strong implication in the onset and progression of multiple diseases, such as neurodegenerative diseases and cancer. Interestingly, in the cancer context, it has been well demonstrated that these proliferating cells are more sensitive to the proteasome blockage, in comparison to the normal cells. Since the tumor cells are characterized by a higher rate of protein synthesis, if the UPS is blocked, a large concentration of aberrant proteins are produced and cell death is triggered (Adams, 2004; Voorhees et al., 2003; Kisselev and Goldberg, 2001). This aspect has elicited an increased interest in the developing UPS inhibitors able to active death programs in cancer cells (Nalepa et al., 2006).

1.2 UPS inhibition as cancer therapeutic strategy

1.2.1 Targeting the proteasome in cancer cells

UPS inhibitors (UPSI) are small molecules able to target and inhibit specific activities of the UPS components, leading to the accumulation of poly-ubiquitinated proteins, activation of multiple stress signals and appearance of cell death. They belong to a heterogeneous class of compounds that can be subdivided into 5 different categories: the peptide aldehydes, peptide boronates, the peptide vinil sulfones, the lactacystins and the peptide epoxyketones (Kisselev and Goldberg, 2001; Adams et al., 1999).

Among them, the dipeptide boronic acid bortezomib (Velcade/PS-341) is of particular interest, since it has been the first UPSI approved for the human application by United States Food and Drug Administration (FDA) and the European Medicine Evaluation Agency (EMEA).

It is a reversible inhibitor of the chymotrypsin-like activity of the 20S proteasome β5-subunit (PSMB5), and of β1-subunit (with lower affinity) (Adams, 2004; Orlowski et al., 2002; Richardson et al., 2003 and 2005).

Specifically, bortezomib was approved for the treatment of relapsed or refractory multiple myeloma in 2008 (Richardson et al., 2003; Kyle and Raijkumar, 2004). However, it is also studied in different haematological malignancies and solid tumors, including non-Hodgkin's lymphoma, prostate, breast and non-small-cell lung cancers, as single agent or in combinatory therapies (Milano et al., 2007). Although this drug has shown promising effects, severe side effects were reported (thrombocytopenia, fatigue, myalgia, neuropathies), and some clinical limiting factors were found (oral administration, off-targets and acquired resistance). In fact, there is evidence about patients who do not respond, or respond briefly to the treatment, and then they relapse (Richardson et al., 2005; Milano et al., 2007). This aspect could be explained by some *in vitro* studies, which reveled the presence of Gly322Ala point mutation in the *PSMB5* gene in the cells resistant to the treatment (Lü et al., 2008). Others mutations have been found around the S1 specificity pocket of the PSMB5, such as the Thr21Ala, Ala49Thr, Ala50Val substitutions, which could be directly involved in the bortezomib-PSMB5 binding. All these acquired mutations negatively influence the binding between bortezomib and its target (Groll et al., 2006; Unno et al., 2002). Surprisingly, no mutations in *PSMB5* gene have been detected in patients with refractory and relapsed multiple myeloma (Lü et al., 2011). Other studies demonstrated that the up-regulation of *PSMB5* gene or the over-expression of the proteasome subunits, which lead to an augmented basal level of the proteasome activity, can explain the nature of the acquired or intrinsic drug resistance phenomena (Lü et al., 2008; de Wilt et al., 2012). Additionally, a significant adverse event, linked with the clinical use of bortezomib, is represented by the peripheral neuropathy. Some studied reported that this clinical issue is due to the inhibition of the neuronal survival protein

called HtrA2/Omi (Arastu-Kapur et al., 2011; Voortman and Giaccone, 2007). For all these reasons, it is urgent to find alternative compounds able to induce the cell death, by targeting the UPS, similarly to bortezomib, but limiting the risk factors.

Among them, it is possible to find:

- the second-generation UPSI, developed to improve the drug efficacy and to reduce the toxicity by targeting the α-subunits or multiple β-subunits of the 20S proteasome in an irreversible way;
- the DUBs inhibitors (Buac et al., 2013).

Concerning the first class, Carfilzomib represents the second UPSI approved, as third line treatment in multiple myeloma, in 2012 and by EMA in 2015 (Kortuem and Stewart, 2013). This drug is characterized by several improvements: the capability to bind irreversibly the β5-subunit (showing a greater selectivity and lower off-target binding activity), the covalent bind (ensuring a prolonged inhibition) and, more prominent, the cytotoxic effects on the bortezomib-resistant cells (Ruschak et al., 2011; Kuhn et al., 2007).

Worthy of note are also ixazomib, since it is the first oral UPSI approved for the myeloma treatment in 2016 (Gupta et al., 2017), and oprozomib, which shows an augmented cytotoxic activity in cancer cells resistant to the other UPSIs (Nooka et al., 2013; Thompson, 2013).

Considering their promising effects in the hematological malignancies, the possibility to use these UPSIs in the treatment of the most common solid malignancies has been explored. Recent studies suggest that they could be used, especially, in combination therapies with the classic anticancer drugs (**Table 1**).

1.2.2 UPSI treatment: cellular effects and cell death activation

The proteasome blockage triggers a multiple, profound and complex number of effects, which they contribute to the onset of cell death. Among them, the endoplasmic reticulum stress (ER stress) is involved (Fribley et al., 2004).

Compound	Combination	Condition	Phase	ClinicalTrials.gov identifier
PS-341	Doxarubicin	Advanced solid tumors	Phase I	NCT00023855
PS-341	Chemotherapy	Advanced solid tumors	Phase I	NCT00028587
PS-341	Topotecan	Advanced malignancies	Phase I	NCT00068484
NPI-0052	–	Solid malignancies or refractory lymphoma	Phase I	NCT00396864
PS-341	–	Advanced or metastatic solid tumors	Phase I	NCT02220049
PS-341	Sorafenib	Advanced cancers	Phase I	NCT00303797
PS-341	–	Children with refractory solid tumors	Phase I	NCT00021216
NPI-0052	–	Advanced malignancies	Phase I	NCT00629473
PS-341	Paclitaxel	Locally advanced or metastatic solid tumor	Phase I	NCT00030368
PS-341	Doxorubicin	Advanced adenoid cystic carcinoma of the head and neck	Phase II	NCT00077428
PS-341	–	Advanced malignancies and kidney dysfunction	Phase I	NCT00054483

Table 1: Summary of the main UPSI clinical trials in different type of solid malignancies (clinicaltrials.gov).

ER stress is activated upon the accumulation of poly-ubiquitinated proteins and misfolded protein aggregates into the cytosol of the UPSI-treated cells (Ri, 2016; Obeng et al., 2006). In parallel, the production of reactive oxygen species (ROS) is facilitated by the high amount of the cytosolic unfolded proteins (Shimizu and Hendershot, 2009). In this context, the activation of the unfolded protein response (UPR) is mediated by three ER stress sensors: PKR-like ER kinase (PERK), inositol requiring kinase1 (IRE1α), and activating transcription factor (ATF6) (Kaufman, 2002; Harding et al., 2002). The UPR plays a pro-survival role, since it stimulates the protein translation blockage, the increase of ER-resident chaperon activities, and the activation of ER-associated degradation pathway (ERAD). All these processes are aimed to resolve the proteotoxic stress, by avoiding a further unfolded protein accumulation and by recovering the physiological folded statement of the cytosolic proteins (Ri, 2016). Analysis of the transcriptional profiling, by DNA microarray, of cancer cells exposed to UPSI reported the up-regulation of heat shock genes, genes encoding for the proteasome subunits and genes implicated in the protein folding regulation (Zimmermann et al., 2000). Nevertheless, if the ER stress is strong or prolonged, cell death occurs (Kaufman, 2002; Ron, 2002). In this context, in which the proteasome is blocked, some critical pro-apoptotic proteins, normally tagged to be degraded, are free to act, as in the case of:

- IkBα, the natural inhibitor of the NF-kB, indispensable for the apoptosis inhibition and pro-survival pathway activation (Lopes et al., 1997);

- p53, a very short-lived protein, whose stabilization and accumulation can strengthen the UPSI pro-apoptotic effects (Rastogi et al., 2015);
- Bim, which when stabilized, favors the accumulation of Bcl-2 family pro-apoptotic proteins (Brancolini, 2008; Demarchi and Brancolini, 2005).

Nevertheless, in the absence of p53 functions and NF-kB inhibition, the UPSI-induced cell death can still be observed (Richardson et al., 2005; Demarchi and Brancolini, 2005).

Caspases are a family of cystein-proteases able to cleave selected substrates after aspartic residues (Demarchi and Brancolini, 2005). They are responsible for the execution of the apoptotic program through two main ways: the extrinsic and intrinsic pathways (**Fig.4**). The extrinsic pathway is activated by the engagement of a death receptor (DR) family member on the cell surface. Caspase-8 (a component of the Death Inducing Signaling Complex (DISC)) is recruited at cytosolic side of DR via the interaction with the adaptor Fas-Associated Death Domain (FADD) protein. At the DISC, also the Fas-like inhibitor protein (FLIP) is recruited. All these proteins modulate the caspase-8 recruitment and its subsequent activation within the cell, in response to pro-apoptotic stimuli (Thorburn, 2004; Oliver and Vallette, 2005). The intrinsic pathway is elicited by the efflux of some mitochondrial pro-apoptotic proteins into the cytosol, such as cytochrome c (cyt c), second mitochondria-derived activator of caspase/ Direct Inhibitor of Apoptosis-Binding protein with LOw pI (Smac/DIABLO) and OMI/ HtrA2. For this reason, the intrinsic pathway is also named mitochondrial pathway. Upon the cytosolic release of these killer proteins, the caspase-9 is activated through the formation of a multi-protein complex known as the apoptosome, driven by the binding of cyt c to Apaf-1 (apoptotic protease activating factor-1). Consequently, the effector caspases-3 and -7 are processed (Jiang and Wang, 2004). Caspases-8 and -9 are the regulatory factors that control the effector caspases, which in turn act on selected cellular substrates to provoke the final cellular disassembly.

In the UPSI-induced cell death, even if there are several controversial points, the mitochondrial outer-membrane permeabilization (MOMP) triggers the release of cyt c and Smac, which in turn elicit the processing and activation of caspases-9, -3 and -7. In this

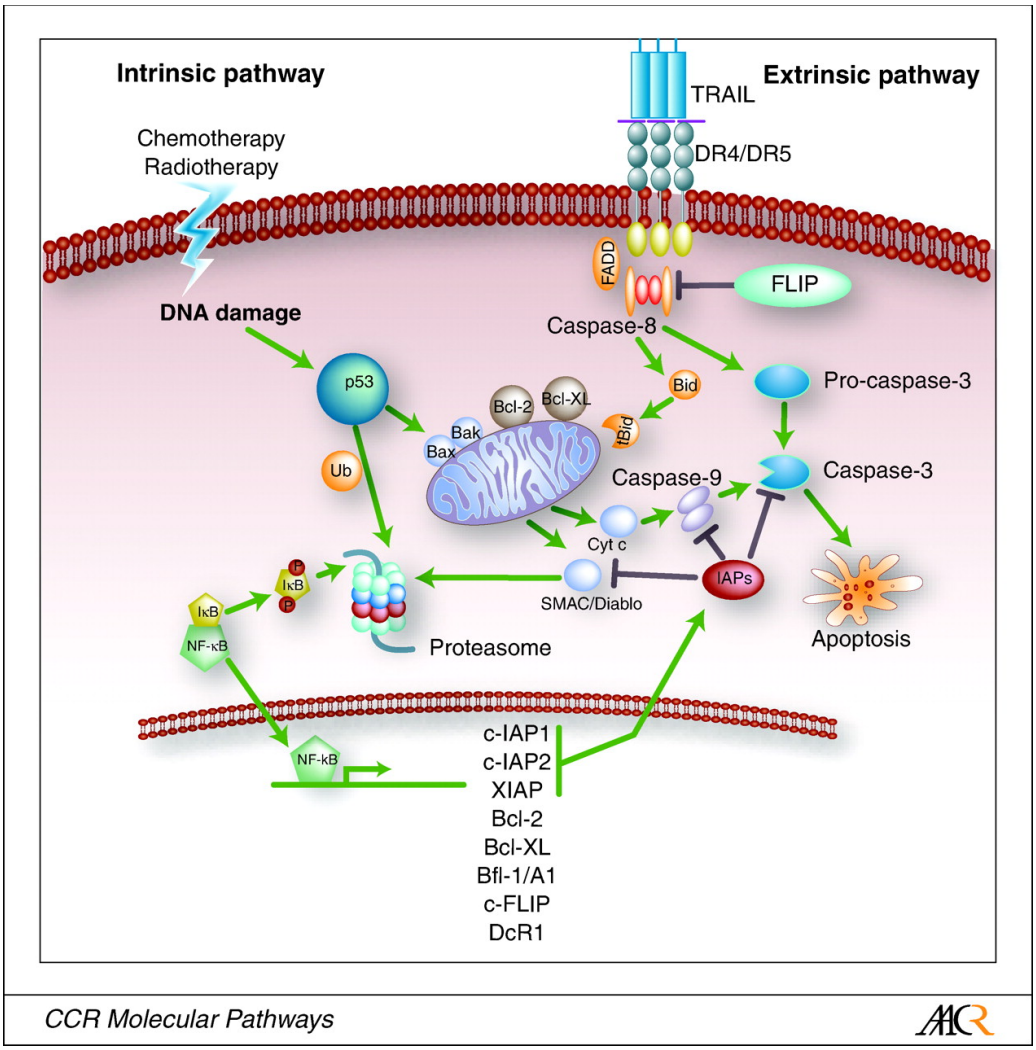

Fig.4: Apoptosis. Schematic representation of the apoptotic mechanisms activated by two ways: the intrinsic and extrinsic pathway (de Vries et al., 2006).

scenario, high levels of cytosolic Smac, allowed by proteasomal blockage, favors an apoptosome-independent apoptotic response (Henderson et al., 2005). Moreover, Inhibitor of Apoptosis Proteins (IAPs), such as XIAP, cIAP1 and cIAP2, are under the proteasome control and, in principle, their increase should prevent the caspases activation (Vaux and Silke, 2005). However, it is reported that bortezomib determines the down-regulation of XIAP *in vivo* (Fernandez et al., 2005; Frankel et al., 2000; Dai et al., 2003), which could be explained by the ability of NF-kB to control some IAPs. Hence, in an indirect way, the NF-kB inhibition could promote the XIAP down-regulation, but a NF-kB independent XIAP down-regulation was reported in response to bortezomib (Kashkar et al., 2007). This event is more complex than expected, since also IAP antagonists exist: they share a sequence at the N-terminus called

IBM (IAP Binding Motif) (Vaux and Silke, 2005), and they can sustain apoptosis by counteracting the IAPs activities (Vaux and Silke, 2005; Schimmer, 2004; Shiozaki and Shi, 2004).

Regarding the extrinsic pathway, it was demonstrated that the UPSI treatment can elicit apoptosis through the DR pathway (Van Geelen and de Vries, 2004; Saule et al., 2007). In fact, in cancer cells, the treatment with these inhibitors leads to the up-regulation of severe DR members and their respective ligands: DR4/TRAIL-R1 (TNF-related apoptosis-inducing ligand (TRAIL)-receptor1), DR5/TRAIL-R2 and DcR2/TRAIL-R4. They are not only accumulated, but also activated in a still unclear way (Liu et al., 2007; Ganten et al., 2005; Aleo et al., 2006; Kabore et al., 2006).

Additional studies are necessary to gain new insights about the UPSI-induced cell death pathways. Until now, it is clear that an unmanageable stress is induced in the UPSI-treated cancer cells, which finally die. The antineoplastic activity of these inhibitors seems to be linked to triggering apoptosis, but new findings are coming out regarding their ability to elicit additional cell death pathways (D'Arcy et al., 2011; Fontanini et al., 2009).

1.2.3 DUBs inhibitors: an emergent class of UPSI

In general, a heterogenous group of small molecule, able to inhibit the DUBs, has been reported: some are broad pan-enzyme inhibitors, others show a more specific inhibitory action (**Fig.5**).

For example, b-AP15 was identified as an inhibitor of the deubiquitinating activities of USP14 and UCHL5, without affecting directly the 20S proteasome (Tian et al., 2014; Wang et al., 2015). Like all UPSIs, the b-AP15 triggers the unfolded protein response (UPR) through the accumulation of poly-ubiquitinated proteins, growth arrest (due to the down-regulation of CDC25C, CDC2 and cyclin B1) and the induction of caspase-dependent apoptosis. *In vivo* xenograft studies reported the promising effects of b-AP15 treatment on human multiple myeloma (Tian et al., 2014), and on solid tumor mouse models of lung, colon, breast, head and neck carcinomas (Dou and Zonder, 2014).

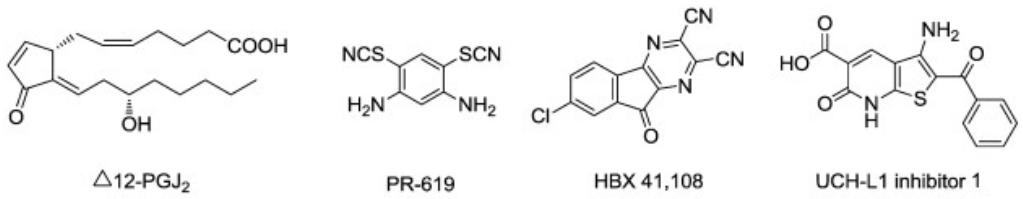

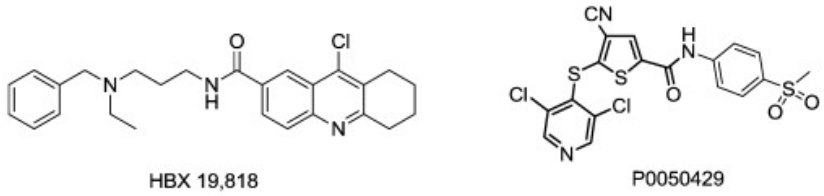

Compound	Enzyme(s)
Δ12PGJ$_2$ (J Prostaglandins)[29]	DUBs (pan)
PR-619[30]	DUBs (pan)
HBX 41,108 [31, 32]	USP7, additional DUBs
UCH-L1 inhibitor 1[33]	Ubiquitin C-terminal hydrolase-L1 (UCH-L1)
HBX 19,818[32]	USP7
P0050429[34]	USP7
WP1130 [35]	USP9X, USP5, USP14, UCH37
GRL0617 [36]	SARS Plpro

Fig.5: Summary of DUB inhibitors and their targets. Some of them are specific for selected DUB enzyme, others show broader activities (Mattern et al., 2012).

b-AP15 shares the pharmacophore with a class of non-selective inhibitors (N-SIIs) previously identified (Aleo et al., 2006; Mullally and Fitzpatrick, 2002). The pharmacophore is characterized by a cross-conjugated α,β-unsaturated dienone with two sterically accessible electrophilic β-carbons (Verbitski et al., 2004). The β-carbons act as Michael acceptors to target nucleophiles, such as the free sulfhydryl groups of catalytic cysteines in the isopeptidases. Indeed, the cysteine is the most nucleophilic and reactive amino acid within a cell (Mullally and Fitzpatrick, 2002).

In vitro studies with recombinant proteins demonstrated the heterogeneity of N-SIIs targets, such as the UCHs, USP2, USP7 and the UbL-protease SENP2 (Nicholson et al., 2008).

Additionally, N-SIIs can react with other thiol-containing compounds. such as the glutathione (GSH) (Foti et al., 2009).

On the contrary to selective inhibitors, the N-SIIs arise interest since, by blocking different enzymes in multiple signaling pathways, they can be more effective in term of toxicity in a wider range of tumors, overcoming in this way the possible onset of drug-resistance. Another relevant advantage, regarding the possible use of N-SIIs as therapeutic agents, is the possibility to modify their chemical structure, thus promoting the triggering of a different type of cell death. In fact, in the anticancer-therapy context, the acquisition of some defects in the execution of the apoptotic program is a problem to be considered. The apoptotic resistance represents one of the major causes of chemotherapy failure. Consequently, a goal to achieve, for the new anti-cancer therapies, is the discovery of compounds able to elicit cell death programs different from apoptosis (Rodriguez-Nieto and Zhivotovsky, 2006). All these reasons led us to focus our attention on a N-SII called G5, especially for its ability to trigger a peculiar necrotic pathway of cell death (Tomasella et al., 2014; Foti et al., 2009).

1.2.4 The promising N-SII G5: its discovery and derivates

The G5, a 4H-thiopyran-4-one, tetrahydro-3,5-bis[(4-nitrophenyl)methylene]-,1,1-dioxide (**Fig.6**), was identified thanks to a screening with a small chemical library (the Developmental Therapeutics Program-National Cancer Institute "challenge set") carried out on cells expressing a dominant-negative form of caspase-9 (C9DN), unable to assemble a functional apoptosome (Aleo et al., 2006). The aim was to identify new drugs able to elicit alternative cell death pathways in apoptosome-defective cells.

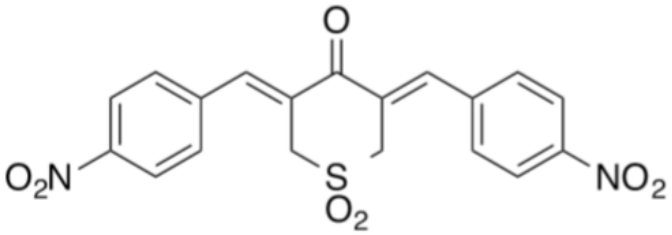

Fig.6: Structure of the N-SII G5 (Cersosimo et al., 2015).

Despite the G5-induced cell death mechanism was not perfectly clear, numerous efforts have been made to optimize this N-SII for *in vivo* use. Indeed, the N-SII G5 compound was modified by varying separately different atoms in different positions (Cersosimo et al., 2015). By testing these variants on glioblastoma U87MG cells, it was observed a different capability to elicit an apoptotic or necrotic response, in base on the chemical substituents of the tested variants. Among all, the compound called 2c raised interest especially for the presence of a reactive -OH group. This group could be easily modified to improve some drug-like properties, such as the *in vivo* delivery (Cersosimo et al., 2015). Functional studies on G5 and 2c inhibitory activities revealed a stronger potential of G5 to inhibit DUBs such as UCHL1, UCHL5 and USP2, but less the deISGylase USP18, which was, on the contrary, more inhibited by 2c. This aspect could explain the differential ability of these inhibitors to trigger necrosis or apoptosis, by reacting with different cysteine proteases (Cersosimo et al., 2015). A further understanding of the intracellular targets bound by this class of inhibitors could shed light on the way through which cell death is engaged.

G5 and 2c are insoluble in aqueous solutions, so the *in vivo* delivery should be improved for their application in the anti-neoplastic therapy. For this reason, the 2c compound was conjugated with polyethylene glycol (PEG) to increase its solubility and bioavailability. This modified version, called 2cPE, represents the first synthesized N-SII pro-drug. Specifically, the phospholipase A2 group 7 (PLA2G7) seems to be the responsible of conversation from the pro-drug 2cPE into the active form 2c (Cersosimo et al., 2015). This pro-drug was tested on A549 lung carcinoma xenografts generated in immunocompromised mice by intravenous injections, and it showed a strong anti-neoplastic activity *in vivo*, as single agent, without significant adverse effects (**Fig.7**). Moreover, the *in vivo* effects of 2cPE are particularly marked in tumor cells than in liver or others organs, highlighting the real possibility to use it in clinic.

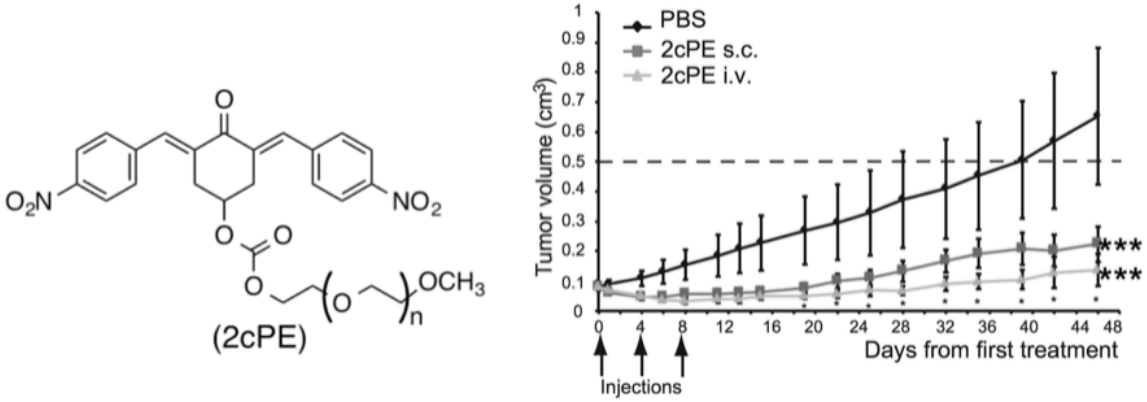

Fig.7: Modified version of the N-SII G5, 2cPEG, and its *in vivo* study. Starting from 2c structure, the OH group has been PEGylated to improve the *in vivo* delivery of the drug. On the right, the development in terms of tumor volume of A549 lung carcinoma xenografts generated in mice upon the subcutaneous (sc) or intravenous (iv) treatments with 2cPE (Cersosimo et al., 2015).

1.2.5 G5: a peculiar necrotic cell death trigger

G5 elicited considerable interest for its ability to trigger a Bcl-2-dependent but apoptosome-independent pathway of cell death (Aleo et al., 2006). G5-treated cells showed a complex response, since different biological processes are affected, and several pro- and anti-apoptotic factors are accumulated. As described for the UPSI, the G5-treatment leads to the expression and activation of the DR pathway, the cytosolic localization of Smac, the engagement of p53 and the inhibition of NF-kB (Richardson et al., 2005; Aleo et al., 2006). Even if the involvement of these two master administrators of survival/death (p53/NF-kB) was reported, the G5-dependent cell death can take place independently from them (Richardson et al., 2005; Demarchi and Brancolini, 2005).

As for the UPSI-elicited cell death, the DR pathway, concomitantly with the reduction of anti-apoptotic c-FLIP levels, can facilitate the cell death induction (Sayers et al., 2003). In this context, also the contribution of Smac should be considered as enforcer of the cell death, especially because it was demonstrated that its cytosolic accumulation can override the protection given by the anti-apoptotic Bcl-2 protein, which can free the effector caspases from IAP inhibition also in absence of the apoptosome formation (Sun et al., 2002; Aleo et al., 2006).

Although the apoptosis is surely involved, recently the contribution of alternative pathways was reported. Indeed, one of the most fascinating aspect of G5 regards its capability to trigger a peculiar necrotic response in cancer cells resistant to apoptosis (Fontanini et al., 2009). A deeper investigation of the G5-elicited molecular pathway was performed on glioblastoma cells, since glioblastomas (GBM) are one of the most lethal tumors characterized by high resistance to radiotherapies and chemotherapies. The resistance to apoptosis and the susceptibility to die by necrosis lead, this type of tumor, to be an ideal model for the characterization of G5 necrotic activity (Furnari et al., 2007).

Study performed on the two GBMs cell lines U87MG and T98G shed some lights on the cell mechanisms triggered by G5 (Foti et al., 2009). U87MG cell line showed an increased susceptibility to die by necrosis upon G5 treatment, in comparison to T98G cells. The expression profile analysis and functional studies, on these two cell lines, unveiled that the differential responsiveness to G5 could be due to the different expression of GSH-detoxification system and to the differential ability to adhere with the extracellular matrix (ECM) (Foti et al., 2009). In fact, the G5-induced necrosis was partially influenced by the ECM adhesion, but not by PARP activation or Bcl-2 or Bcl-xL inhibition, as shown in the study on murine embryonic fibroblasts derived from mice double-deficient for Bax and Bak (double knock-out; DKO) (Fontanini et al., 2009). PARP (poly(ADP-ribose) polymerases) is a well-known enzyme involved in the DNA damage repair response, and it has a role in the induction of necrosis in presence of DNA-alkylating compounds (Zong et al., 2004). In the PARP-induced pathway, the receptor-interacting protein 1 (RIP1) and c-Jun N-terminal kinase (JNK) are activated by various environmental stresses leading the cell to die by necrosis (Xu et al., 2006). By inhibiting separately these elements of the necrotic response, the G5-induced cell death was not affected (Fontanini et al., 2009), emphasizing the possibility of a new peculiar mechanism of cell death.

Starting to understand the capability of G5 to induce necrosis, an another study was performed to clarify if this pathway is similar to the necrosome-dependent cell death: the necroptosis.

Necroptosis was described as regulated cell death program activated by tumor necrosis factor α (TNF-α), TLR (toll-like receptors), interferon, and also by viral and bacterial agents or multiple pathophysiological signals (Berghe et al., 2014). The morphological features were described, for the first time, by Vercammen and colleagues on L929 cells upon the caspases blockage by the inhibitor z-Val-Ala-Asp.fluoromethylketone (zVAD-fmk) (Vercammen et al., 1998). They also observed that this pathway stimulates an inflammatory response since the treated cells, after the increase of cell volume and plasma membrane rupture, collapse and release the cellular content in the surrounding environment.

Several studies in the following years identified the nature of the execution complex involved in this type of cell death: the necrosome, which is the responsible of the final cellular demise. This multi-protein complex includes the receptor interacting protein kinase 1 (RIPK1), RIPK3 and mixed kinase domain-like (MLKL) (Berghe et al., 2014; Newton et al., 2016). Upon its activation, MLKL translocates on the plasma membrane to bind phosphoinositolphosphate (PIPs) molecules, and it forms some pore-forming structures, through which ions (as sodium) diffuse (Chen et al., 2014). The intracellular osmotic pressure is increased and the membrane collapse appears (Dondelinger et al., 2014). The MLKL behavior recalls the Bax and Bak proteins function on the outer mitochondrial membrane.

Another recent study described the capability of RIPK3-MLKL complex to translocate on mitochondria membranes to initiate the intrinsic pathway of necroptosis (Chen et al., 2014). This event together with the participation of the mitochondrial phosphatase PGAM5, which in turn activates the dynamin-related protein 1 (Drp1), seems to be essential for the mitochondrial fragmentation and for the final execution of the necroptotic pathway (Wang et al., 2012). The PGAM5 and Drp1 involvement is still unclear and debated, since several studies excluded their requirement in this type of cell death (Moujalled et al., 2014; Tait et al., 2013). Nevertheless, it is emerging an even more close connection between this regulated mechanism of necrosis and the intrinsic pathway of apoptosis, since they can proceed simultaneously, rendering more complex to define in which way a cell can die (Belizário et al., 2015; **Fig.8**).

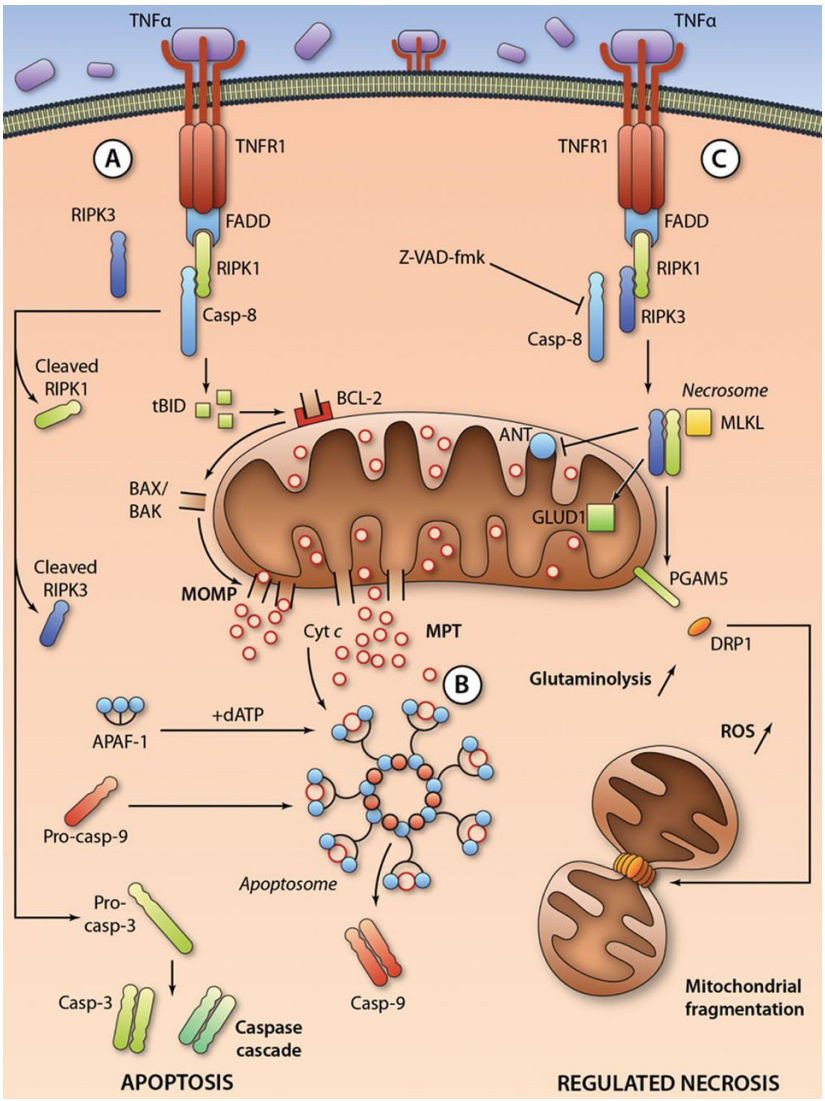

Fig.8: Cell death mechanisms. Comparison between the molecular mechanisms of apoptosis: the extrinsic pathway in **A** and the intrinsic pathway in **B**. The necroptosis (here called regulated necrosis) is shown in **C**. The differential complexes involved in the execution of the cell death pathways are reported (Galluzzi et al., 2012).

To better understand on which components of the cell death G5 relies, a comparative study was performed between this N-SII and DMNQ. The DMNQ (2,3-Dimethoxy-1,4-naphthoquinone) acts as redox-cycling agent, and it is normally used as a tool to generate reactive oxygen species (ROS), especially the superoxide and hydrogen peroxide species (Kaas et al., 1989). In fact, this drug is able to cross the plasma membrane and, in the intracellular environment, it is reduced by flavoenzymes (such as NADPH-cytochrome P450 reductase) producing semiquinone radicals. These species can react with the oxygen, forming

superoxide and, in turn, hydrogen peroxide. Not only, reactive and unstable hydroxyl radicals can be produced in presence of Fenton metals, determining the onset of the oxidative stress within the cell (Shi et al., 1994; Gant et al., 1988). The generated oxidative stress alters multiple cellular parameters, including the mitochondrial membrane potential (Klotz et al., 2014).

Comparing the responses of U87MG cells to these two drugs, different aspects were observed. The DMNQ-induced cell death requires the necroptotic components RIP1 and Drp1 and mitochondrial fragmentation, whereas the G5-triggered pathway occurs independently from them (Tomasella et al., 2014). In the G5-elicited mechanism, others components were pointed out: the phosphatase PP2A and its substrate Cofilin-1. Specifically, the catalytic subunit, of the Ser/Thr phosphatase PP2A, is stabilized upon the G5 treatment, and also an increase of its enzymatic activity was reported. Although in the cell death induced by the two stressors, an opposite role for PP2A was described, this phosphatase translocates from the nucleus into the cytoplasm, concomitantly with the well-known necrotic marker HMGB1. This aspect leaves open the possibility that the PP2A enzyme can organize a specific cytosolic necrotic complex able to drive the cell death (Tomasella et al., 2014).

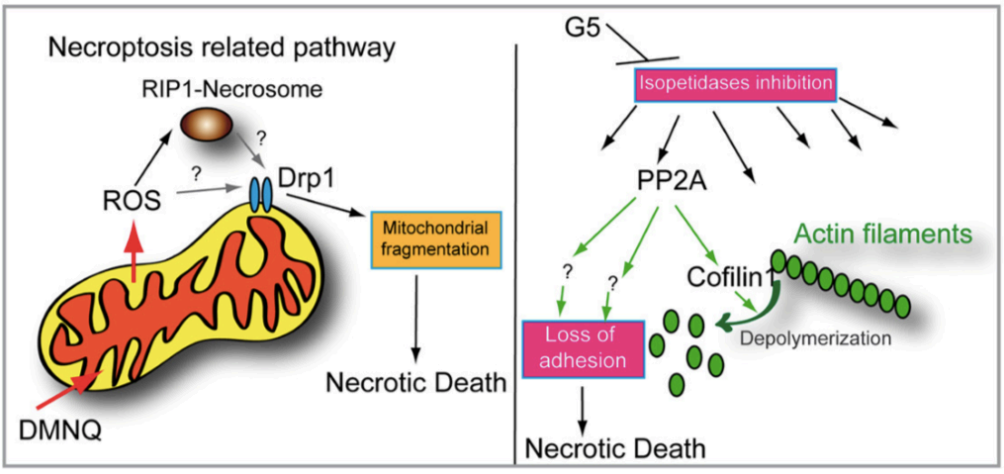

Fig.9: Comparison of DMNQ- and G5-induced cell death pathways. Different intracellular effects and activated pathways are involved in response to the two necrotic stressors: the ROS generator DMNQ and the N-SII G5 (Tomasella et al., 2014).

Since cytoskeletal alterations are evident in the G5-treated cells, it was thought to study Cofilin-1, the PP2A substrate, which is characterized by an actin depolymerizing activity. G5 treatment induces the activation of Cofilin-1, by dephosphorylating its Ser3, in a PP2A-dependent manner. Nevertheless, the expression of a Cofilin-1 phosphomimic mutant in the U87MG cells, and their following treatment with G5, reveal a partial involvement of this actin-binding protein, emphasizing that others elements are required for the execution of G5-elicited pathway (Tomasella et al., 2014; **Fig.9**).

Obviously, a complete and clear description of the peculiar necrotic program elicited by G5 is necessary. In fact, the promising effect of G5 is given by its capability to trigger a different pathway of cell death in those cancer cells which acquired resistance to the traditional pro-apoptotic drugs.

2. Aim of the study

Acquisition of mutations/alterations in the apoptotic machinery is one of the main cause of the chemotherapy failure in cancer cells. For this reason, it is interesting to find new compounds able to elicit alternative cell death pathways. Among them, the non-selective DUB inhibitor G5 represents a promising therapeutic agent for its ability to induce a proteotoxic stress-dependent necrotic pathway. This pathway is largely unexplored. Previous studies have demonstrated the role played by the PP2A/Cofilin-1 axis, but other key proteins and signaling events are possible involved. To better dissect the G5-elicited death mechanisms, two strategies have been followed: i) a proteomic approach to map additional cellular targets of this compound, and ii) an unbiased screening using a shRNA library to identify critical genes in the G5-induced necrotic death. The general aim of this thesis was to reveal new death signaling pathways, operating in glioblastoma cells, by using different genome and genetic editing approaches, such as the RNA interference and the CRISPR-Cas9 system.

In parallel, the effects of the G5-derivate 2cPE, optimized for *in vivo* delivery, has been studied in a different cancer context: the B-cell chronic lymphocytic leukemia (B-CLL) in comparison to bortezomib, the first UPS inhibitor approved in clinic. Since these results have been already published they are included as appendix of this thesis. Hence, the result section will be focused on the recently obtained and still unpublished results.

3. Results

3.1 High-throughput shRNA library screening to identify genes involved in transducing G5-induced cell death

To uncover key genes controlling the G5-induced necrosis, we conducted an unbiased pooled short hairpin RNA (shRNA) screening on U87MG cells, a cellular model chosen for its natural propensity to die by necrosis (Foti et al., 2009). The used DECIPHER™ human module 1 of the library contains 27500 shRNAs targeting 5046 signaling components.

The basis of this type of technology is the stable suppression of thousands of different targets on a large scale, allowing us to obtain a simultaneous loss-of-function screening in a single experiment. In this way, it is possible to identify genes functionally involved in triggering the G5-induced pathway, since they ablation should promote a growth advantage.

U87MG cells were infected with the lentiviral library encoding the highly heterogeneous population of barcoded shRNA constructs for two days. The infection was performed into a population of 33 millions of cells, to exceed the complexity of the library for at least 200 times. A very low multiplicity of infection (MOI of 0,1) was selected, in order to have the expression of a single shRNA in single cells. Two days later, the infected cells were selected with puromycin and after three days, the surviving population of cells, harboring different shRNAs, was treated with G5 for 60 hours. G5-treatment should permit the exclusive survival of those cells, which contain and express shRNAs able to silence genes required for G5 death-related activities (**Fig.10*A***). To discover the identity of these genes, the genomic DNA was extracted from the surviving cells and the abundance of every integrated shRNA-specific barcode was amplified by PCR with vector-specific primers and identified using high-throughput (HT) sequencing. The barcodes are unique and specific sequences of 18-nucleotides permanently associated with the shRNA expression cassette. These sequences enable an unambiguous identification of each shRNA upon the HT sequencing. The deconvolution and normalization of the reads for each barcode respect to “neutral” shRNAs, present in the library, reveled the identity of the most enriched shRNAs. Moreover, since in the library, for every target were present from 5 to 6 different shRNAs, relevant “hits” were defined those genes with at least two different shRNAs enriched in comparison to the

shRNAs against the luciferase ($N_{shRNAs} \geq 2$), the control gene (**Fig.10*B***). As it is shown in the graph, among the top target genes were identified: RNASEL, POU5F1, GSK3β, CAPN1 and DUSP10. We focused our attention on glycogen synthase kinase-3 β (GSK3β), since it is well known to be a stress-induced kinase (Cheng et al., 2016; Song et al., 2002), and because it is involved in different cell death pathways under specific cellular contexts (Beurel and Jope, 2006; Sun et al., 2008; Gómez-Sintes and Lucas, 2010). Finally and most important, among other hits, well-known interacting proteins/regulators of GSK3β were detected, such as Calpain 1 (CAPN-1) (Goñi-Oliver et al., 2007), and the protein phosphatase-1 (PPP1) (Felgueiras and Fardilha, 2014) (**Fig.10*C***).

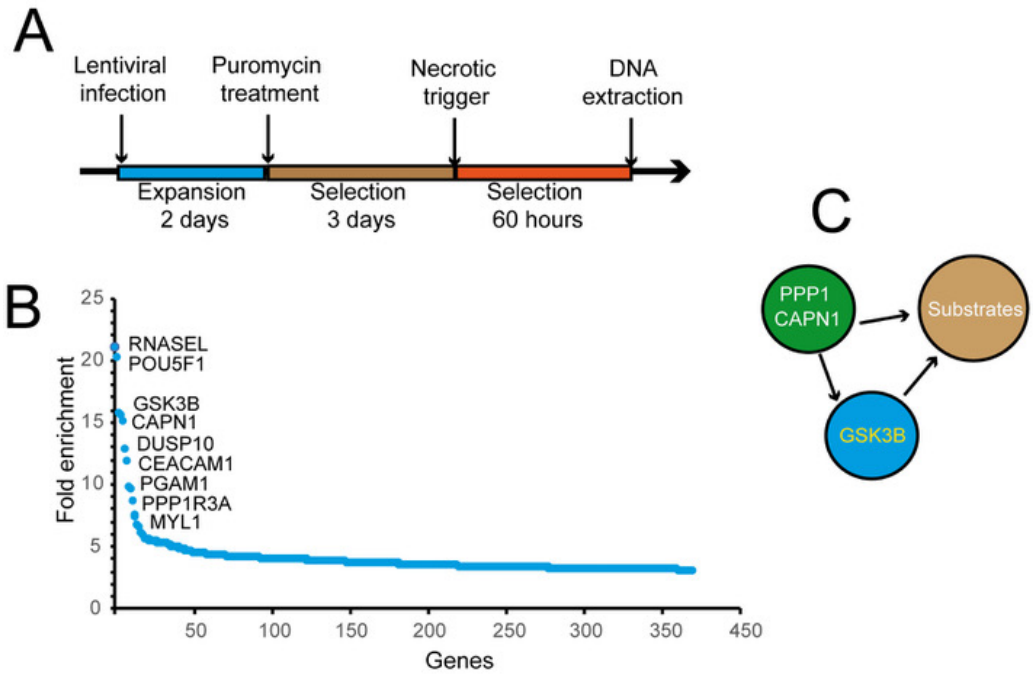

Fig.10: Followed experimental approach and identification of hits by the DECIPHER™ pooled shRNA library. (**A**) Schematic representation of the screening protocol. 33 millions of U87MG cells were infected with the lentiviral particles containing the shRNA plasmids for two days. For the selection of the expressing-shRNAs, the cells were selected with puromycin (2 µg/ml) for three days. Later, the selected cells were treated with the necrotic tigger G5 (2,5 µM) for 60 hours and the surviving cells were harvested to recover the genomic DNA. (**B**) By PCR-amplification, HT sequencing, and normalization on Luciferase shRNAs, the most enriched hits were represented ($N_{shRNAs} \geq 2$). (**C**) Among the identified hits, the GSK3β and its specific interacting proteins, such as CAPN1 and PPP1, were detected.

3.2 Validation of hits library through RNAi

Since the involvement of CAPN1 in different cell death programs is well known, and, to validate our shRNA library screening, the silencing of CAPN1 was performed using a siRNA targeting a different region of the gene. In addition, a siRNA against PP2AC was used as positive control. In fact, it was previously demonstrated that PP2AC down-regulation decreased G5-induced cell death (Tomasella et al., 2014).

U87MG cells with down-regulated CAPN1 and PP2AC proteins were less sensitive to the G5-treatment, in comparison with the control transfected cells. The potency of silencing was confirmed by the reduction of the respective protein levels, as shown in the immunoblot analysis (**Fig.11*A***).

To validate GSK3β as an element of G5-induced cell death pathway, a specific siRNA was transfected in both U87MG and U87MG-BCLXL cells. U87MG-BCLXL cells were used to confirm the role of GSK3β in the necrosis regulation and, not in the apoptosis, since BCLXL over-expression further suppresses the apoptotic cascade activation. Cells were subjected to 72 hours of silencing. In both cell lines, when GSK3β was down-regulated and, cells were treated with G5, the reduction of the GSK3β mRNA expression was correlated with a slight decrease in cell death in comparison to cells transfected with a control siRNA (**Fig.11*B***).

In summary, the involvement of GSK3β in the necrotic pathway triggered by G5 is unclear, given that its silencing was not able to strongly affect the cell death appearance. To clarify if this partial effect was due to the modest RNAi-mediated down-regulation of the kinase under consideration, the CRISPR/Cas9 system was applied to obtain the full abolition of GSK3β protein in U87MG cells.

3.3 Generation of GSK3β knock-out cells and their characterization

To apply the CRISPR/Cas9 system and to generate knock-out (KO) cells for GSK3β, a single guide RNA (sgRNA) complementary to the exon 1 of *GSK3β* gene was designed and the wild type (wt) Cas9 was used. After the screening of 253 isolated clones, one putative U87MG/ GSK3β KO clone (number 19) was identified. The immunoblot analysis demonstrated the complete absence of the GSK3β protein in these cells, in comparison to two types of U87MG/

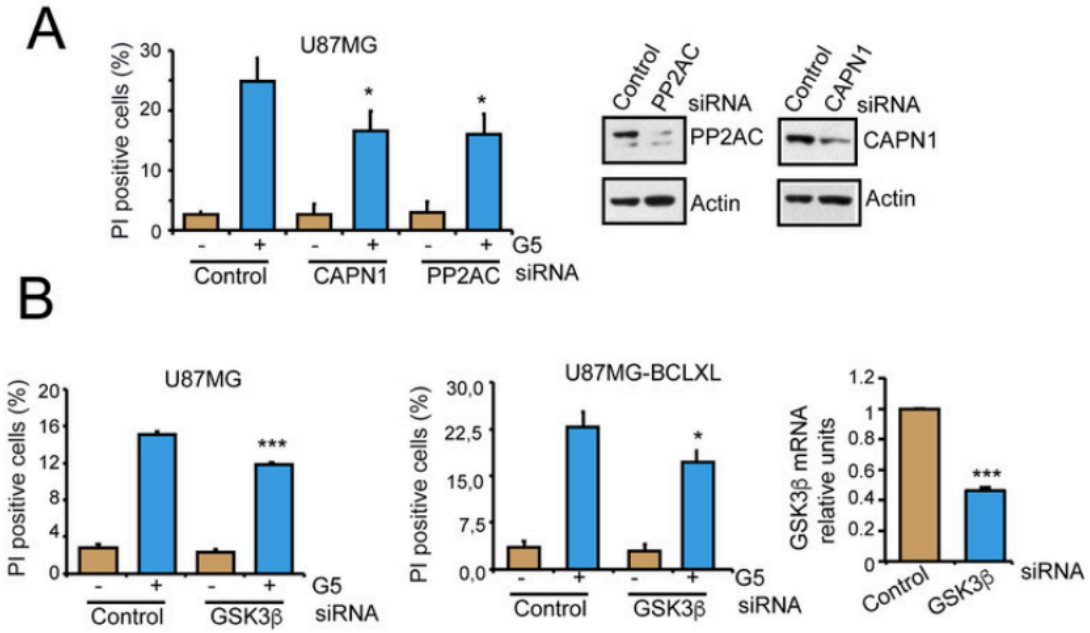

Fig.11: Validation of identified hits in U87MG G5-treated cells. (**A**) Cytofluorimetric analysis showing the percentage of cell death in U87MG cells silenced for 48 hours for CAPN1 or PP2AC, and G5-treated for 24 hours (10 μM). The cellular lysates from down-regulated cells were tested by immunoblot. Antibodies anti-CAPN1, anti-PP2AC, and anti-actin (as loading control) were used. (**B**) Cytofluorimetric analysis showing the percentage of cell death in U87MG and U87MG-BCLXL cells silenced for 48 hours for GSK3β, and G5-treated for 24 hours (10 μM). GSK3β mRNA levels, in the down-regulated U87MG cells, were reported in comparison to GSK3β mRNA expression in control transfected cells. Data were from 3 experiments. Columns mean loss of viability + SD. *=p<0.05; **=p<0.01; ***=p<0.01.

GSK3β$^{+/+}$ control cells (**Fig. 12*A***). The GSK3β$^{+/+}$ control cells were represented by a clone derived from U87MG cells infected exclusively with Cas9 wt, but not with the sgRNA (control sample), and by other clone (number 63), which was one of the screened clones that resulted wild-type for GSK3β (WT sample).

The genomic DNA (gDNA) of the putative GSK3β$^{-/-}$ clone was extracted and sequenced in order to find the origin of the mutation that causes the absence of the kinase. The sequencing demonstrated that the *GSK3β* gene in the KO cells was characterized by the insertion of one thymidine in the exon 1, exactly two nucleotides later the PAM, in both the alleles. Consequently, in the corresponding amino acid sequence the introduction of a premature stop codon was observed as product of the frameshift dictated by the insertion. This event explains the total absence of the GSK3β protein in U87MG KO cells (**Fig. 12*B***).

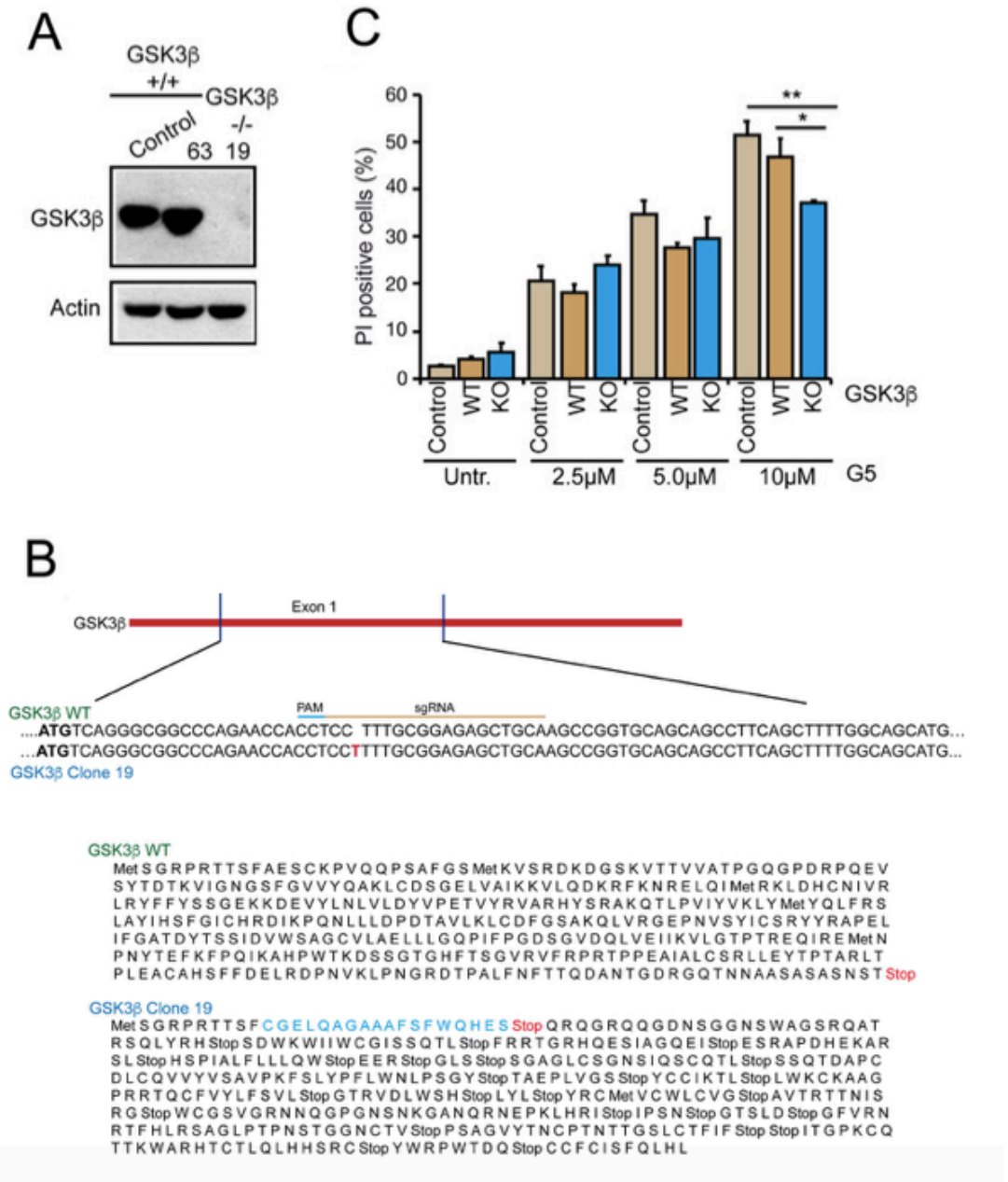

Figure 12: Generation of U87MG/GSK3β KO clone and its response to G5 treatment. (**A**) Immunoblot analysis of GSK3β protein expression on lysates obtained from U87MG control cells (infected with Cas9 wt, without the sgRNA), from the clone 63 (infected with Cas9 wt and the sgRNA, but resulted wt for GSK3β), and from GSK3β$^{-/-}$ cells (clone 19). Antibodies anti-GSK3β and anti-actin (as loading control) were used. (**B**) Nucleotide sequence of *GSK3β* gene in the U87MG/GSK3β$^{-/-}$ cells aligned to the wt sequence. In the exon 1 of the *GSK3β* gene, two nucleotide after the PAM, an insertion of one thymidine (in red) was found in both the alleles (only one allele is reported). The corresponding amino acid sequence of the KO clone is shown. The frameshift due to the mutation is highlighted in blue and the introduction of a premature stop codon (in red) explains the absence of the kinase in the clone 19. (**C**) Cytofluorimetric analysis showing the percentage of cell death in GSK3β control, GSK3β WT and GSK3β KO cells treated with G5 for 24 hours (2,5-5-10 μM). Data were from 3 experiments. Columns mean loss of viability + SD. *=p<0.05; **=p<0.01; ***=p<0.01.

The U87MG/GSK3β$^{-/-}$ cells represent the ideal model to study the role of this kinase in the

cell death pathway elicited by G5. For this reason, these cells and the relative control cells were treated with an increasing concentration of the inhibitor for 24 hours. Surprisingly, the GSK3β KO cells showed a modest resistance to the G5-treatment exclusively with the higher concentration (10 μM), similarly to cells knocked-down by RNAi (**Fig. 12*C***). The obtained results suggest a partial role for GSK3β in transducing the G5-induced cell death signals, leaving unsolved the question about the nature of other regulators possible involved in this peculiar cell death pathway. On the other hand, these data strengthened the role of GSK3β in the necrotic regulation, given that the G5-treatment is able to directly elicit a necrotic response in the cells treated with highest concentration of the drug (Fontanini et al., 2009).

G5 triggers pleiotropic stresses, which can drive cells to death, such as: proteotoxic stress, oxidative stress and cytoskeletal malfunctions, thus, the partial impact of GSK3β knock-out could stem from a co-existence of multiple cell death pathways.

To prove this hypothesis, we selected DMNQ, an inducer of oxidative stress. DMNQ-induced cell death involves the necroptotic component RIP1, Drp1, and mitochondrial fragmentation. G5, by contrast, acts mainly through different pathways, even if it affects the mitochondria.

The DMNQ-treatment of U87MG/GSK3β$^{-/-}$ cells and relative control cells (control and WT) showed that GSK3β was strongly required to trigger cell death in response to DMNQ (**Fig. 13*A***). The contribution of GSK3β to the DMNQ-induced cell death, it was validated by RNAi experiments. In fact, U87MG cells, down-regulated for GSK3β, were less sensitive to the oxidative stress-induced cell death pathway caused by DMNQ exposure. The decreased protein levels of GSK3β, in the corresponding silenced cells, was confirmed by immunoblot analysis (**Fig.13*B***).

In summary, GSK3β plays a minor role during G5-induced cell death, but a major role in the DMNQ-elicited cell death pathway.

3.4 Phenotype rescue in the U87MG/GSK3β$^{-/-}$ cells re-expressing GSK3β

To further confirm that GSK3β was effectively involved in the onset of cell death, in response to the oxidative stress generated by DMNQ, we re-expressed GSK3β in the U87MG/GSK3β$^{-/-}$ cells. Specifically, two variants of the GSK3β protein were re-expressed: GSK3β wild type (WT) and GSK3β kinase mutant (KM), both C-terminal GFP-tagged. The DNA sequencing

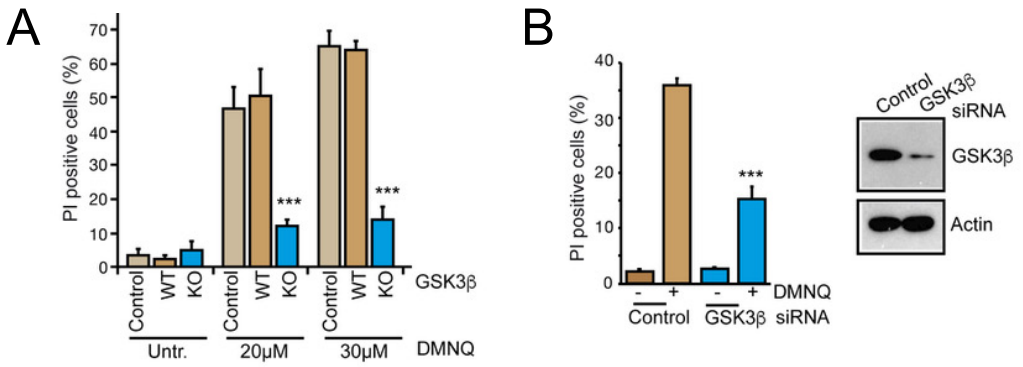

Figure 13: Resistance phenotype correlated to the absence and down-regulation of GSK3β upon the DMNQ-treatment. (**A**) Cytofluorimetric analysis showing the percentage of cell death in U87MG/GSK3β control, GSK3β WT and GSK3β KO cells treated with DMNQ for 24 hours (20 and 30 μM). (**B**) Cytofluorimetric analysis showing the percentage of cell death in U87MG cells silenced for 48 hours for GSK3β, and treated with DMNQ for further 24 hours (30 μM). At 48 hours of silencing, cellular lysates, from the down-regulated control and GSK3β cells, were harvested and tested by immunoblot. Antibodies anti-GSK3β, and anti-actin (as loading control) were used. Data were from 3 experiments. Columns mean loss of viability + SD. *=p<0.05; **=p<0.01; ***=p<0.01.

confirmed, in the GSK3β KM sequence, the presence of a mutation located in the amino acid 85 (K85A) in the kinase domain (data not shown). This mutation determines the inability of the kinase to act on its substrates. Thus, in the U87MG/GSK3β$^{-/-}$ cells re-expressing GSK3β KM, the kinase can be activated, but it cannot phosphorylate the specific intracellular substrates.

The re-expression of the two GSK3β variants was performed into the U87MG/GSK3β$^{+/+}$ and GSK3β$^{-/-}$ cells. U87MG/GSK3β$^{+/+}$ and GSK3β$^{-/-}$ cells expressing only the Neomycin resistance were used as control (Neo cells). In **Fig.14*A***, the immunoblot analysis proved the successful re-expression of WT and KM versions in both the GSK3β$^{+/+}$ and GSK3β$^{-/-}$ cells. Subsequently, the engineered cell lines were treated with DMNQ, in order to understand, if the re-expression of the WT form of GSK3β, was able to re-establish the sensitivity to die. The reported results showed that only the U87MG/GSK3β$^{-/-}$ cells expressing GSK3β WT, but not the KM version, entered cell death after DMNQ treatment (**Fig.14*B***). On the contrary, the DMNQ-treated U87MG/GSK3β$^{-/-}$ cells re-expressing the inactive form of GSK3β were not rescued in terms of cell death. The morphology of the different cell lines before and after DMNQ treatment is reported in **Fig.14*D***. Here, it is possible to recognize the presence of dead cells, upon DMNQ treatment, in the case of U87MG/GSK3β$^{-/-}$ cells re-expressing GSK3β

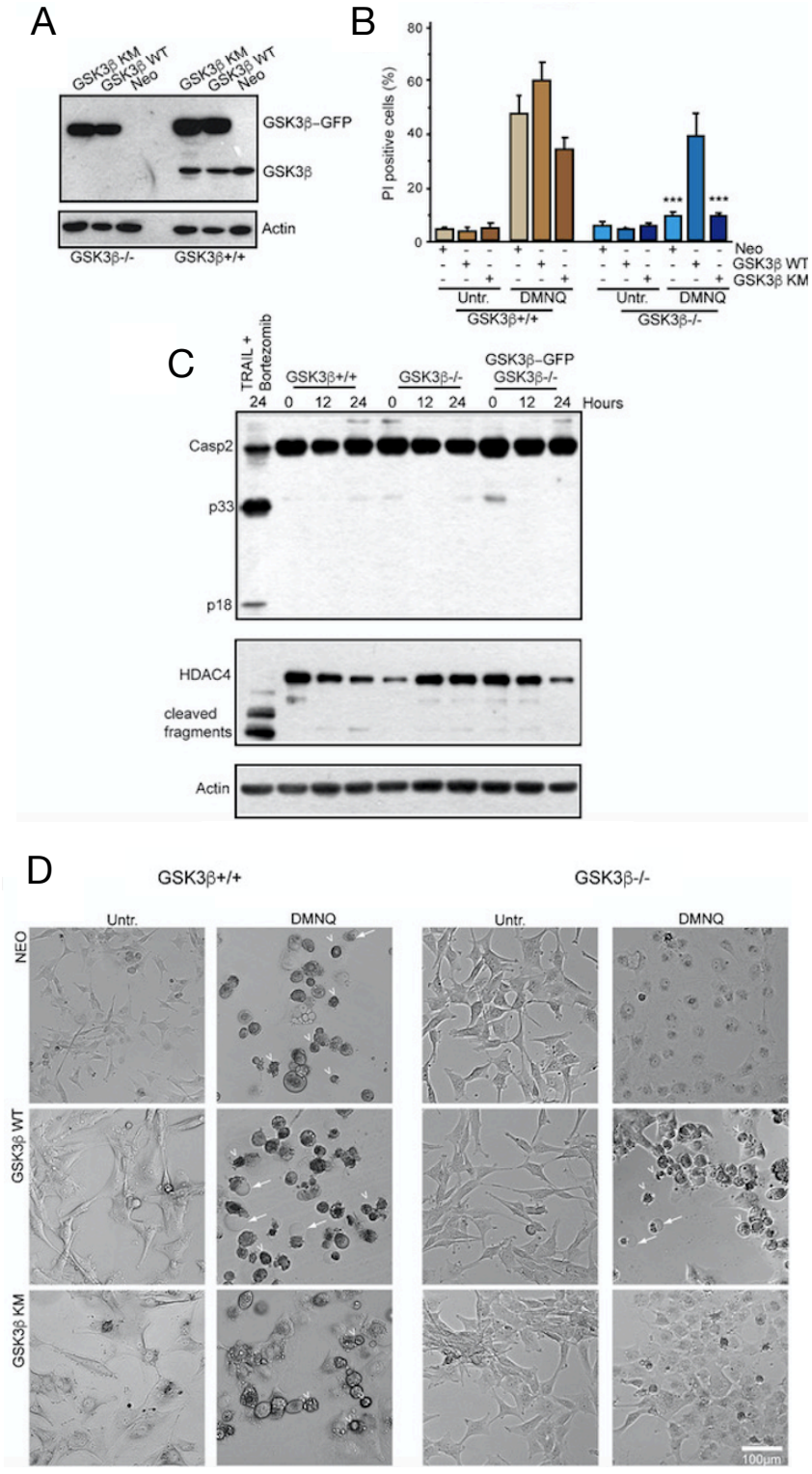

Figure 14: Phenotype rescue in response to DMNQ in the U87MG/GSK3β$^{-/-}$ cells re-expressing GSK3β wild type. (**A**) Immunoblot analysis of lysates obtained from U87MG/GSK3β$^{+/+}$ and GSK3β$^{-/-}$ cells re-expressing GSK3β WT or KM version. The exogenous form of GSK3β in frame with GFP was reveled at 75 kDa (GSK3β-GFP) and the endogenous one at 45 kDa. Antibodies anti-GSK3β, and anti-actin (as loading control) were used. (**B**) Cytofluorimetric analysis showing the percentage of cell death in U87MG/ GSK3β$^{+/+}$ and GSK3β$^{-/-}$ cells re-expressing GSK3β WT or KM, treated with DMNQ for 24 hours (30 μM). Data were from 3 experiments. Columns mean loss of viability + SD. ***=p<0.01. (**C**) Immunoblot analysis of lysates obtained from U87MG/GSK3β$^{+/+}$, GSK3β$^{-/-}$ and GSK3β$^{-/-}$ cells re-expressing GSK3β WT, treated with DMNQ (30 μM, for the indicated times) or bortezomib (100nM) for 4 hours plus TRAIL (2,5 ngr/ml) for further 20 hours. Anti-Casp2, anti-HDAC4 and anti-actin antibodies were used. (**D**) The same cells in B were imaged with Leica DMi1 microscope with a 10x objective before and after the DMNQ treatment (30 μM); white arrows indicate dying cells; scale bar: 100 μm.

WT, but not in the case of cells expressing the kinase death mutant KM or the Neo gene alone. Overall, these results further validate the crucial role of GSK3β in the DMNQ-induced oxidative stress death pathway and prove the dependence on the kinase activity.

Finally, to confirm that death induced by DMNQ was necrotic/caspase-independent, two caspase substrates were tested: Caspase-2 and HDAC4. It is known that, during apoptosis, HDAC4 translocates into the nucleus upon its cleavage, and this event is mediated by the activated Caspase-3/-2 (Paroni et al., 2004).

U87MG/GSK3β$^{+/+}$ cells, treated with an apoptotic stimulus (bortezomib and TRAIL co-treatment), were used to compare the two different cell death responses (Unterkircher et al., 2011). Immunoblot analysis of DMNQ-treated U87MG/GSK3β$^{+/+}$, GSK3β$^{-/-}$ and GSK3β$^{-/-}$ re-expressing GSK3β-WT cells, in comparison to bortezomib/TRAIL-treated U87MG/GSK3β$^{+/+}$ cells, showed that the cleaved forms of Caspase-2 (p33 and p18), and cleaved fragments of HDAC4, were detected only in the lysates obtained from cells treated with the combination of the two apoptotic stressors (**Fig.14*C***). Moreover, the reduction in HDAC4 levels, observed at later time points from DMNQ treatment (only in the presence of GSK3β), could be related to the ability of the kinase to influence HDAC4 poly-ubiquitylation and degradation (**Fig.14*C***).

To conclude, the role played by GSK3β in necrosis, triggered by oxidative stress, was fully confirmed.

3.5 DMNQ activates GSK3β and triggers mitochondrial dysfunction

To explore whether GSK3β is activated in the pathways triggered by DMNQ and G5, the phosphorylation status of Ser9 GSK3β was evaluated. This amino acid residue is well-know to be the main responsible for the regulation of the kinase. In particular, once phosphorylated, it inhibits the kinase activity of GSK3β (Cross et al., 1995). Molecularly, it happens because the phosphorylated N-terminus end of GSK3β occupies the site for the primed substrates, by acting as a pseudosubstrate, and by blocking in this way the catalytic activity of the kinase (Frame et al., 2001).

A time course analysis of the phosphorylation status of Ser9 residue (p-GSK3β S9), in the U87MG/GSK3β$^{+/+}$ cells, was performed, upon DMNQ or G5 treatments. A strong difference in terms of GSK3β activation was observed (**Fig.15**). In DMNQ-treated cells an early and

marked dephosphorylation of Ser9 was detected as soon as after 1 hour of treatment, which became stronger after 3 hours. At later time points (from 6 hours), GSK3β was again phosphorylated at Ser9, and subsequently inactivated. On the contrary, in G5-treated cells, the initial phosphorylation of Ser9 was modestly affected by G5 treatment throughout the period of the analysis.

These results could explain the differential dependence of two necrotic insults from GSK3β, given the divergent responses of U87MG/GSK3β$^{-/-}$ cells to the two treatments.

To support these data, we investigated the status of Akt activation, a main up-stream regulator of GSK3β activity. Once Akt is activated, it is able, by phosphorylating GSK3β on Ser9, to inactivate it (Cross et al., 1995; Alessi and Cohen, 1998). To this purpose, the Thr308 and Ser473 phosphorylation status of Akt (p-Akt T308 and p-Akt S473) were followed. Immunoblot analysis showed a correspondence between the decrease of the p-GSK3β S9 and the inactivation of Akt, given by an early dephosphorylation of Thr308, in response to the DMNQ exposure. In opposite, the phosphorylation of Ser473 was not strongly affected in response to DMNQ treatment (**Fig.15**).

In the G5-treated cells, the phosphorylation status of Akt did not correspond with the GSK3β status, since an early and strong Akt activation was detected later 1 hour from the treatment. p-GSK3β S9 status was independent from the p-Akt T308. In contrast to the DMNQ, Thr308-dependent activation of Akt was strongly involved during the G5 exposure (**Fig.15**).

DMNQ treatment can elicit a profound re-organization of the mitochondrial network, which depends on Drp1 activities (Tomasella et al., 2014).

To gain further insight into the intracellular effects supervised by GSK3β, in response to DMNQ treatment, U87MG/GSK3β$^{+/+}$ and GSK3β$^{-/-}$ cells were analyzed for the integrity and morphology of mitochondrial network. In particular, Smac localization was studied, since it allows to monitor the mitochondrial morphology and the integrity of the outer mitochondrial membrane (OMM) (Lim et al., 2002; Newmeyer and Ferguson-Miller, 2003). By immunofluorescence analysis of the Smac localization, in the DMNQ-treated U87MG/ GSK3β$^{+/+}$ and GSK3β$^{-/-}$ cells, it was noticed that in both cellular contexts (hence, in a GSK3β-independent way), the mitochondria underwent fragmentation in response to DMNQ treatment (**Fig.16*A***). Next, we evaluated the total levels of Smac in DMNQ-treated cells. The

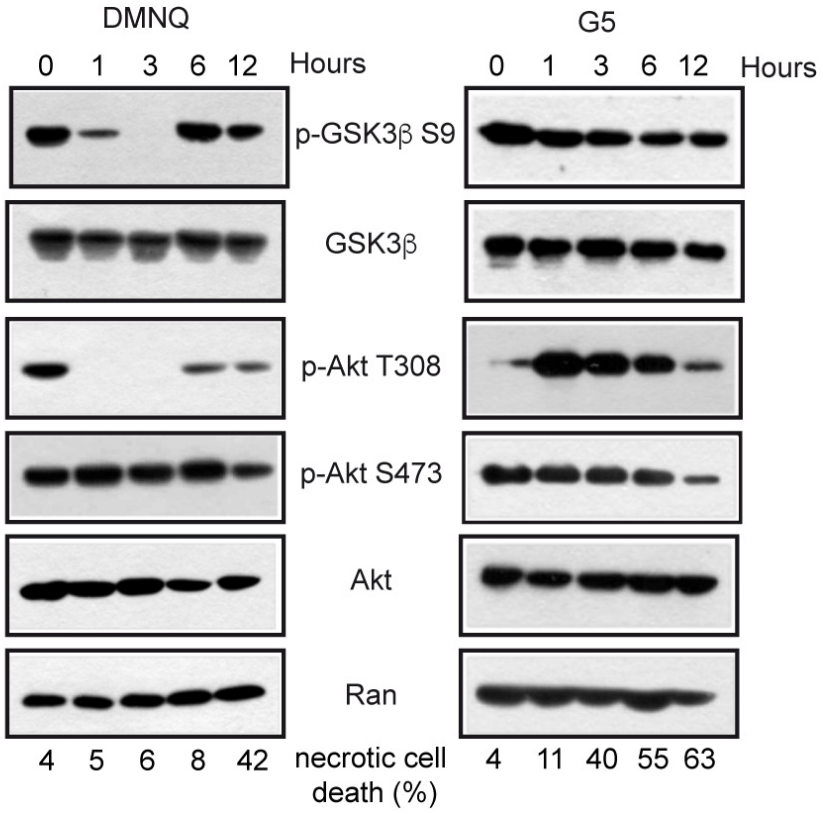

Figure 15: Differential activated signaling pathways in DMNQ- and G5-treated U87MG/GSK3β +/+ cells. Comparative immunoblot analysis between U87MG GSK3β +/+ cells treated with DMNQ (30 μM) or G5 (10 μM) for the indicated times. p-GSK3β S9, GSK3β, p-Akt T308, p-Akt S473, Akt and Ran (as loading control) antibodies were used.

Smac levels were clearly reduced in U87MG/GSK3β$^{+/+}$ cells, whereas they were unaffected in the U87MG/GSK3β$^{-/-}$ cells (**Fig.16*B***). Re-expression of GSK3β promoted the decrease of Smac protein. The degradation of Smac, in response to DMNQ, could be related to its release into the cytoplasm as consequence of the rupture of the OMM (Henderson et al., 2005).

In fact, although the mitochondria of U87MG/GSK3β$^{+/+}$ and GSK3β$^{-/-}$ cells present the same morphology upon the DMNQ exposure, the mitochondrial membrane potential ($\Delta\psi_m$) was completely different. The cytofluorimetric measurements, using the probe TMRM, demonstrated that, in the U87MG/GSK3β$^{-/-}$ cells, the mitochondrial potential is well maintained, also after 24 hours of DMNQ treatment. By contrast, in U87MG/GSK3β$^{+/+}$ cells a dramatic drop of the mitochondrial potential was measured in response to DMNQ (**Fig.16*C***). TMRM probe was recording effectively the $\Delta\psi_m$ of the treated cells, since the incubation with the mitochondrial uncoupler FCCP drastically reduced the TMRM fluorescence, given by the

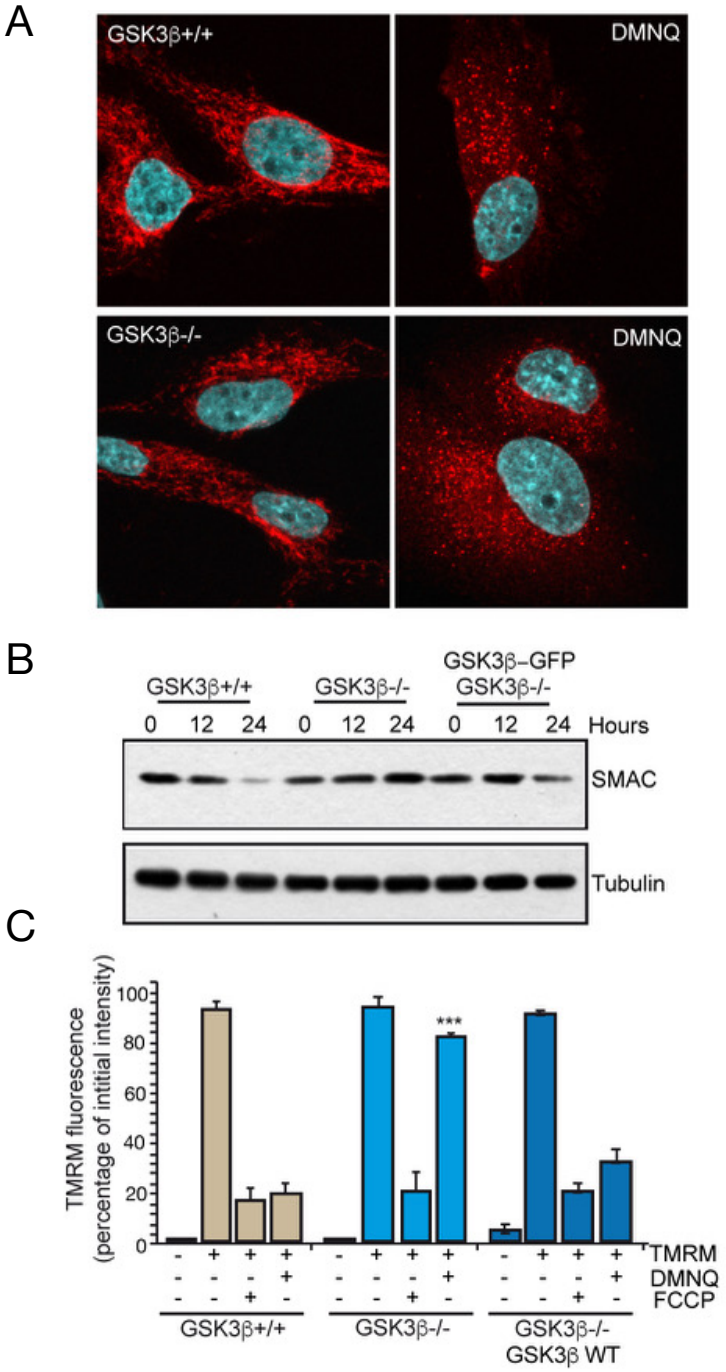

Figure 16: Mitochondria state and functionality in the DMNQ-treated U87MG/ GSK3β$^{+/+}$ and U87MG/GSK3β$^{-/-}$ cells. (**A**) Immunofluorescence of Smac subcellular localization and mitochondrial morphology in DMNQ-treated U87MG/GSK3β$^{+/+}$ and U87MG/GSK3β$^{-/-}$ cells (30 μM for 24 hours). Cells were analyzed and imaged at confocal microscopy. (**B**) Comparative immunoblot analysis of lysates obtained from U87MG/ GSK3β$^{+/+}$, U87MG/GSK3β$^{-/-}$ and U87MG/GSK3β$^{-/-}$ re-expressing GSK3β WT-GFP cells treated with DMNQ (30 μM) for the indicated times. Anti-Smac and anti-Tubulin (as loading control) antibodies were used. (**C**) Comparison of the $\Delta\psi_m$ in the U87MG/ GSK3β$^{+/+}$, U87MG/GSK3β$^{-/-}$ and U87MG/GSK3β$^{-/-}$ re-expressing GSK3β WT cells after 24 hours of DMNQ treatment (30 μM), measuring, by cytofluorimetric analysis, the TMRM fluorescence. Cells were incubated with TMRM (1 μM) for 30 minutes, then FCCP was added for 5 minutes (10 μM) before the FACS analysis. Data were from 3 experiments. Columns represent the percentage of initial intensity of TMRM fluorescence+ SD. ***=p<0.01.

mitochondrial membrane depolarization. This effect was GSK3β independent (**Fig.16*C***).

3.6 $\Delta\psi_m$ dissipation and nuclear GSK3β translocation

The oxidative stress and ROS generation mainly relies on the mitochondrial functions, influencing the cell viability. In fact, the mitochondrial respiratory chain is considered one of the major source for ROS generation and spreading, within a cell. At the same time, the mitochondria are very susceptible targets of the damaging effects related to the oxidative stress (Marchi et al., 2012). GSK3β is mainly a cytosolic protein, however its localization in other sub-cellular compartments, including the nucleus and the mitochondria, has been reported (Bijur and Jope, 2001; 2003).

For these reasons, we investigated *in vivo*, the sub-cellular localization of GSK3β and the mitochondrial membrane potential in U87MG/GSK3β$^{-/-}$ cells re-expressing GSK3β WT-GFP, during the DMNQ exposure. A time-lapse experiment of 24 hours was performed, and the $\Delta\psi_m$ dissipation was evaluated by measuring TMRM fluorescence in single cells. In parallel, GSK3β localization was observed through the GFP. The integrity of the GSK3β-GFP probe during the period of analysis was verified by immunblot (**Fig.17*A***).

Single-cell imaging analysis of DMNQ-treated cells showed that the DMNQ treatment determines a gradual nuclear translocation of GSK3β, followed by $\Delta\psi_m$ collapse, cell detachment and death (**Fig.17*A***). Measuring changes of the cytosolic TMRM fluorescence, and in parallel, of the nuclear/cytosolic GSK3β-GFP fluorescence ratio, in DMNQ treated-cells, it was possible to appreciate that the kinetic of the kinase nuclear translocation is gradual and linked to the $\Delta\psi_m$ loss. Since the single cells depolarize at different times from DMNQ treatment, the potential collapse was set to time zero. With some peculiarities, 3 hours before $\Delta\psi_m$ collapse, some nuclear accumulation of GSK3β can be appreciated (**Fig.17*B***).

On the contrary, the untreated cells were characterized by "physiological fluctuations" of the $\Delta\psi_m$ (Hüser and Blutter, 1999), and by a stable nuclear/cytosolic GSK3β-GFP fluorescence ratio, during all the recorded time. These data indicate that the nuclear translocation of GSK3β-GFP seems to be specifically caused by the DMNQ treatment and that it appears in a late phase of the necrotic response, but before $\Delta\psi_m$ collapse.

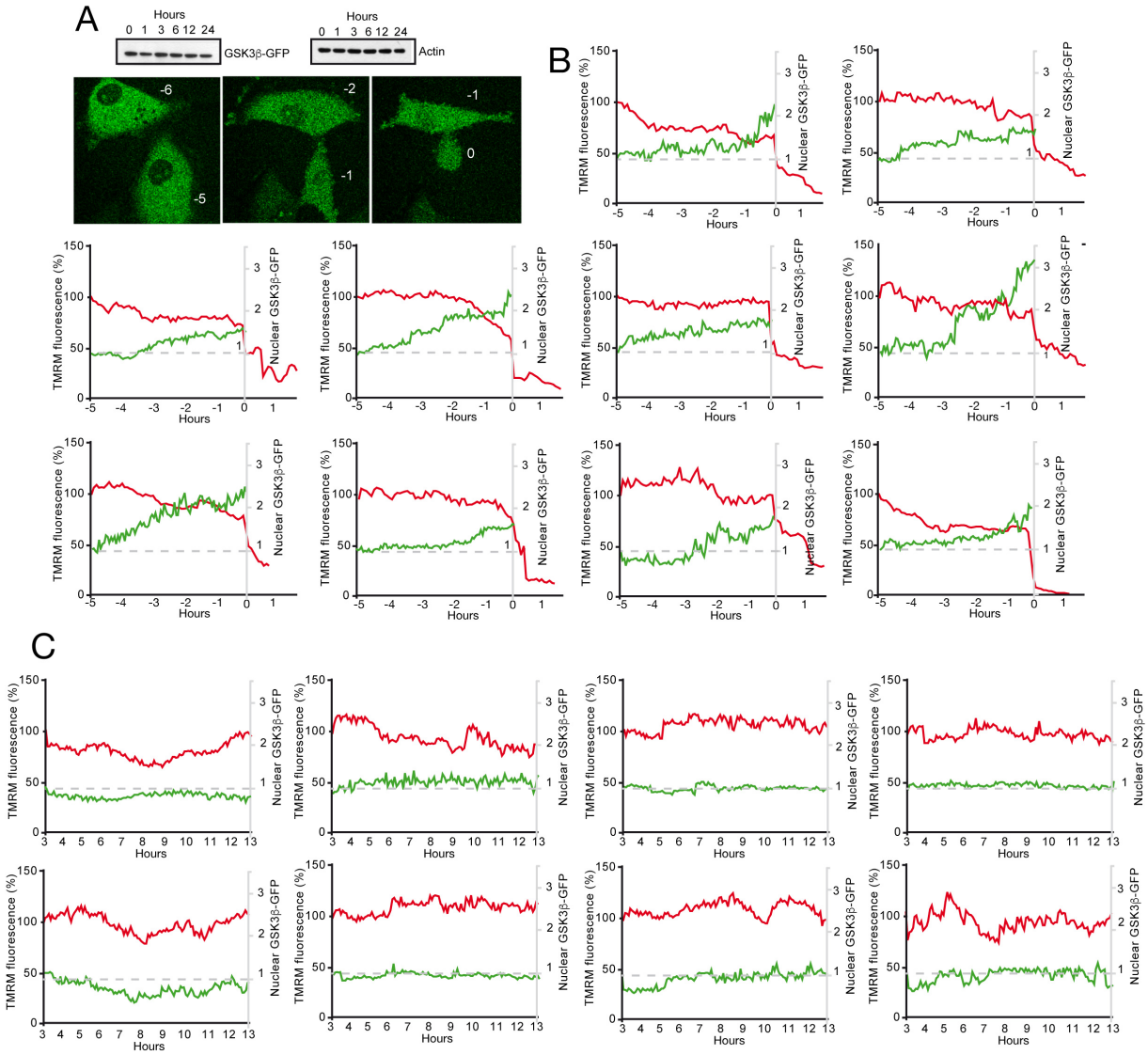

Figure 17: Nuclear translocation of GSK3β-GFP during DMNQ treatment and mitochondrial $\Delta\psi_m$ dissipation in single cells. (**A**) Frames of two U87MG/GSK3β$^{-/-}$ re-expressing GSK3β WT-GFP cells, examined in B at the indicated times. Immunoblot analysis of lysates obtained from U87MG/GSK3β$^{-/-}$ re-expressing GSK3β-GFP cells during the DMNQ treatment (30 μM) at the indicates times. Anti-GSK3β and anti-actin (as loading control) antibodies were used. (**B**) Individual traces of TMRM fluorescence (in red) and of nuclear/cytosolic GSK3β WT-GFP fluorescence ratio (in green) in ten U87MG/GSK3β$^{-/-}$ re-expressing GSK3β-GFP cells, treated with DMNQ (30 μM) for 24 hours. (**C**) Individual traces of TMRM fluorescence (in red) and of nuclear/cytosolic GSK3β-GFP fluorescence ratio (in green) in ten untreated U87MG/GSK3β$^{-/-}$ re-expressing GSK3β-GFP cells.

4. Discussion

The importance of discovery new therapeutic targets is dictated by the frequent appearance/ emergence of resistance, in cancer cells, to the pro-apoptotic chemotherapeutic agents. Chemoresistance represents one of the major causes of cancer therapy failure (Longley and Johnston, 2005).

A promising therapeutic target is the UPS, including some of its components, such as the class of isopeptidases, known as DUBs. These enzymes are interesting targets since their inhibition can trigger different death pathways including a peculiar necrotic response in apoptosis-resistant cancer cells (Fontanini et al., 2009). Moreover, during this thesis we have demonstrated that G5, a N-SII, can react with exposed cysteines present in additional proteins not limited to the catalytic site of isopeptidases (Ciotti et al., 2018).

G5-treatment promotes the proteasome blockage and the accumulation of poly-ubiquitinated proteins (Aleo et al., 2006), which in turn determine a strong proteotoxic stress followed by a peculiar necrotic pathway, as confirmed through the work performed in this thesis (Tomasella et al. 2016). Beside the induction of proteotoxic stress, the molecular elements of the necrotic pathway elicited by G5 are still undefined.

The final aim of this thesis was to better dissect the necrotic mechanism induced by this drug, by identifying the critical genes required for the process. To this aim, genome editing approaches, such as the CRISPR-Cas9 system and the RNA interference, were used in a glioblastoma cell line.

The unbiased screening of the DECIPHER library, composed by 27500 shRNAs directed against 5000 signaling-involved genes, revealed that the Ser/Thr kinase GSK3β could play a role in the G5-elicited death pathway.

Since GSK3β acts on more than 100 known substrates, it is considered one of the busiest kinase in most of the cells (Sutherland, 2011). GSK3β is an unconventional kinase because it shows some peculiar characteristics. It is constitutively active. Hence, environmental signals trigger its inhibition rather than its activation. Second its substrates have to be phosphorylated at the fourth amino acid at the C-terminal end of GSK3β consensus site to allow the GSK3β

action. The concept of primed substrates (Fiol et al., 1987). This cooperation process, between the pre-phosphorylation of the specific substrate by different up-stream kinases and the following binding by GSK3β, consents signaling integration from different pathways (Grimes and Jope, 2001). In fact, although GSK3β has been originally identified as an important regulator of glycogen metabolism (Embi et al., 1980), its contribution to different cellular processes, including: cell proliferation, gene expression, cellular morphology, neural development and plasticity, cell survival and cell death, is well established (Cohen and Frame, 2001; Frame and Cohen, 2001; Doble and Woodgett, 2003; Jope and Johnson, 2004). Not surprisingly, GSK3β is also involved in a wide number of diseases, such as in the bipolar depression, Parkinson's disease, Alzheimer's disease, cardiovascular diseases, diabetes, inflammatory dysfunctions and cancer (Gao et al., 2012; Forlenza et al., 2012; Amar et al., 2011).

In the context of tumor, GSK3β has raised interest as a potential therapeutic target in different types of cancer. However, this possibility was complicated by the recent findings about controversial roles of GSK3β as tumor promoter or tumor suppressor in a context-dependent manner (McCubrey, 2014).

GSK3β can act as a tumor suppressor modulating the phosphorylation of β-catenin and its subsequent proteasome-dependent degradation (Polakis, 2007). This activity has been well demonstrated in skin and breast cancers, in which the GSK3β inhibition promotes proliferation and tumorigenesis through the β-catenin stabilization (Leis et al., 2002; Farago et al., 2005; Armanious et al., 2010). On the contrary, a role for GSK3β as tumor promoter has been described in colon, pancreatic cancers, liver and ovarian cancers. In these contexts GSK3β is highly expressed and a correlation between its inhibition and anti-proliferative effects was described (Shakoori et al., 2005; Ougolkov et al., 2005; Zhou et al., 2012; Luo et al., 2009). In these type of tumors, which exhibit a pathological GSK3β over-expression, the kinase could be seen as a promising therapeutic target. Currently, more than 50 GSK3β inhibitors have been described and some of them are under clinical investigations not limited to cancer (Ougolkov and Billadeau, 2008; McCubrey, 2014).

In the glioblastoma model, chosen for this thesis work, some findings suggest a pro-survival role for GSK3β, since its chemical inhibition decreased the cellular proliferation (Furuta et al.,

2017) and promoted cell death by apoptosis (Kotliarova et al., 2008). Another study also revealed that GSK3β sustained the survival and proliferation of glioblastoma cells by counteracting apoptosis (Miyashita et al., 2009).

On the opposite, our data indicate that GSK3β plays a pro-death role in glioblastoma cells in response to treatment with specific necrotic stressors. The effects were less pronounced in the case of the N-SII G5, but they were prominent in DMNQ-treated cells. Thus, given that DMNQ is a mitochondrial ROS generator, GSK3β could be a key kinase in the transducing the death signals triggered by oxidative stress.

Our results suggest that GSK3β plays a minor role during G5-induced necrosis. We hypothesize that although G5 can induce some oxidative stress (Tomasella et al., 2016), the engagement of other stresses including protein misfolding (Tomasella et al., 2016; Chitta et al., 2015) renders the cells less dependent on GSK3β activities.

If this hypothesis holds true, GSK3β mainly controls the oxidative stress-induced necrosis and much less the proteotoxic-induced cell death. Alternatively, it is also possible that other kinases, in cooperation with GSK3β, act in controlling the G5-induced pathway. Hence, the only absence of GSK3β, in the GSK3β KO clone, it is not sufficient to completely abrogate the necrotic response to G5.

A contribution of GSK3β in oxidative-induced cell death was previously observed. An increased cellular survival following glutamate and hydrogen peroxide exposure was reported in the neuronal HT22 cells, when they were pharmacological inhibited for GSK3β (Schäfer et al., 2004). Another study described the GSK3β involvement in the ROS-mediated signals triggered by an array of redox stressors in the retinoblastoma mutated cells. The treatment with 4HPR (retinoid N-(4-hydroxyphenyl)retinamide), PEITC (phenylethyl isothiocyanate) and As_2O_3 (arsenic trioxide) affected the cell viability of Y79 cells, by inducing the inhibition of GSK3β. This inactivation favors the activities of survival pathways. An up-regulation of the anti-oxidant heme oxygenase (HO-1) and an augmentation in the glutathione (GSH) levels were reported. Furthermore, retinoblastoma and prostate cancer cells resistant to 4HPR were characterized by a sustained inhibition of GSK3β, HO-1 over-expression and high GSH levels, confirming the role of GSK3β in controlling cell death during acute oxidative stress (Venè et al., 2014).

Reports on a different cellular context, the DCLF-treated tubular epithelial cells, showed that the GSK3β inactivation was associated with sustained viability and the suppression of necrosis and apoptosis. DCFL (diclofenac) is a non-steroidal anti-inflammatory drug able to elicit oxidative stress. In response to this drug, the treated cells activated GSK3β and stimulated the opening of the mitochondrial permeability transition (MPT) pore. This event seemed positively controlled by cyclophilin D, which promotes the MPT pore opening. Cyclophilin D was phosphorylated by GSK3β on two amino acid residues: Ser118 and Ser190. Hence, the DCFL-induced GSK3β activation could determine cell death by triggering the opening of the MPT pores. The same cells treated by TDZD-8 and DCLF, an inhibitor of GSK3β, were characterized by attenuated swelling of mitochondria, MPT suppression, and reduced cell death (Bao et al., 2012).

The involvement of GSK3β in the oxidative stress-induced necrosis is further strengthened by the observation that this kinase is promptly activated in response to DMNQ, as monitored by Serine-9 dephosphorylation in its inhibitory N-terminal domain. It occurs within 1 hour to reach the full activation after 3 hours. Concomitantly, we observed an inactivation of Akt, which is one of the most relevant up-stream kinase able to inhibit GSK3β (Cross et al., 1995; Alessi and Cohen, 1998). This event could permit to GSK3β to be activated by a specific phosphatase such as PP1 (Szatmari et al., 2005) in response to the oxidative stress, which in turn, dephosphorylating the Ser9, leading to its activation. Interestingly, in our shRNA screening among genes, which down-regulation favors survival in response to G5, the protein phosphatase 1 regulatory subunit 3A was found.

The re-activation of Akt 6 hours later determines the GSK3β inhibition. Later from the DMNQ incubation, necrosis appears. This means that in this time interval GSK3β activates or inactive different substrates, so the outcome of cell death is not directly mediated by GSK3β, but by its substrates. It seemed that once GSK3β defines the cell fate, it can be inactivated. Alternatively, the inhibition of GSK3β could be manifested by cells that resisted to the oxidative crisis and survive.

Regarding the phosphorylation status of Akt Ser473, it did not show a phosphorylation pattern as the Akt T308. Several studies showed that the Akt full activation depends on these two

critical residues, but a partial activation can be achieved by only the phosphorylation of T308 (Alessi and Cohen, 1998; Alessi et al., 1996).

In contrast to our results, a previous study showed that Akt is activated and phosphorylated on both T308 and S473 in an early and transient manner during the incubation with hydrogen peroxide in Jurkat cells, thus inactivating GSK3β (LaHair et al., 2006). These data are in line with the results obtained also in different cellular contexts (Huang et al., 2001; Howe et al., 2002). They further reported that, the phosphorylation of Akt, and consequently GSK3β inactivation in response to the oxidative stress, plays an anti-apoptotic role, sustaining the cellular survival. Most probably, Akt inactivation and GSK3β activation, that we detected upon DMNQ exposure, could explain the role of the Akt/GSK3β axis in controlling the life/ death balance.

An opposite response of Akt was reveled in the G5-treated cells. Here a strong phosphorylation of the T308 appeared in response to G5, as previously noted (Tomasella et., 2014). The differences in Akt activation and in parallel the partial contribution of GSK3β to G5-induced cell death can explain the different behavior of U87MG/GSK3β KO clone to the two treatments.

Generally, an enhanced oxidative stress can impair the mitochondrial state, influencing cell survival. Mitochondria can be considered as an important source of intracellular ROS producing cellular superoxide anion (O_{2-}) and hydrogen peroxide (H_2O_2), and, concomitantly, them-self are a direct targets of the damaging effects of the produced ROS (Griendling and FitzGerald 2003). In this context, mitochondria undergo to evident fragmentation in response to oxidative stress (Wu et al., 2011; Iqbal and Hood, 2014).

Regarding the mitochondria morphology, it was observed that they underwent fragmentation in response to the DMNQ treatment (Tomasella et al., 2014). We observed that this response is GSK3β-independent. By contrast, we showed that mitochondrial integrity and functionality is strongly dependent on GSK3β.

Specifically, it is well know that the oxidative phosphorylation is ensured by complexes I to II, III and IV, which drives the proton translocation across the inner membrane to the intermembrane space, forming a proton gradient measured as mitochondrial membrane potential ($\Delta\psi_m$) (Duchen and Surin et al. 2003; Chen, 1988). This gradient maintains all

cellular functions, by driving the production of ATP by complex V (ATP synthetase). The preservation of the mitochondrial membrane potential represents a vital parameter for the cell. Its complete lost or collapse in the majority of mitochondria within a cell can be considered a point of no-return from cell death (Green and Amarante-Mendes, 1998; Ichim et al., 2015). The collapse of $\Delta\psi_m$, after the treatment with DMNQ is suppressed in absence of GSK3β activity.

Curiously, in DMNQ-treated cells, some GSK3β translocates into the nucleus before the collapse of mitochondrial potential. GSK3β can translocate in the nucleus thanks to its bipartite nuclear localization sequence (NLS), which is normally hidden when GSK3β is complexed with interacting proteins in the cytosol. In a stimuli-dependent manner, GSK3β dissociates and the NLS drives the kinase into the nucleus. A previous study reported the nuclear moving of this kinase in the TNF-treated HeLa cells. They demonstrated that an anti-apoptotic role of GSK3β seems to be exercised by the cytosolic form (Meares and Jope, 2007). Another report described the GSK3β translocation as a consequence of different apoptotic stimuli, but independently from its Ser9 and Tyr216 phosphorylation status (Bijur and Jope, 2001). Interestingly, in a complete different context, the murine embryonic stem cells (mESCs), GSK3β was able to shuttle from the cytoplasm into the nucleus. Once Akt was activated, it promoted the cytosolic accumulation of GSK3β, its phosphorylation and inactivation. This means that activated GSK3β works in the nucleus and mediates the differentiation signal (Bechard and Dalton, 2009).

In our case, the nuclear translocation of GSK3β occurs at a later step after DMNQ treatment. Further studies will be necessary to reveal the mechanisms controlling GSK3β translocation.

Moreover, because the limited definition of the time-lapse analysis in vivo, a partial re-localization of GSK3β at mitochondrial level, as described by Chiara et al., cannot be excluded (Chiara et al., 2012).

In the literature it has been described the capability of GSK3β to exert some effects on gene expression, indirectly, by affecting several transcription factors and, directly, by modifying epigenetic mechanisms. Among the transcription factors known as GSK3β substrates, there are Fos/Jun AP-1, heat shock factor 1, myc, NF-kB, p53, STAT3, as well as many others (Grimes and Jope, 2001; Jope and Johnson, 2004). Regarding the involvement of GSK3β in

the epigenetic regulation, some evidences reported that GSK3β contributes to the regulation of some important histone modification, as the phosphorylation of histone 1.5 (Happel et al., 2009) and histone 3 (Zhou et al., 2016). Moreover, this kinase can also act on the histone deacetylases (HDACs), by modulating the activity of HDAC3, and the degradation of HDAC4 (Bardai and D'Mello, 2011; Cernotta et al., 2011). A better investigation of the nuclear function played by GSK3β in the DMNQ response is necessary to understand in which way the cell death is carried out.

To conclude, since the DMNQ has not a clinical use, the acknowledgment about the role of GSK3β in the oxidative stress response could be useful for those therapies in which the oxidative stress played a central role, as in the case of Photodynamic Therapy (PDT). PDT is able to induce oxidative stress using a photosensitizer and the correct light based on the absorption and emission spectra of the photosensitizer (Gomer et al. 1996). The PDT is under studies for several types of cancers and it could be possible to study the behavior of the U87MG/GSK3β KO cells in response to this type of treatment. If in the absence of the kinase, the cells are resistant to this type of treatment, the GSK3β expression in the cancer cells can be seen as a predictive factor of the therapeutic outcome.

In addition GSK3β and oxidative stress seems to be involved in neurodegenerative disorders, including Alzheimer's disease and Parkinson's disease (Behl, 1997; Behl et al., 1997; Butterfield and Kanski, 2001; Halliwell, 2001; Jenner and Olanow, 1996; Moosmann and Behl, 2002). The central nervous system is an important target for this type of stress, mainly due to its consistent oxygen turnover. This could be the reason for which the oxidative stress can be considered as the cause of these pathologies. Since they are characterized by the lost of neural cells, signaling pathways able to protect these cells from the death induced by an excessive production of ROS are of interest. Working on GSK3β and its inactivation may provide a promising therapy for the prevention and treatment of these oxidative stress and aging-associated neurodegenerative diseases.

5. Materials & Methods

5.1 Cell culture conditions and reagents

The Human glioblastoma cell line Uppsala 87 Malignant Glioma (U87MG), the Human Embryonic Kidney cells 293 T1 (HEK293T1) and the Phoenix Amphotropic (AMPHO) were maintained at 37°C in 5% CO_2 atmosphere in Dulbecco's Modified Eagle's Medium (DMEM, Sigma-Aldrich) supplemented with 10% Fetal Bovine Serum (FBS; Euroclone), glutamine (2 mmol/L, Lonza), penicillin (100 U/mL) and streptomycin (100 μg/mL). The following chemicals agent were used: 4H-thiopyran-4-one, tetrahydro-3,5-bis[(4-nitrophenyl) methylene]-1,1-dioxide (G5; Aleo et al., 2006), 2,3-dimethoxy-1,4-naphthoquinone (DMNQ; Sigma Aldrich), Propidium Iodide (PI; Sigma Aldrich), DMSO (Sigma Aldrich), Tetramethyl Rhodamine Methyl-ester (TMRM, Scorrano et al., 1999), Bortezomib (LC Laboratories), TNF-related apoptosis-inducing ligand (TRAIL, Sgorbissa et al., 2011), carbonilcyanide *p*-triflouromethoxyphenylhydrazone (FCCP, Sigma Aldrich).

5.2 shRNA library: production, application and "hits" selection

The DECIPHER™ shRNA lentiviral Human Module 1 (HM1) library (Cellecta Inc.) was provided by the DECIPHER Open Source RNAi Screening Project (http://www.decipherproject.net/). The DECIPHER™ HM1 library was composed of 27500 shRNA sequences targeting 5,043 genes (5–6 shRNAs/mRNA). Among the targeted genes, members of major canonical and non-canonical signaling pathways were represented. Each shRNA was tagged with an unique 18 nucleotide sequence termed "barcode", which permits the final identification after the Illumina Next-Generation Sequencing (NGS). The HTS3 (DECIPHER pRSI9-U6-(sh)-HTS3-UbiC-TagRFP-2A-Puro-dW) cassette of each shRNA contained the following elements: (i) U6 RNA polymerase III promoter, necessary to drive the shRNA expression, (ii) the specific and unique 18-nucleotide DNA barcode sequence, (iii) UbiC promoter responsible of red fluorescence protein (RFP) expression into the infected cells, (iv) the puromycin selection gene, and v) three different set of primers, two for the final barcode-amplification PCR and one for the sub-sequential DNA sequencing.

Lentiviral packaging was performed following manufacturer instructions (Cellecta Inc.). The HEK293T1 packaging cells were transfected with a solution given by 60 μg of the shRNA library and 300 μg of the packaging plasmid mix (psPAX2 and pMD2.G; Cellecta Inc.) in DMEM without serum or antibiotics, in the presence of Plus Reagent™ and Lipofectamin™ (Life Technologies). HEK293T1 cells were incubated with this mix solution for 24 h. Viral

supernatant was collected at 48 h and 72 h after transfection, filtered through a 0.45 μm filter and concentrated using LentiFuge™ (Cellecta Inc.) following the manufacturer's protocol. The concentrated lentiviral particles were re-suspended in 3 ml of PBS/10% FBS and stored at −80 °C. For the lentiviral titer estimation, the U87MG cells were seeded in a 12-well plate and, they were infected with 15 μl of thawed solution containing the lentivirus. After 24 hours, these cells were harvested and the RFP positivity (corresponding to the infected $shRNA^+$ RFP^+ cells) was measured by fluorescence-activated cell sorting (FACS; Beckman Dickinson). Using a table providing by Cellecta, it was possible to calculate the Transduction Units of the solution containing the viral particles (TU/ml). One TU corresponds to one integration event in the target cells.
Thus, using the following formula:

$$\text{TU/ml} = (\#\ of\ cells\ at\ Transduction) * [\ \text{MOI} / (ml\ of\ Viral\ Stock\ used\ at\ Transduction)\ ]$$

the calculated TU/ml was 440000 TU/ml.

Considering the obtained TU/ml, the MOI of 0,1, and the number of U87MG cells to infect, the volume of the viral stock to use for the infection was calculated by using the previous formula.
The number of U87MG cells to infect was chosen considering that it should exceeded the complexity of the library of at least 200 times. For a library with 27500 shRNAs, the starting population should be at least 5,5 million of cells. Regarding the multiplicity of infection (MOI), in a pooled shRNA screen, the starting number of cells should be 2-3 times more than the infecting viral particles to ensure that ~90% of the cells are infected with one shRNA-carrying virus. For all these reasons, 33 millions of U87MG cells were seeded. After the infection with the calculated viral volume, which was carried on for 48 hours, the $shRNA^+$ U87MG cells were selected by adding Puromycin (2 μg/ml) at 37 °C for 72 hours. Later, the selected cells were treated with G5 (2,5 μM) for 60 hours. Genomic DNA (gDNA) was purified from the surviving cells using the QIAamp DNA Micro Kit (Qiagen) following the manufacturer's instructions. Pooled barcodes were PCR-amplified starting from 100 μg of gDNA and they were identified by Illumina High-throughput (HT) sequencing. The conversion of raw sequencing data into summary files, that include annotation for each identified gene and the sequence frequencies, was performed using the barcode deconvoluter software (Cellecta Inc.). The target proteins, of whom at least two different shRNAs were represented by higher frequencies in comparison to the control luciferase shRNA frequencies, were defined "Hits" ($N_{shRNAs} \geq 2$).

5.3 RNA interference

The RNA interference (RNAi) was performed using the following siRNAs direct against:
- Calpain-1 (CAPN1) (Santa Cruz Biotechnology);

- PP2AC (Fw 5'-GCAAGAGGUUCGAUGUCCAGUUACU-3', Rv 5'-AGUAACUGGACA UCGAACCUCUUGC - 3', Invitrogen);
- GSK3β (Fw 5'-GCAUUUAUCGUUAACCUAA-3', Rv 5'-UUAGGUUAACGAUA AAUGC - 3', Sigma Aldrich);
- control siRNA (Fw 5'-UAAGGCUAUGAAGAGAUAC-3', 5'- GUAUCUCUUCAUA GCCUUA - 3' (Sigma Aldrich).

U87MG and U87MG BCLXL cells were transfected 24 hours after the seeding in Opti-MEM medium without antibiotics and containing Lipofectamine (Invitrogen) plus siRNAs (75nM). After 6 hours the medium was changed, and after 48 hours of silencing, the cells were treated with G5 or DMNQ for further 24 hours. In parallel, the RNA was extracted and the protein lysates were collected. As last step, the FACS analysis was performed on the down-regulated and treated cells.

5.4 PI- and TMRM- assays

For cytofluorimetric analysis, the cells were treated, one day after the seeding, with different concentrations of G5 (2.5 μM, 5 μM or 10 μM) or DMNQ (20 μM or 30 μM). DMSO was used for the untreated cells. Upon 24 hours of treatment, the cell death was measured adding PI (10 μg/ml) to the dead and living cells, which were resuspended in 200 μl of Phosphate-Buffered Saline (PBS) for 5 minutes at room temperature. PI fluorescence was determined by FACS. Before to be analyzed, the untreated and treated cells were imaged with Leica DMi1 microscope (10x objective).

Data were represented as arithmetic mean of PI positivity percentage ± SD.

For TMRM assay used to follow the $\Delta\psi_m$, the cells were firstly DMNQ-treated (30 μM) for 24 hours and they were incubated with TMRM (1 μM) for 30 minutes at 37 °C in 5% CO_2 atmosphere. FCCP (10 μM) was used to promote the mitochondrial membrane potential collapse and it was added 5 minutes before the TMRM fluorescence measure by FACS. Data were represented as arithmetic mean of TMRM positivity percentage ± SD.

5.5 Cell lysis and Western Blotting

The cellular lysis was performed using an SDS denaturing lysis solution, in which the Protease Inhibitor Cocktail (PIC), PhenylMethane Sulfonyl Fluoride (PMSF), Na_3VO_4 and β-mercaptoethanol were added. The protein lysates were sonicated for 5 minutes at 4°C and they were boiled for 5 minutes. The denaturated proteins were loaded into a Sodium Dodecyl Sulfate (SDS) polyacrylamide gel to perform the electrophoresis. After the run, the proteins were transferred from the gel to a 0.2 μm-pore-sized nitrocellulose membrane. The aspecific sites of the membrane were blocked through the incubation with Milk 5% (Delikat Gramm), TrisHCl pH 7,5 1M, NaCl 5M, and Tween-20 (Riedel De-Haen) for 1 hour at room

temperature. Then the membranes were incubated with the specific primary antibodies for 4 hours at room temperature or overnight at 4°C. The used primary antibodies were anti-CAPN1 (1:1000; Santa Cruz Biotechnology), anti-PP2Ac (1:2000; Upstate, Lake Placid, NY), anti-actin (1:4000; Sigma Aldrich), anti-GSK3β (1:3000; Santa Cruz Biotechnology), anti-p-GSK3β S9 (1:1000; Cell Signaling), anti-p-Akt T308, anti-p-Akt S473, anti-Akt (1:1000, 1:3000, 1:1000; Cell Signaling), anti-Smac (1:2000; Henderson et al., 2005), anti-Casp2 (1:3000; Foti et al., 2009), anti-HDAC4 (1:1000; Paroni et al., 2004), anti-tubulin (1:3000; Paroni et al., 2001). The same membranes were incubated with the horseradish peroxidase (HRP)-conjugated secondary antibody for 1 hour at room temperature. The used secondary antibodies were goat anti-mouse (Sigma Aldrich) or goat anti-rabbit (Sigma Aldrich). Finally, the blots were developed using Super Signal West Dura as recommended by the vendor (Pierce), impressing the signal on the photographic film through the produced chemiluminescence reaction.

5.6 RNA extraction and qRT-PCR

For the RNA extraction, the TRIzol (Molecular Research Center) was added to the cells. Then, the chloroform was added to the samples to separate the RNA from the DNA and proteins. The obtained RNA was precipitated using the isopropanol, and it was washed two times with ethanol 75% and resuspended in sterile water. The retro-transcription PCR (RT-PCR) of 1 μg of extracted RNA was performed using a mix composed by First Strand Buffer (Invitrogen), dithiotreitol (DTT; 0,1 M; Invitrogen), dNTP Mix (2,5 mM; Thermo Scientific), oligo dT (20 μM; Eurofins Genomics), random primers (Promega), Rnase OUT Recombinant Ribonuclease inhibitor (30 U/μl; Invitrogen), and the Moloney murine leukemia virus reverse transcriptase (M-MLV; 200 U/μl; Invitrogen). The obtained cDNAs were analyzed by Quantitative Real Time PCR (qRT-PCR) using the SYBR Green technology (KAPA Biosystems). The studied genes were: Glyceraldehyde 3-phosphate dehydrogenase (GAPDH), Hypoxanthine-guanine phosphoribosyltransferase (HPRT) and GSK3β. The obtained data were analyzed using the ΔΔCt method, considering HPRT and GAPDH as normalizer genes. All the reactions were performed in triplicate.

5.7 Generation of GSK3β knock-out clone

The generation of U87MG Knock-Out cells for GSK3β (termed GSK3β KO or GSK3β$^{-/-}$) was achieved using the CRISPR/Cas9 technology. In particular, the single guide RNA (sgRNA) was designed using the bioinformatic tool “CRISPR design” (http://crispr.mit.edu/) and the sequence was the following:
5’ - CCTTTGCGGAGAGCTGCAAG - 3’.

Firstly, this sgRNA was cloned into the lentiviral pLENTIV2 plasmid which contains the sequence of Cas9 wt, then the obtained plasmid was introduced in the U87MG cells through lentiviral infection. Specifically, the HEK293T1 packaging cells were transfected with the pLENTIV2-sgRNA-Cas9 wt, together with the Δ8.9 and VSV-G packaging plasmids, through the calcium phosphate method. The transfected cells were incubated for 48 hours at 37°C. After, the viral particles present in the supernatant were collected, diluted 1:1 with fresh medium, added with polybrene (8 μg/ml), filtered through 45 μm filters and used to infect U87MG cells. Later 24 hours at 37°C, the virus was removed and the infected cells were selected using the specific antibiotic (Puromycin 2 μg/ml). The selected U87MG cells were seeded 1 cell/well in 96-wells plates to promote the monoclonal growth of each cell. After 20 days, the grown clones were screened through Western Blot. The found putative KO clone was further validated by Sanger sequencing. A screened clone resulted wt for GSK3β was used as control. The same protocol was followed to infect the U87MG cells with the empty pLENTIV2 plasmid expressing only Cas9 wt but not the sgRNA, in order to have an additional control clone.

5.8 Cloning of GSK3β WT and KM

To generate the U87MG cells expressing the two variants of GSK3β, the wild-type (WT) and the kinase-mutant (KM), the respective sequences were firstly cloned into pEGFP-N1 plasmid in order to add to the GSK3β sequence the Green Fluorescence Protein (GFP) tag at the C-terminus end. Through a second step of cloning, the two sequences GSK3β WT-GFP and GSK3β KM-GFP were cloned into the retroviral plasmid pWZL-Neo.

The coding sequence of GSK3β was amplified by PCR, using the following primers (Sigma):

- AGATCTATGTCAGGGCGGCCCAG, as forward primer with in addition the restriction site for BglII;
- GAATTCTGGTGGAGTTGGAAGCTGATG, as reverse primer with in addition the restriction site for EcoRI.

The PCR products were ran on 1% agarose gel electrophoresis and the DNA molecules were extracted from the gel through the QIAquick Gel Extraction Kit (Qiagen). The used gels were produced in Tris-Acetate-EDTA (TAE) buffer 1X and the ethidium bromide was added in order to visualize the DNA. The extracted DNA was digested with the restriction enzymes BglII (Thermo Scientific) and EcoRI (Thermo Scientific) for 40 minutes at 37°C. The pEGFP-N1 plasmid was digested with the same restriction enzymes. The digested DNA fragments were ligated with the digested plasmid pEGFP-N1 in a ratio 3:1 by using the T4 DNA Ligase (Thermo Scientific) and its specific 10x T4 DNA Ligase Buffer (Thermo Scientific) for 20 minutes at 24°C. Subsequently, STBL3 bacteria cells were transformed, plated onto Lysogeny Broth (LB)-agar plates and incubated overnight at 37°C. The grown colonies were picked from the plates, and incubated with LB overnight at 37°C. The day after,

the bacteria were harvested and the pEGFP-N1 plasmids were extracted using the Plasmid Plus Midi Kit (Qiagen), following the manufacturer's instructions. After the control of the cloning, the same steps were repeated to clone the GSK3β WT-GFP and GSK3β KM-GFP into the retroviral plasmid pWZL-Neo. Therefore, the two sequences GSK3β-WT and GSK3β-KM from the pEGFP-N1 plasmids were amplified by PCR using the following primers (Sigma):

- AGATCTATGTCAGGGCGGCCCAG as forward primer with in addition the restriction site for BglII;
- CTCGAGTTACTTGTACAGCTCGTCC as reverse primer with in addition the restriction site for XhoI.

Repeating the steps of extraction from the gel, digestion, and ligation, the GSK3β WT-GFP and GSK3β KM-GFP sequences were cloned into pWZL-Neo plasmids, which were used to transform STBL3 bacteria cells. These GSK3β-WT and GSK3β-KM constructs were used to perform the retroviral infection of the U87MG cells.

5.9 Transfection and retroviral infection

U87MG cells expressing BCL-XL, GSK3β-WT-GFP or KM-GFP constructs were generated by retroviral infection. Briefly, retroviral vectors were transfected in the AMPHO cells through the calcium phosphate method. After 48 hours, the viral supernatants were collected, filtered, supplemented with 8 μg/ml Polybrene, and combined with fresh medium in a ratio of 1:1 in order to infect U87MG cells. The infection was maintained for 48 hours at 32°C and the selection with the specific antibiotic was applied: G418 (1000 μg/ml) for the selection of GSK3β WT-GFP and GSK3β KM-GFP expressing cells and Hygromycin (200 μg/ml) for the selection of BCL-XL expressing cells.

The control cells were obtained infecting the U87MG cells with the two empty pWZL-Hygro and pWZL-Neo plasmids.

5.10 Immunofluorescence

U87MG/GSK3$\beta^{+/+}$ and GSK3$\beta^{-/-}$ cells were fixed with 3% paraformaldehyde (PFA) and permeabilized with 0.5 % Triton X-100. The primary antibody was anti-Smac (Henderson et al., 2005), and the secondary antibody Alexa Fluor 546-conjugated anti-rabbit (Molecular Probes). Cells were imaged with a Leica confocal microscopy SP equipped with a 488 λ Ar laser and a 543 to 633 λ HeNe laser.

5.11 Time-lapse confocal fluorescence microscopy

U87MG/GSK3$\beta^{-/-}$ re-expressing GSK3β WT-GFP cells were seeded 200000 cells/glass-bottom dish 35 mm and, the day after, they were incubated with the $\Delta\psi_m$-sensitive dye TMRM (20 μM; Henderson et al. 2005) and with DMNQ (30 μM). After 1 hour of treatment,

the time-lapse analysis was performed. The imaging of the fluorescence relative to the GSK3β-GFP and TMRM was evaluated every 5 minutes for 24 hours using the time-lapse imaging system (Leica). The image analysis was obtained using the Leica Acquired Software X (LASX). For the $\Delta\psi_m$ analysis, the fluorescence of the mitochondria was evaluated drawing a region around the cell (Region Of Interest; ROI) and measuring the Mean fluorescence Intensity of TMRM ($MI_{TMRMcell}$). The fluorescence of the background (BK_{TMRM}), which is another ROI located in a non-fluorescent region, was subtracted to the $MI_{TMRMcell}$ and the obtained data was multiplied for the area of the cell ($Area_{cell}$), according to the following equation:

$$TMRM\ fluorescence\ (\%) = (MI_{TMRMcell} - BK_{TMRM}) * Area_{cell}$$

The same steps were followed for the untreated cells, which were not incubated with the DMNQ, but only with the TMRM. A similar calculation was used to quantify the increase of nuclear GSK3β-GFP fluorescence, according to the following formula:

$$Nuclear\ GSK3\beta\text{-}GFP = (MI_{GSK3\beta\text{-}GFPnucl} - BK_{GSK3\beta\text{-}GFP}) * Area_{nucl} / (MI_{GSK3\beta\text{-}GFPcytosol} - BK_{GSK3\beta\text{-}GFPcytosol}) * Area_{cytosol}$$

5.12 Statistics

Results were expressed as means ± standard deviations (SD) from at least three independent experiments. Statistical analysis was performed using the Student's t-test of Excel software and p values represented as: * $p < 0.05$; ** $p < 0.01$; *** $p < 0.005$.

6. Publications

1. **Cell Death and Disease**. 2018 Feb 7;9(2):184.
doi: 10.1038/s41419-017-0259-1.

The binding landscape of a partially-selective isopeptidase inhibitor with potent pro-death activity, based on the bis(arylidene)cyclohexanone scaffold.

Ciotti S, Sgarra R, Sgorbissa A, Penzo C, Tomasella A, Casarsa F, Benedetti F, Berti F, Manfioletti G, Brancolini C.

2. **Oncotarget.** 2016 Jul 19;7(29):45429-45443.
doi: 10.18632/oncotarget.9742.

The isopeptidase inhibitor 2cPE triggers proteotoxic stress and ATM activation in chronic lymphocytic leukemia cells.

Tomasella A, Picco R, Ciotti S, Sgorbissa A, Bianchi E, Manfredini R, Benedetti F, Trimarco V, Frezzato F, Trentin L, Semenzato G, Delia D, Brancolini C.

7. Bibliography

Adams J. *The proteasome: structure, function, and role in the cell*. Cancer Treat Rev, May;29 Suppl1: 3-9 (2003);

Adams J. *The development of proteasome inhibitors as anticancer drugs.* Cancer Cell, May;5(5): 417-21 (2004);

Adams J, Palombella VJ, Sausville EA, Johnson J, Destree A, Lazarus DD, Maas J, Pien CS, Prakash S and Elliott PJ. *Proteasome inhibitors: a novel class of potent and effective antitumor agents.* Cancer Res, Jun 1;59(11): 2615-22 (1999);

Aleo E, Henderson CJ, Fontanini A, Solazzo B and Brancolini C. *Identification of new compounds that trigger apoptosome-independent caspase activation and apoptosis*. Cancer Res, Sep 15;66(18): 9235-44 (2006);

Alessi DR, Andjelkovic M, Caudwell B, Cron P, Morrice N, Cohen P, et al. *Mechanism of activation of protein kinase B by insulin and IGF-1*. EMBO J, 15: 6541-6551 (1996);

Alessi DR and Cohen P. *Mechanism of activation and function of protein kinase B*. Curr Opin Genet Dev, 8: 55–62, (1998);

Alessi DR, Andjelkovic M, Caudwell B, Cron P, Morrice N, Cohen P, et al. *Mechanism of activation of protein kinase B by insulin and IGF-1*. EMBO J, 15: 6541-6551 (1996);

Almond JB and Cohen GM. The proteasome: a novel target for cancer chemotherapy. Leukemia, Apr;16(4): 433-43 (2002);

Amar S, Belmaker RH and Agam G. *The possible involvement of glycogen synthase kinase-3 (GSK-3) in diabetes, cancer and central nervous system diseases.* Current Pharmaceutical Design, 17: 2264-2277 (2011);

Arastu-Kapur S, Anderl JL, Kraus M, Parlati F, Shenk KD, Lee SJ, Muchamuel T, Bennett MK, Driessen C, Ball AJ and Kirk CJ. *Nonproteasomal targets of the proteasome inhibitors bortezomib and carfilzomib: a link to clinical adverse events.* Clin Cancer Res, May 1;17(9): 2734-43 (2011);

Armanious H, Deschenes J, Gelebart P, Ghosh S, Mackey J and Lai R. *Clinical and biological significance of GSK-3β inactivation in breast cancer-an immunohistochemical study.* Hum Pathol, Dec;41(12): 1657-63 (2010);

Atkins RJ, Stylli SS, Luwor RB, Kaye AH and Hovens CM. *Glycogen synthase kinase-3β (GSK-3β) and its dysregulation in glioblastoma multiforme.* J Clin Neurosci, Sep;20(9): 1185-92 (2013);

Bao H, Ge Y, Zhuang S, Dworkin LD, Liu Z and Gong R. *Inhibition of glycogen synthase kinase-3β prevents NSAID-induced acute kidney injury.* Kidney Int, 81: 662-673 (2012);

Bardai FH and D'Mello SR. *Selective toxicity by HDAC3 in neurons: regulation by Akt and GSK3beta.* J Neurosci, Feb 2;31(5): 1746-51 (2011);

Bechard M and Dalton S. *Subcellular localization of glycogen synthase kinase 3beta controls embryonic stem cell self-renewal.* Mol Cell Biol, Apr;29(8): 2092-104 (2009);

Behl C. *Amyloid beta-protein toxicity and oxidative stress in Alzheimer's disease.* Cell Tissue Res, 290: 471-480 (1997);

Behl C, Skutella T, Lezoualc'h F, Post A, Widmann M, Newton C and Holsboer F. *Neuroprotection against oxidative stress by estrogens: structure–activity relationship.* Mol Pharmacol. 51: 535-541 (1997);

Belizário J, Vieira-Cordeiro L and Enns S. *Necroptotic Cell Death Signaling and Execution Pathway: Lessons from Knockout Mice.* Mediators Inflamm, 2015: 128076 (2015);

Berghe TV, Linkermann A, Jouan-Lanhouet S, Walczak H and Vandenabeele P. *Regulated necrosis: the expanding network of non-apoptotic cell death pathways.* Nature Reviews Molecular Cell Biology**,** 15: 135-147 (2014);

Beurel E and Jope RS. *The paradoxical pro- and anti-apoptotic actions of GSK3 in the intrinsic and extrinsic apoptosis signaling pathways.* Prog Neurobiology, 79: 173-189 (2006);

Bijur GN and Jope RS. *Dynamic regulation of mitochondrial Akt and GSK3β.* J Neurochem, 87: 1427-1435 (2003);

Bijur GN and Jope RS. *Proapoptotic Stimuli Induce Nuclear Accumulation of Glycogen Synthase Kinase-3β.* The Journal of Biological Chemistry, 276: 37436-37442 (2001);

Brancolini C. *Inhibitors of the Ubiquitin-Proteasome System and the cell death machinery: How many pathways are activated?* Curr Mol Pharmacol, Jan;1(1): 24-37 (2008);

Buac D, Shen M, Schmitt S, Kona FR, Deshmukh R, Zhang Z, Neslund-Dudas C, Mitra B and Dou QP. *From bortezomib to other inhibitors of the proteasome and beyond*. Curr Pharm Des, 19(22): 4025-38 (2013);

Buetow L and Huang DT. *Structural insights into the catalysis and regulation of E3 ubiquitin ligases.* Nat Rev Mol Cell Biol, Oct;17(10): 626-42 (2016);

Burgie ES, Craig A. Bingman CA, Soni AB and Phillips GN Jr. *Structural characterization of human Uch37*. Proteins, Feb; 80(2): 649–654 (2012);

Butterfield DA and Kanski J. *Brain protein oxidation in age-related neurodegenerative disorders that are associated with aggregated proteins.* Mech Ageing Dev, 1222: 945-962 (2001);

Cernotta N, Clocchiatti A, Florean C and Brancolini C. *Ubiquitin-dependent degradation of HDAC4, a new regulator of random cell motility.* Mol Biol Cell, Jan 15;22(2): 278-89 (2011);

Cersosimo U, Sgorbissa A, Foti C, Drioli S, Angelica R, Tomasella A, Picco R, Semrau MS, Storici P, Benedetti F, Berti F and Brancolini C. *Synthesis, characterization, and optimization for in vivo delivery of a nonselective isopeptidase inhibitor as new antineoplastic agent.* J Med Chem, Feb 26;58(4): 1691-704 (2015);

Chau V, Tobias JW, Bachmair A, Marriott D, Ecker DJ, Gonda DK and Varshavsky A. *A multiubiquitin chain is confined to specific lysine in a targeted short-lived protein.* Science Mar 24; 243(4898):1576-83 (1989);

Chen LB. *Mitochondrial membrane potential in living cells.* Annu Rev Cell Biol, 4: 155-81 (1988);

Chen X, Li W, Ren J, Huang D, He WT, Song Y, Yang C, Li W, Zheng X, Chen P and Han J. *Translocation of mixed lineage kinase domain-like protein to plasma membrane leads to necrotic cell death*. Cell Res, Jan;24(1): 105-21 (2014);

Cheng Y, Pardo M, Armini RS, Martinez A, Mouhsine H, Zagury JF, Jope RS and Beurel E. *Stress-induced neuroinflammation is mediated by GSK3-dependent TLR4 signaling that promotes susceptibility to depression-like behavior.* Brain Behav Immun, Mar;53: 207-222 (2016);

Chiara F, Gambalunga A, Sciacovelli M, Nicolli A, Ronconi L, Fregona D, Bernardi P, Rasola A and Trevisan A. *Chemotherapeutic induction of mitochondrial oxidative stress activates GSK-3α/β and Bax, leading to permeability transition pore opening and tumor cell death.* Cell Death Dis, Dec; 3(12): e444 (2012);

Chitta K, Paulus A, Akhtar S, Blake MK, Caulfield TR, Novak AJ, Ansell SM, Advani P, et al. *Targeted inhibition of the deubiquitinating enzymes, USP14 and UCHL5, induces proteotoxic stress and apoptosis in Waldenstrom macroglobulinaemia tumour cells.* Br J Haematol, 169: 377-90 (2015);

Ciechanover A. *Proteolysis: from the lysosome to ubiquitin and the proteasome.* Nat Rev Mol Cell Biol, Jan, 6(1):79-87 (2005);

Ciechanover A and Stanhill A. *The complexity of recognition of ubiquitinated substrates by the 26S proteasome.* Biochimica et Biophysica Acta, 1843: 86–96 (2014);

Clague MJ, Barsukov I, Coulson JM, Liu H, Rigden DJ and Urbé S. *Deubiquitylases from genes to organism.* Physiol Rev, Jul;93(3):1289-315 (2013);

Cohen P and Frame S. *The renaissance of GSK3.* Nat Rev Mol Cell Biol, 2: 769-776 (2001);

Cross DA, Alessi DR, Cohen P, Andjelkovich M and Hemmings BA. *Inhibition of glycogen synthase kinase-3 by insulin mediated by protein kinase B.* Nature, 378: 785-789 (1995);

D'Arcy P, Brnjic S, Olofsson MH, Fryknäs M, Lindsten K, De Cesare M, Perego P, Sadeghi B, Hassan M, Larsson R and Linder S. *Inhibition of proteasome deubiquitinating activity as a new cancer therapy.* Nat Med, Nov 6;17(12):1636-40 (2011);

Dai Y, Rahmani M and Grant S. *Proteasome inhibitors potentiate leukemic cell apoptosis induced by the cyclin-dependent kinase inhibitor flavopiridol through a SAPK/JNK- and NF-kappaB- dependent process.* Oncogene, 22, 7108-7122 (2003);

de Vries EG, Gietema JA and de Jong S. *Tumor necrosis factor-related apoptosis-inducing ligand pathway and its therapeutic implications.* Clin Cancer Res, Apr 15;12(8):2390-3 (2006);

de Wilt LH, Jansen G, Assaraf YG, van Meerloo J, Cloos J, Schimmer AD, Chan ET, Kirk CJ, Peters GJ and Kruyt FA. *Proteasome-based mechanisms of intrinsic and acquired bortezomib resistance in non-small cell lung cancer*. Biochem Pharmacol, Jan 15;83(2): 207-17 (2012);

Demarchi F and Brancolini C. *Altering protein turnover in tumor cells: new opportunities for anti-cancer therapies.* Drug Resist Updat, Dec;8(6): 359-68 (2005);

Dikic I, Wakatsuki S and Walters KJ. *Ubiquitin-binding domains - from structures to functions.* Nat Rev Mol Cell Biol, Oct; 10(10):659-71 (2009);

Doble BW and Woodgett JR. *GSK-3: tricks of the trade for a multi-tasking kinase.* J Cell Sci, 116: 1175–1186 (2003);

Dondelinger Y, Declercq W, Montessuit S, Roelandt R, Goncalves A, Bruggeman I, Hulpiau P, Weber K, Sehon CA, Marquis RW, Bertin J, Gough PJ, Savvides S, Martinou JC, Bertrand MJ and Vandenabeele P. *MLKL compromises plasma membrane integrity by binding to phosphatidylinositol phosphates.* Cell Rep, May 22,7(4): 971-81 (2014);

Dou QP and Zonder JA. *Overview of proteasome inhibitor-based anti-cancer therapies: perspective on bortezomib and second generation proteasome inhibitors versus future generation inhibitors of ubiquitin-proteasome system.* Curr Cancer Drug Targets, 14(6): 517-36 (2014);

Duchen MR, Surin A and Jacobson J. *Imaging mitochondrial function in intact cells.* Methods Enzymol, 361: 353-89 (2003);

Embi N, Rylatt DB and Cohen P. *Glycogen synthase kinase-3 from rabbit skeletal muscle. Separation from cyclic-AMP- dependent protein kinase and phosphorylase kinase*. Eur J Biochem, 107: 519-527 (1980);

Farago M, Dominguez I, Landesman-Bollag E, Xu X, Rosner A, Cardiff RD, Seldin DC. *Kinase-inactive glycogen synthase kinase 3beta promotes Wnt signaling and mammary tumorigenesis.* Cancer Res, Jul 1;65(13): 5792-801 (2005);

Felgueiras J and Fardilha M. *Phosphoprotein phosphatase 1-interacting proteins as therapeutic targets in prostate cancer.* World J Pharmacol, 9,3(4): 120-139 (2014);

Fernandez Y, Verhaegen M, Miller TP, Rush JL, Steiner P, Opipari AWJ, Lowe SW and Soengas MS. *Differential regulation of noxa in normal melanocytes and melanoma cells by proteasome inhibition: therapeutic implications.* Cancer Res*,* 65, 6294-6300 (2005);

Fiol CJ, Mahrenholz AM, Wang Y, Roeske RW and Roach PJ. *Formation of protein kinase recognition sites by covalent modification of the substrate. Molecular mechanism for the synergistic action of casein kinase II and glycogen synthase kinase 3*. J Biol Chem, 262: 14042–14048 (1987);

Fontanini A, Foti C, Potu H, Crivellato E, Maestro R, Bernardi P, Demarchi F and Brancolini C. *The Isopeptidase Inhibitor G5 Triggers a Caspase-independent Necrotic Death in Cells Resistant to Apoptosis: A COMPARATIVE STUDY WITH THE PROTEASOME INHIBITOR BORTEZOMIB.* J Biol Chem, Mar 27;284(13): 8369-81 (2009);

Forlenza OV, de Paula VJ, Machado-Vieira R, Diniz BS and Gattaz WF. *Does lithium prevent Alzheimer's disease?* Drugs & Aging, 29: 335-342 (2012);

Foti C, Florean C, Pezzutto A, Roncaglia P, Tomasella A, Gustincich S and Brancolini C. *Characterization of caspase-dependent and caspase-independent deaths in glioblastoma cells treated with inhibitors of the ubiquitin-proteasome system*. Mol Cancer Ther, Nov;8(11): 3140-50 (2009);

Frame S and Cohen P. *GSK3 takes centre stage more than 20 years after its discovery*. Biochem J, 359: 1-16 (2001);

Frame S, Cohen P and Biondi RM. *A Common Phosphate Binding Site Explains the Unique Substrate Specificity of GSK3 and Its Inactivation by Phosphorylation*. Molecular Cell, June, Vol7: 1321–1327 (2001);

Frankel A, Man S, Elliott P, Adams J and Kerbel RS. *Lack of multicellular drug resistance observed in human ovarian and pros- tate carcinoma treated with the proteasome inhibitor PS-341*. Clin Cancer Res, 6, 3719-3728 (2000);

Fribley A, Zeng Q and Wang CY. *Proteasome inhibitor PS-341 induces apoptosis through induction of endoplasmic reticulum stress-reactive oxygen species in head and neck squamous cell carcinoma cells.* Mol Cell Biol, 24:9695–9704 (2004);

Fulda S, Rajalingam K and Dikic I. *Ubiquitylation in immune disorders and cancer: from molecular mechanisms to therapeutic implications.* Ubiquitylation in immunity and cancer, EMBO Molecular Medicine (2012);

Furnari FB, Fenton T, Bachoo RM, Mukasa A, Stommel JM, Stegh A, Hahn WC, Ligon KL, Louis DN, Brennan C, Chin L, DePinho RA and Cavenee WK. *Malignant astrocytic glioma: genetics, biology, and paths to treatment.* Genes Dev, Nov 1;21(21): 2683-710 (2007);

Furuta T, Sabit H, Dong Y, Miyashita K, Kinoshita M, Uchiyama N, Hayashi Y, Hayashi Y, Minamoto T and Nakada M. *Biological basis and clinical study of glycogen synthase kinase- 3β-targeted therapy by drug repositioning for glioblastoma.* Oncotarget, Apr 4;8(14): 22811-22824 (2017);

Gadhave K, Bolshette N, Ahire A, Pardeshi R, Thakur K, Trandafir C, Istrate A, Ahmed S, Lahkar M, Muresanu DF and Balea M. *The ubiquitin proteasomal system: a potential target for the management of Alzheimer's disease*. J Cell Mol Med, Jul; 20(7): 1392–1407 (2016);

Galluzzi L, Vitale I, Abrams JM, Alnemri ES, Baehrecke EH, Blagosklonny MV, et al. *Molecular definitions of cell death subroutines: recommendations of the Nomenclature Committee on Cell Death 2012.* Cell Death Differ, Jan,19(1): 107-20 (2012);

Gant W, Rao DN, Mason RP, et al. *Redox cycling and sulphydryl arylation; their relative importance in the mechanism of quinone cytotoxicity to isolated hepatocytes.* Chemico-Biological Interactions, 65(2): 157-173 (1988);

Ganten TM, Koschny R, Haas TL, Sykora J, Li-Weber M, Herzer K and Walczak H. *Proteasome inhibition sensitizes hepatocellular carcinoma cells, but not human hepatocytes, to TRAIL.* Hepatology, 42, 588-597 (2005);

Gao C, Holscher C, Liu Y and Li L. *GSK3: a key target for the development of novel treatments for type 2 diabetes mellitus and Alzheimer disease.* Reviews in the Neurosciences, 23: 1-11 (2012);

Goldberg AL. *Degradation of abnormal proteins in E. coli.* Proc Natl Acad Sci, USA 69, 422–426 (1972);

Goldberg AL and Dice JF. *Intracellular protein degradation in mammalian and bacterial cells.* Annu Rev Biochem 43, 835–869 (1974);

Gomer CJ, Ryter SW, Ferrario A, Rucker N, Wong S and Fisher AM. *Photodynamic therapy-mediated oxidative stress can induce expression of heat shock proteins.* Cancer Res, May 15;56(10): 2355-60 (1996);

Gómez-Sintes R and Lucas JJ. *NFAT/Fas signaling mediates the neuronal apoptosis and motor side effects of GSK-3 inhibition in a mouse model of lithium therapy.* J Clin Invest, 120: 2432-2445 (2010);

Goñi-Oliver P, Lucas JJ, Avila J and Hernández F. *N-terminal cleavage of GSK-3 by calpain: a new form of GSK-3 regulation.* J Biol Chem, Aug 3;282(31): 22406-13 (2007);

Green DR and Amarante-Mendes GP. *The Point of No Return: Mitochondria, Caspases, and the Commitment to Cell Death.* In: Kumar S. (eds) Apoptosis: Mechanisms and Role in Disease. Results and Problems in Cell Differentiation, vol 24. Springer, Berlin, Heidelberg (1998);

Gregori L, Poosch MS, Cousins G and Chau V. *A uniform isopeptide-linked multiubiquitin chain is sufficient to target substrate for degradation in ubiquitin-mediated proteolysis*. J Biol Chem 265, 8354–8357 (1990);

Griendling KK and FitzGerald GA. *Oxidative stress and cardiovascular injury: Part I: basic mechanisms and in vivo monitoring of ROS.* Circulation, Oct 21;108(16): 1912-6 (2003);

Grimes CA and Jope RS. *The multifaceted roles of glycogen synthase kinase 3beta in cellular signaling.* Prog Neurobiol, Nov;65(4): 391-426 (2001);

Groll M, Celia R, Hidde B, Ploegh L and Ovaa H. *Crystal Structure of the Boronic Acid-Based Proteasome Inhibitor Bortezomib in Complex with the Yeast 20S Proteasome.* Structure, 14,3: 451-456 (2006);

Gupta N,Yang H, Hanley MJ, Zhang S, Liu R, Kumar S, Richardson PG, Skacel T and Venkatakrishnan K. *Dose and Schedule Selection of the Oral Proteasome Inhibitor Ixazomib in Relapsed/Refractory Multiple Myeloma: Clinical and Model-Based Analyses.* Target Oncol, 12(5): 643–654 (2017);

Haas AL, Ahrens P, Bright PM and Ankel H. *Interferon induces a 15-kilodalton protein exhibiting marked homology to ubiquitin.* J Biol Chem 262: 11315–11323 (1987);

Halliwell B. *Role of free radicals in the neurodegenerative diseases: therapeutic implications for antioxidant treatment.* Drugs Aging, 18: 685-716 (2001);

Happel N, Stoldt S, Schmidt B and Doenecke D. *M phase-specific phosphorylation of histone H1.5 at threonine 10 by GSK-3.* J Mol Biol, Feb 20;386(2): 339-50 (2009);

Harding HP, Calfon M, Urano F, Novoa I and Ron D. *Transcriptional and translational control in the Mammalian unfolded protein response.* Annu Rev Cell Dev Biol, 18: 575-99 (2002);

Henderson CJ, Aleo E, Fontanini A, Maestro R, Paroni G and Brancolini C. *Caspase activation and apoptosis in response to proteasome inhibitors.* Cell Death and Differentiation, 12: 1240-1254 (2005);

Hershko A. *Ubiquitin: roles in protein modification and breakdown.* Cell, Aug; 34(1): 11-2 (1983);

Hershko A, Ciechanover A and Varshavsky A. *The ubiquitin system*. Nature Medicine, volume 6: 1073–1081 (2000);

Hickey CM, Wilson NR and Hochstrasser M. *Function and regulation of SUMO proteases.* Nat Rev Mol Cell Biol, Dec;13(12): 755-66 (2012);

Howe CJ, LaHair MM, Maxwell JA, Lee JT, Robinson PJ, Rodriguez-Mora O, McCubrey JA and Franklin RA. *Participation of the calcium/calmodulin-dependent kinases in hydrogen peroxide-induced Ikappa B phosphorylation in human T lymphocytes.* J Biol Chem, Aug 23;277(34): 30469-76 (2002);

Huang C, Li J, Ding M, Leonard SS, Wang L, Castranova V, Vallyathan V and Shi X. *UV Induces phosphorylation of protein kinase B (Akt) at Ser-473 and Thr-308 in mouse epidermal Cl 41 cells through hydrogen peroxide.* J Biol Chem, 276: 40234–40240 (2001);

Hurley JH, Lee S and Prag G. *Ubiquitin-binding domains.* Biochem J, Nov 1;399(3): 361-72 (2006);

Hüser J and Blatter LA. *Fluctuations in mitochondrial membrane potential caused by repetitive gating of the permeability transition pore.* Biochem J, Oct 15;343,Pt2: 311-7 (1999);

Ichim G, Lopez J, Ahmed SU, Muthalagu N, Giampazolias E, Delgado ME, Haller M, Riley JS, Mason SM, et al. L*imited Mitochondrial Permeabilization Causes DNA Damage and Genomic Instability in the Absence of Cell Death.* Mol Cell, Mar 5; 57(5): 860-872 (2015);

Iqbal S and Hood DA. *Oxidative stress-induced mitochondrial fragmentation and movement in skeletal muscle myoblasts.* Am J Physiol Cell Physiol, Jun 15; 306(12): C1176-C1183 (2014);

Jackson SP and Durocher D. *Regulation of DNA damage responses by ubiquitin and SUMO.* Mol Cell, Mar 7;49(5):795-807 (2013);

Jenner P and Olanow CW. *Oxidative stress and the pathogenesis of Parkinson's disease.* Neurology, 47:S161-S170 (1996);

Jesenberger V and Jentsch S. *Deadly encounter: ubiquitin meets apoptosis.* Nat Rev Mol Cell Biol, Feb; 3(2): 112-21 (2002);

Jiang X and Wang X. *Cytochrome C-mediated apoptosis.* Annu Rev Biochem, 73:87-106 (2004);

Jin J1, Li X, Gygi SP and Harper JW. *Dual E1 activation systems for ubiquitin differentially regulate E2 enzyme charging.* Nature, Jun 28;447(7148): 1135-8 (2007);

Jope RS and Johnson GV. *The glamour and gloom of glycogen synthase kinase-3.* Trends Biochem Sci, 29: 95–102 (2004);

Kaas GEN, Duddy SK and Orrenius S. *Activation of hepatocyte protein kinase C by redox-cycling quinones.* Biochemistry Journal, 260(2): 499-507 (1989);

Kabore AF, Sun J, Hu X, McCrea K, Johnston JB and Gibson SB. *The TRAIL apoptotic pathway mediates proteasome inhibitor induced apoptosis in primary chronic lymphocytic leukemia cells.* Apoptosis, 11: 1175-1193 (2006);

Kashkar H, Deggerich A, Seeger JM, Yazdanpanah B, Wiegmann K, Haubert D, Pongratz C and Kronke M. *NF-kappaB- independent down-regulation of XIAP by bortezomib sensitizes HL B cells against cytotoxic drugs.* Blood, 109: 3982-3988 (2007);

Kerscher O, Felberbaum R and Hochstrasser M. *Modification of proteins by ubiquitin and ubiquitin-like proteins.* Annu Rev Cell Dev Biol, 22: 159-80 (2006);

Kim HT, Kim KP, Lledias F, Kisselev AF, Scaglione KM, Skowyra D, Gygi SP and Goldberg AL. *Certain pairs of ubiquitin-conjugating enzymes (E2s) and ubiquitin-protein ligases (E3s) synthesize nondegradable forked ubiquitin chains containing all possible isopeptide linkages.* J Biol Chem, 282: 17375-17386 (2007);

Kim W, Bennett EJ, Huttlin EL, Guo A, Li J, Possemato A, Sowa ME, Rad R, Rush J, Comb MJ, Harper JW and Gygi SP. *Systematic and quantitative assessment of the ubiquitin-modified proteome.* Mol Cell, Oct 21;44(2): 325-40 (2011);

Kisselev AF and Goldberg AL. *Proteasome inhibitors: from research tools to drug candidates.* Chem Biol, Aug; 8(8):739-58 (2001);

Klotz LO, Hou X and Jacob C. *1,4-Naphthoquinones: From oxidative damage to cellular and inter-cellular signaling.* Molecules, 19(9): 14902-14918 (2014);

Kodadek T. *No Splicing, no dicing: non-proteolytic roles of the ubiquitin-proteasome system in transcription*. J Biol Chem, Jan 22;285(4): 2221-6 (2010);

Komander D. *The emerging complexity of protein ubiquitination*. Biochem Soc Trans, Oct;37(Pt 5): 937-53 (2009);

Komander D, Clague MJ and Urbé S. *Breaking the chains: structure and function of the deubiquitinases*. Nat Rev Mol Cell Biol, 10(8): 550–63 (2009);

Kortuem KM and Stewart AK. *Carfilzomib*. Blood, Feb 7;121(6): 893-7 (2013);

Kotliarova S, Pastorino S, Kovell LC, Kotliarov Y, Song H, Zhang W, Bailey R, Maric D, Zenklusen JC, Lee J and Fine HA. *Glycogen Synthase Kinase 3 inhibition Induces Glioma Cell Death through c-MYC, NF-κB and Glucose Regulation.* Cancer Res, Aug 15; 68(16): 6643–6651 (2008);

Kuhn DJ, Chen Q, Voorhees PM, Strader JS, Shenk KD, Sun CM, Demo SD, Bennett MK, van Leeuwen FW, Chanan-Khan AA and Orlowski RZ. *Potent activity of carfilzomib, a novel, irreversible inhibitor of the ubiquitin-proteasome pathway, against preclinical models of multiple myeloma.* Blood, Nov 1;110(9): 3281-90 (2007);

Kyle RA and Rajkumar SV. *DRUG THERAPY. Multiple Myeloma*. N Engl J Med, 351: 1860-1873 (2004);

LaHair MM, Howe CJ, Rodriguez–Mora O, McCubrey JA and Franklin RA. *Molecular Pathways Leading to Oxidative Stress-Induced Phosphorylation of Akt.* ANTIOXIDANTS & REDOX SIGNALING, Volume 8, Numbers 9: 10 (2006);

Lee BH, Lee MJ, Park S, Oh DC, Elsasser S, Chen PC, Gartner C, Dimova N, et al. *Enhancement of proteasome activity by a small-molecule inhibitor of USP14*. Nature, Sep 9;467(7312):179-84 (2010);

Lee BH, Lu Y, Prado MA, Shi Y, Tian G, Sun S, Elsasser S, Gygi SP, King RW and Finley D. *USP14 deubiquitinates proteasome-bound substrates that are ubiquitinated at multiple sites.* Nature, Apr 21;532(7599): 398-401 (2016);

Leis H, Segrelles C, Ruiz S, Santos M and Paramio JM. *Expression, localization, and activity of glycogen synthase kinase 3β during mouse skin tumorigenesis.* Mol Carcinog, 35: 180–185 (2002);

Lim MLR, Lum MG, Hansen TM, Roucou X and Nagley P. *On the release of cytochrome c from mitochondria during cell death signaling.* J Biomed Sci, 9: 488-506 (2002);

Liu, X, Yue P, Chen S, Hu L, Lonial S, Khuri FR and Sun SY. *The proteasome inhibitor PS-341 (bortezomib) up-regulates DR5 expression leading to induction of apoptosis and enhancement of TRAIL-induced apoptosis despite up-regulation of c-FLIP and survivin expression in human NSCLC cells.* Cancer Res, 67: 4981-4988 (2007);

Longley DB and Johnston PG. *Molecular mechanisms of drug resistance.* J Pathol, 205: 275–292 (2005);

Lopes UG, Erhardt P, Yao R and Cooper GM. *p53-dependent induction of apoptosis by proteasome inhibitors.* J Biol Chem, 272: 12893-12896 (1997);

Lu J, Lu J, Chen W, Huo Y, Huang X, Hou J and the Chinese Medical Doctor Association Hematology Branch. *Clinical features and treatment outcome in newly diagnosed Chinese patients with multiple myeloma: results of a multicenter analysis.* Blood Cancer J, Aug; 4(8): e239 (2014);

Lü S, Yang J, Song X, Gong S, Zhou H, Guo L, Song N, Bao X, Chen P and Wang J. *Point Mutation of the Proteasome β5 Subunit Gene Is an Important Mechanism of Bortezomib Resistance in Bortezomib-Selected Variants of Jurkat T Cell Lymphoblastic Lymphoma/Leukemia Line.* Journal of Pharmacology and Experimental Therapeutics August, 326(2): 423-431 (2008);

Luo J. *Glycogen synthase kinase 3beta (GSK3beta) in tumorigenesis and cancer chemotherapy.* Cancer Lett, 273: 194–200 (2009);

Maiti TK, Permaul M, Boudreaux DA, Mahanic C, Mauney S and Das C. *Crystal structure of the catalytic domain of UCHL5, a proteasome-associated human deubiquitinating enzyme, reveals an unproductive form of the enzyme.* FEBS J, Dec; 278(24): 4917–4926 (2011);

Marchi S, Giorgi C, Suski J, Pinton P et al. *Mitochondria-Ros Crosstalk in the Control of Cell Death and Aging.* Journal of Signal Transduction, Vol2012, Article ID 32635,17 (2012);

Mattern MR, Wu J and Nicholson B. *Ubiquitin-based anticancer therapy: carpet bombing with proteasome inhibitors vs surgical strikes with E1, E2, E3, or DUB inhibitors.* Biochim Biophys Acta, Nov;1823(11): 2014-21 (2012);

McCubrey JA, Steelman LS, Bertrand FE, Davis NM, Sokolosky M, Abrams SL, Montalto G, D'Assoro AB, Libra M, Nicoletti F, Maestro R, Basecke J, Rakus D, Gizak A, et al. *GSK-3 as potential target for therapeutic intervention in cancer.* Oncotarget, May 30;5(10): 2881-911 (2014);

Meares GP and Jope RS. *Resolution of the Nuclear Localization Mechanism of Glycogen Synthase Kinase-3 : FUNCTIONAL EFFECTS IN APOPTOSIS.* J Biol Chem, June(8);282(23): 16989-17001 (2007);

Milano A, Iaffaioli RV and Caponigro F. *The proteasome: A worthwhile target for the treatment of solid tumours.* European Journal of Cancer, 43,7: 1125-1133 (2007);

Mitsiades N, Mitsiades CS, Richardson PG, Poulaki V, Tai YT, Chauhan D, Fanourakis G, Gu X, Bailey C, Joseph M, Libermann TA, Schlossman R, Munshi NC, Hideshima T and Anderson KC. *The proteasome inhibitor PS-341 potentiates sensitivity of multiple myeloma cells to conventional chemotherapeutic agents: therapeutic applications.* Blood, Mar 15;101(6): 2377-80 (2003);

Miyashita K, Kawakami K, Nakada M, Mai W, Shakoori A, Fujisawa H, Hayashi Y, Hamada J and Minamoto T. *Potential therapeutic effect of glycogen synthase kinase 3beta inhibition against human glioblastoma.* Clin Cancer Res, Feb 1;15(3): 887-97 (2009);

Moosmann B and Behl C. A*ntioxidants as treatment for neurodegenerative disorders.* Expert Opin Investig Drugs, 11:1407-1435 (2002);

Morreale FE and Walden H. *Types of Ubiquitin Ligases*. Cell, Mar 24;165(1): 248-248.e1 (2016);

Moujalled DM, Cook WD, Murphy JM and Vaux DL. *Necroptosis induced by RIPK3 requires MLKL but not Drp1*. Cell Death Dis, Feb; 5(2): e1086 (2014);

Mullally JE And Fitzpatrick FA. *Pharmacophore model for novel inhibitors of ubiquitin isopeptidases that induce p53-independent cell death.* Mol Pharmacol, 62: 351-358 (2002);

Muratani M and Tansey WP. *How the ubiquitin-proteasome system controls transcription.* Nat Rev Mol Cell Biol, Mar;4(3): 192-201 (2003);

Nalepa G, Rolfe M and Harper JW. *Drug discovery in the ubiquitin-proteasome system.* Nat Rev Drug Discov, Jul;5(7):596-613 (2006);

Newmeyer DD and Ferguson-Miller S. *Mitochondria: releasing power for life and unleashing the machineries of death.* Cell, 112: 481-490 (2003);

Newton K, Dugger DL, Maltzman A, Greve JM, Hedehus M, Martin-McNulty B, Carano RAD, Cao TC, van Bruggen N, Bernstein L, Lee WP, et al. *RIPK3 deficiency or catalytically inactive RIPK1 provides greater*

benefit than MLKL deficiency in mouse models of inflammation and tissue injury. Cell Death Differ, Sep 1,23(9): 1565-1576 (2016);

Nicholson B, Leach CA, Goldenberg SJ, Francis DM, Kodrasov MP, Tian X, et al. *Characterization of ubiquitin and ubiquitin-like-protein isopeptidase activities.* Protein Sci, 17: 1035-1043 (2008);

Nishio K, Kim SW, Kawai K, Mizushima T, Yamane T, Hamazaki J, Murata S, Tanaka K and Morimoto Y. *Crystal structure of the de-ubiquitinating enzyme UCH37 (human UCH-L5) catalytic domain.* Biochem Biophys Res Commun, Dec 18;390(3): 855-60 (2009);

Nooka A, Gleason C, Casbourne D and Lonial S. *Relapsed and refractory lymphoid neoplasms and multiple myeloma with a focus on carfilzomib.* Biologics, 7: 13–32 (2013);

Obeng EA, Carlson LM, Gutman DM, Harrington WJ Jr, Lee KP and Boise LH. *Proteasome inhibitors induce a terminal unfolded protein response in multiple myeloma cells.* Blood, Jun 15;107(12): 4907-16 (2006);

Oliver L and Vallette FM. *The role of caspases in cell death and differentiation.* Drug Resist Updat, 8: 163–170 (2005);

Orlowski RZ, Stinchcombe TE, Mitchell BS, Shea TC, Baldwin AS, Stahl S, Adams J, Esseltine DL, Elliott PJ, Pien CS, Guerciolini R, Anderson JK, Depcik-Smith ND, et al. *Phase I trial of the proteasome inhibitor PS-341 in patients with refractory hematologic malignancies.* J Clin Oncol, Nov 15;20(22): 4420-7 (2002);

Ougolkov AV and Billadeau DD. *Inhibition of glycogen synthase kinase-3.* Methods Mol Biol, 468: 67-75 (2008);

Ougolkov AV, Fernandez-Zapico ME, Savoy DN, Urrutia RA and Billadeau DD. *Glycogen synthase kinase-3beta participates in nuclear factor kappaB-mediated gene transcription and cell survival in pancreatic cancer cells.* Cancer Res, 65: 2076-2081 (2005);

Paroni G, Henderson C, Schneider C and Brancolini C. *Caspase-2-induced apoptosis is dependent on caspase-9, but its processing during UV- or tumor necrosis factor-dependent cell death requires caspase-3.* J Biol Chem, Jun 15;276(24):21907-15 (2001);

Paroni G, Mizzau M, Henderson C and Brancolini C. *Caspase-dependent Regulation of Histone Deacetylase 4 Nuclear-Cytoplasmic Shuttling Promotes Apoptosis*. Molecular Biology of the Cell, July,15(6): 2804-18 (2004);

Peng J. et al. *A proteomics approach to understanding protein ubiquitination.* Nature Biotechnol, 21, 921–926 (2003);

Pickart CM. *Ubiquitin in chains.* Trends Biochem Sci, Nov;25(11): 544-8 (2000);

Pickart CM and Eddins MJ. *Ubiquitin: structures, functions, mechanisms*. Biochim Biophys, Acta 1695: 55–72 (2004);

Polakis P. *The many ways of Wnt in cancer.* Curr Opin Genet Dev, Feb;17(1): 45-51 (2007);

Randal JK. *Orchestrating the unfolded protein response in health and disease.* J Clin Invest, Nov 15; 110(10): 1389–1398 (2002);

Rastogi N, Duggal S, Singh SK, Porwal K, Srivastava VK, Maurya R, Bhatt ML and Mishra DP. *Proteasome inhibition mediates p53 reactivation and anti-cancer activity of 6-gingerol in cervical cancer cells.* Oncotarget, Dec 22;6(41):43310-25 (2015);

Rehman SAA, Kristariyanto YA, Choi SY Labib K, Hofmann K and Kulathu Y. *MINDY-1 Is a Member of an Evolutionarily Conserved and Structurally Distinct New Family of Deubiquitinating Enzymes.* Molecular Cell, Volume 63, 1: 146-155 (2016);

Reyes-Turcu FE, Ventii KH and Wilkinson KD. *Regulation and cellular roles of ubiquitin-specific deubiquitinating enzymes.* Annu Rev Biochem, 78: 363-97 (2009);

Ri M. *Endoplasmic-reticulum stress pathway-associated mechanisms of action of proteasome inhibitors in multiple myeloma.* Int J Hematol, Sep;104(3): 273-80 (2016);

Richardson PG, Sonneveld P, Schuster MW, Irwin D, Stadtmauer EA, Facon T, Harousseau JL, Ben-Yehuda D, Lonial S, Goldschmidt H, Reece D, San-Miguel JF, Bladé J, Boccadoro M, Cavenagh J, Dalton WS, Boral AL, Esseltine DL, Porter JB, Schenkein D, Anderson KC and Assessment of Proteasome Inhibition for Extending Remissions (APEX) Investigators. *Bortezomib or high-dose dexamethasone for relapsed multiple myeloma.* N Engl J Med, Jun 16;352(24):2487-98 (2005);

Rodriguez-Nieto S and Zhivotovsky B. *Role of alterations in the apoptotic machinery in sensitivity of cancer cells to treatment.* Curr Pharm Des, 12(34): 4411-25 (2006);

Ron D. *Translational control in the endoplasmic reticulum stress response.* J Clin Invest, Nov 15; 110(10): 1383–1388 (2002);

Ruschak AM, Slassi M, Kay LE and Schimmer AD. *Novel proteasome inhibitors to overcome bortezomib resistance.* J Natl Cancer Inst, 2011 Jul 6;103(13): 1007-17 (2011);

Saeki Y, Kudo T, Sone T, Kikuchi Y, Yokosawa H, Toh-e A and Tanaka K. *Lysine 63-linked polyubiquitin chain may serve as a targeting signal for the 26S proteasome*. EMBO J, 28, 359-371 (2009);

Saulle E, Petronelli A, Pasquini L, Petrucci E, Mariani G, Biffoni M, Ferretti G, Scambia G, Benedetti-Panici P, Cognetti F, Humphreys R, Peschle C and Testa U. *Proteasome inhibitors sensitize ovarian cancer cells to TRAIL induced apoptosis.* Apoptosis, 12*,* 635-655 (2007);

Sayers TJ, Brooks AD, Koh CY, Ma W, Seki N, Raziuddin A, Blazar BR, Zhang X, Elliott PJ and Murphy WJ. *The proteasome inhibitor PS-341 sensitizes neoplastic cells to TRAIL-mediated apoptosis by reducing levels of c-FLIP.* Blood, Jul 1;102(1):303-10 (2003);

Schäfer M, Goodenough S, Moosmann B and Behl C. *Inhibition of glycogen synthase kinase 3 beta is involved in the resistance to oxidative stress in neuronal HT22 cells.* Brain Res, Apr 16;1005(1-2): 84-9 (2004);

Schimmer AD. *Inhibitor of apoptosis proteins: translating basic knowledge into clinical practice.* Cancer Res, Oct 15;64(20): 7183-90 (2004);

Schulman BA and Harper JW. *Ubiquitin-like protein activation by E1 enzymes: the apex for downstream signalling pathways*. Nat Rev Mol Cell Biol, 10(5):319-31 (2009);

Schwartz AL and Ciechanover A. *Targeting proteins for destruction by the ubiquitin system: implications for human pathobiology.* Annu Rev Pharmacol Toxicol, 49:73-96// 051208.165340 (2009);

Schwartz DC and Hochstrasser M. *A superfamily of protein tags: ubiquitin, SUMO and related modifiers.* Trends Biochem Sci, Jun;28(6):321-8 (2003);

Scorrano L, Petronilli V and Bernardi P. *Chloromethyltetramethylrosamine (Mitotracker OrangeTM) Induces the Mitochondrial Permeability Transition and Inhibits Respiratory Complex I: IMPLICATIONS FOR THE MECHANISM OF CYTOCHROME c RELEASE.* Journal of Biological Chemistry, 274(35): 24657-63 (1999);

Sgorbissa A, Tomasella A, Potu H et al. *Type I IFNs signaling and apoptosis resistance in glioblastoma cells.* Apoptosis, December 16: 1229 (2011);

Shakoori A, Ougolkov A, Yu ZW, Zhang B, Modarressi MH, Billadeau DD, Mai M, Takahashi Y and Minamoto T. *Deregulated GSK3beta activity in colorectal cancer: its association with tumor cell survival and proliferation.* Biochem Biophys Res Commun, 334: 1365-1373 (2005);

Sherman M and Goldberg AL. *Cellular defenses against unfolded proteins: a cell biologist thinks about neurodegenerative diseases.* Neuron 29, 15–32 (2001);

Shi MM, Kugelman A, Iwamoto T, et al. *Quinone-induced oxidative stress elevates glutathione and induces γ-glutamylcysteine synthetase activity in rat lung epithelial L2 cells.* The Journal of Biological Chemistry, 269(42): 26512-26517 (1994);

Shimizu Y and Hendershot LM. *Oxidative Folding: Cellular Strategies for Dealing with the Resultant Equimolar Production of Reactive Oxygen Species.* Antioxid Redox Signal, 11(9): 2317–2331 (2009);

Shin EJ, Shin HM, Nam E, Kim WS, Kim JH, Oh BH and Yun Y. *DeSUMOylating isopeptidase: a second class of SUMO protease.* EMBO Rep, 2012 Apr;13(4):339-46 (2012);

Shiozaki EN and Shi Y. *Caspases, IAPs and Smac/DIABLO: mechanisms from structural biology.* Trends Biochem Sci, 29, 486-494 (2004);

Song L, De Sarno P and Jope RS. *Central role of glycogen synthase kinase-3beta in endoplasmic reticulum stress-induced caspase-3 activation.* J Biol Chem, Nov 22;277(47): 44701-8 (2002);

Sun M, Song L, Li Y, Zhou T and Jope RS. *Identification of an anti-apoptotic protein complex at death receptors.* Cell Death Differentiation, 15: 1887-1900 (2008);

Sun XM, Bratton SB, Butterworth M, MacFarlane M and Cohen GM. *Bcl-2 and Bcl-xL inhibit CD95-mediated apoptosis by preventing mitochondrial release of Smac/DIABLO and subsequent inactivation of X-linked inhibitor-of-apoptosis protein.* J Biol Chem, Mar 29;277(13): 11345-51 (2002);

Sutherland C. *What Are the bona fide GSK3 Substrates?* Int J Alzheimers Dis, 2011: 505607 (2011);

Szatmari E, Habas A, Yang P, Zheng JJ, Hagg T and Hetman M. *A positive feedback loop between glycogen synthase kinase 3beta and protein phosphatase 1 after stimulation of NR2B NMDA receptors in forebrain neurons.* J Biol Chem, 280: 37526-37535 (2005);

Tait SWG, Oberst A, Quarato G, Milasta S, Haller M, Wang R, Karvela M, Ichim G, Yatim N, Albert ML, Kidd G, Wakefield R, Frase S, Krautwald S, Linkermann A and Green DR. *Widespread mitochondrial depletion via mitophagy does not compromise necroptosis.* Cell Rep, Nov 27,5(4): 878–885 (2013);

Thompson JL. *Carfilzomib: a second-generation proteasome inhibitor for the treatment of relapsed and refractory multiple myeloma.* Ann Pharmacother, 47:56–62 (2013);

Thorburn A. *Death receptor-induced cell killing*. Cell Signal, 16: 139-144 (2004);

Thrower JS, Hoffman L, Rechsteiner M and Pickart CM. *Recognition of the polyubiquitin proteolytic signal.* EMBO J, 19, 94-102 (2000);

Tian Z, D'Arcy P, Wang X, Ray A, Tai YT, Hu Y, Carrasco RD, Richardson P, Linder S, Dand C and Kenneth CA. *A novel small molecule inhibitor of deubiquitylating enzyme USP14 and UCHL5 induces apoptosis in multiple myeloma and overcomes bortezomib resistance.* Blood, Jan 30; 123(5): 706–716 (2014);

Tomasella A, Blangy A and Brancolini C. *A receptor-interacting protein 1 (RIP1) -independent necrotic death under the control of protein phosphatase PP2A that involves the reorganization of actin cytoskeleton and the action of cofilin-1*. J Biol Chem, Sep 12;289(37):25699-710 (2014);

Unno M, Mizushima T, Morimoto Y, Tomisugi Y, Tanaka K, Yasuoka N and Tsukihara T. *The structure of the mammalian 20S proteasome at 2.75 A resolution.* Structure, May;10(5):609-18 (2002);

Unterkircher T, Cristofanon S, Vellanki SH and Fulda S. *Bortezomib Primes Glioblastoma, Including Glioblastoma Stem Cells, for TRAIL by Increasing tBid Stability and Mitochondrial Apoptosis.* Clinical Cancer Research, 17(12):4019-30 (2011);

Van Geelen CM, de Vries EG and de Jong S. *Lessons from TRAIL-resistance mechanisms in colorectal cancer cells: paving the road to patient-tailored therapy.* Drug Resist Updat, 7, 345-358 (2004);

Vaux DL and Silke J. *IAPs, RINGs and ubiquitylation.* Nat Rev Mol Cell Biol, 6 287 (2005);

Venè R, Cardinali B, Arena G, Ferrari N, Benelli R, Minghelli S, Poggi A, Noonan DM, Albini A and Tosetti F. *Glycogen Synthase Kinase 3 Regulates Cell Death and Survival Signaling in Tumor Cells under Redox Stress.* Neoplasia, Sep; 16(9): 710-722 (2014);

Verbitski SM, Mullally JE, Fitzpatrick FA and Ireland CM. *Punaglandins, chlorinated prostaglandins, function as potent Michael receptors to inhibit ubiquitin isopeptidase activity.* J Med Chem, 47: 2062–2070 (2004);

Vercammen D, Beyaert R, Denecker G, Goossens V, Van Loo G, Declercq W, Grooten J, Fiers W and Vandenabeele P. *Inhibition of caspases increases the sensitivity of L929 cells to necrosis mediated by tumor necrosis factor.* J Exp Med, May 4;187(9): 1477-85 (1998);

Verma R, Aravind L, Oania R, McDonald WH, Yates JR 3rd, Koonin EV and Deshaies RJ. *Role of Rpn11 metalloprotease in deubiquitination and degradation by the 26S proteasome.* Science, Oct 18;298(5593):611-5 (2002);

Vijay-Kumar S, Bugg CE and Cook WJ. *Structure of ubiquitin refined at 1. 8 A resolution.* J Mol Biol, 194, 531–544 (1987);

Voorhees PM, Dees EC, O'Neil B and Orlowski RZ. *The proteasome as a target for cancer therapy.* Clin Cancer Res, Dec 15;9(17):6316-25 (2003);

Voortman J, Checińska A and Giaccone G. *The proteasomal and apoptotic phenotype determine bortezomib sensitivity of non-small cell lung cancer cells.* Mol Cancer, Nov 17;6:73 (2007);

Wang Y, Wang J, Zhong J, Deng Y, Xi Q, He S, Yang S, Jiang L, Huang M, Tang C and Liu R. *Ubiquitin-specific protease 14 (USP14) regulates cellular proliferation and apoptosis in epithelial ovarian cancer.* Med Oncol, Jan; 32(1):379 (2015);

Wang Z, Jiang H, Chen S, Du F and Wang X. *The mitochondrial phosphatase PGAM5 functions at the convergence point of multiple necrotic death pathways.* Cell, Jan 20;148(1-2): 228-43 (2012);

Wilkinson JC, Wilkinson AS, Scott FL, Csomos RA, Salvesen GS and Duckett CS. *Neutralization of Smac/Diablo by Inhibitors of Apoptosis (IAPs): A caspase-independent mechanism for apoptotic inhibition.* J Biol Chem, 279, 51082-51090 (2004);

Wu S, Zhou F, Zhang Z and Xing D. *Mitochondrial oxidative stress causes mitochondrial fragmentation via differential modulation of mitochondrial fission-fusion proteins.* FEBS J, Apr;278(6): 941-54 (2011);

Xu Y, Huang S, Liu ZG and Han J. *Poly(ADP-ribose) polymerase-1 signaling to mitochondria in necrotic cell death requires RIP1/TRAF2-mediated JNK1 activation.* J Biol Chem, Mar 31;281(13): 8788-95 (2006);

Yao T and Cohen RE. *A cryptic protease couples deubiquitination and degradation by the proteasome*. Nature, Sep 26;419(6905):403-7 (2002);

Yao T, Song L, Jin J, Cai Y, Takahashi H, Swanson SK, Washburn MP, Florens L, Conaway RC, Cohen RE and Conaway JW. *Distinct modes of regulation of the Uch37 deubiquitinating enzyme in the proteasome and in the Ino80 chromatin-remodeling complex.* Mol Cell, Sep 26;31(6):909-17 (2008);

Yao T, Song L, Xu W, DeMartino GN, Florens L, Swanson SK, Washburn MP, Conaway RC, Conaway JW and Cohen RE. *Proteasome recruitment and activation of the Uch37 deubiquitinating enzyme by Adrm1.* Nat Cell Biol, Sep;8(9):994-1002 (2006);

Ye Y and Rape M. *Building ubiquitin chains: E2 enzymes at work.* Nat Rev Mol Cell Biol, Nov;10(11):755-64 (2009);

Zhou A, Lin K, Zhang S, Chen Y, Zhang N, Xue J, Wang Z, Aldape KD, Xie K, Woodgett JR and Huang S. *Nuclear GSK3β promotes tumorigenesis by phosphorylating KDM1A and inducing its deubiquitylation by USP22.* Nat Cell Biol, Sep;18(9): 954-966 (2016);

Zhou W, Wang L, Gou SM, Wang TL, Zhang M, Liu T and Wang CY. *shRNA silencing glycogen synthase kinase-3 beta inhibits tumor growth and angiogenesis in pancreatic cancer.* Cancer Letters, 316: 178-186 (2012);

Zimmermann J, Erdmann D, Lalande I, Grossenbacher R, Noorani M and Furst P. *Proteasome inhibitor induced gene expression profiles reveal overexpression of transcriptional regulators ATF3, GADD153 and MAD1*. Oncogene, 19: 2913-2920 (2000);

Zong WX, Ditsworth D, Bauer DE, Wang ZQ and Thompson CB. *Alkylating DNA damage stimulates a regulated form of necrotic cell death.* Genes Dev, Jun 1;18(11): 1272-82 (2004).

1. Acknowledgements

I would like to express my sincere gratitude to my Supervisor Prof. Claudio Brancolini for giving me the possibility to be his PhD student and for driving me, constantly and strongly, throughout the period of my research study, and especially during the writing thesis. Thanks to him, I understood how the research field is and how to survival in it.

A special thanks to PhD Eros Di Giorgio for sharing with me his invaluable biological knowledge, and for showing me how to really chase a dream.

I would like also to thank my external reviewer, Christian Widmann, whom sincerely helped me to better face my PhD project.

My deepest gratitude goes to my "Lab Team": Valentina Cutano, Elisa Franforte, Harikrishnareddy Paluvai, and to new students Martina Minisini, Luca Iuliano, Alice Cellot and Gabriele Pellegrini, for allowing me to life the funniest moments of the lab.

I am also greatly thankful to "Cutanina" and "Franca", whom have been my second family in the lab.

Thanks to all my closest friends and family, because they are my real life's treasure.

Thanks to my deepest love Peppe.

Research Paper

The isopeptidase inhibitor 2cPE triggers proteotoxic stress and ATM activation in chronic lymphocytic leukemia cells

Andrea Tomasella[1], Raffaella Picco[1], Sonia Ciotti[1], Andrea Sgorbissa[1], Elisa Bianchi[2], Rossella Manfredini[2], Fabio Benedetti[3], Valentina Trimarco[4], Federica Frezzato[4], Livio Trentin[4], Gianpietro Semenzato[4], Domenico Delia[5], Claudio Brancolini[1,2]

[1]Department of Medical and Biological Sciences, Università degli Studi di Udine, Udine, Italy

[2]Centre for Regenerative Medicine "Stefano Ferrari", Department of Life Sciences, University of Modena and Reggio Emilia, Modena, Italy

[3]Dipartimento di Scienze Chimiche e Farmaceutiche, Università degli Studi di Trieste, Trieste, Italy

[4]Department of Medicine, Hematology and Clinical Immunology Branch, Padua University School of Medicine, Padua, Italy

[5]Department of Experimental Oncology and Molecular Medicine, Fondazione IRCCS Istituto Nazionale dei Tumori, Milan, Italy

Correspondence to: *Claudio Brancolini,* ***email:*** *claudio.brancolini@uniud.it*

Keywords: *CLL, apoptosis, proteasome, proteotoxic stress, deubuquitylases*

Received: *November 15, 2015* ***Accepted:*** *May 22, 2016* ***Published:*** *May 31, 2016*

ABSTRACT

Relapse after treatment is a common and unresolved problem for patients suffering of the B-cell chronic lymphocytic leukemia (B-CLL). Here we investigated the ability of the isopeptidase inhibitor 2cPE to trigger apoptosis in leukemia cells in comparison with bortezomib, another inhibitor of the ubiquitin-proteasome system (UPS). Both inhibitors trigger apoptosis in CLL B cells and gene expression profiles studies denoted how a substantial part of genes up-regulated by these compounds are elements of adaptive responses, aimed to sustain cell survival. 2cPE treatment elicits the up-regulation of chaperones, proteasomal subunits and elements of the anti-oxidant response. Selective inhibition of these responses augments apoptosis in response to 2cPE treatment. We have also observed that the product of the ataxia telangiectasia mutated gene (ATM) is activated in 2cPE treated cells. Stimulation of ATM signaling is possibly dependent on the alteration of the redox homeostasis. Importantly ATM inhibition, mutations or down-modulation increase cell death in response to 2cPE. Overall this work suggests that 2cPE could offer new opportunities for the treatment of B-CLL.

INTRODUCTION

B-cell chronic lymphocytic leukemia (B-CLL) is the most prevalent leukemia in Western countries and it is characterized by accumulation of malignant cells in the blood, lymph nodes, spleen and bone marrow. B-CLL is a severe disease with heterogeneous clinical course and although new therapies have significantly prolonged the overall survival, most patients relapse [1]. Augmented expression of anti-apoptotic Bcl-2 family members and up-regulation of pro-survival pathways contribute to the resistant phenotype [1–5].

Among drugs tested for the ability to trigger apoptosis in B-CLL cells, inhibitors of the ubiquitin-proteasome system (UPS) have raised some interest. Bortezomib, the first UPS inhibitor approved for the use in clinic, efficiently triggers apoptosis in *in vitro* cultured B-CLL cells [6, 7]. Unfortunately, clinical trials evaluating bortezomib in B-CLL patients were unsatisfactory [8]. Several constrains can explain this failure, including the chemical reaction between the boronate moiety of bortezomib and dietary flavonoids [9]. Furthermore bortezomib induces thrombocytopenia and neuropathy possibly due to proteasomal independent activities [10]. Hence, evaluating alternative compounds targeting the UPS for the treatment of B-CLL is of primary importance.

Small molecules characterized by the presence of a cross-conjugated α,β-unsaturated dienone with two sterically accessible electrophilic β-carbons can act as Michael acceptors to target nucleophiles, such

as cysteine residues [11–14]. Highly susceptible to these compounds are the isopeptidases, which contain a cysteine in the catalytic core. Isopeptidases include DUBs (deubiquitylases) and ubiquitin-like proteases. Although the presence of different groups, in addition to the pharmacophore, can enhance or limit the promiscuity of these compounds, we refer to them as partially-selective isopeptidase inhibitors (P-SIIs) [11–16].

P-SIIs are potent inducers of apoptosis and of additional types of cell death, particularly in cells showing extreme apoptotic resistance [17–19]. We have recently developed a PEG-conjugated P-SII, named 2cPE optimized for the *in vivo* delivery. 2cPE is a pro-drug version of G5 [11], which can be activated by secreted esterase and exhibits promising anti-neoplastic activities *in vivo* [20]. In this manuscript, we have investigated the effect of 2cPE against B-CLL cells, in comparison with bortezomib. Our results prove that induction of proteotoxic stress is a key aspect of 2cPE activity and discovered an unexpected contribution of ATM in influencing 2cPE-induced apoptosis.

RESULTS

The UPS inhibitors bortezomib, G5 and 2cPE cause loss of viability of CD19$^+$ B-CLL cells

Bortezomib and the isopeptidase inhibitor G5, or its PEGylated derivative 2cPE, induce loss of viability in primary CLL cells (Figure 1A and 1B). Cytofluorimetric analysis proved that, for all inhibitors, the loss of viability is largely caused by the induction of apoptosis, with only a minor fraction of the cells exhibiting markers (Annexin-V$^-$ and PI$^+$) of primary necrosis (Figure 1C and 1D).

Gene expression profiles of B-CLL cells treated with the UPS inhibitors bortezomib and 2cPE

To explore whether bortezomib and 2cPE elicit similar or different biological responses, we performed microarray experiments in primary B-CLL cells. Leukemia CD19$^+$ B-cells from 10 different patients were treated or not for 3, 6, 12 and 24 hours with 6nM of bortezomib or with 4μM of 2cPE. Under these conditions the two compounds induce equivalent levels of apoptosis, at 24 hours. For the microarray analysis the 6 hours time-point was selected in order to observe early adaptive responses to the inhibitors and to exclude changes in mRNA expression depending on cellular demise. The clinical and prognostic features of each of the 10 primary CLL samples and their responsiveness in terms of apoptosis are described in Table 1.

Data analysis identified a list of common genes, which expression is influenced by both compounds. Venn diagrams (Figure 2A) illustrate that only few genes were commonly modulated by 2cPE and bortezomib in different patients (19 up-regulated and 15 down-regulated). Overall 2cPE influences the expression of a wider number of genes compared to bortezomib, 169 and 95 genes respectively, including both up and down-regulated ones.

The vast majority of the commonly up-regulated genes encode for chaperones implicated in the regulation of protein folding (Figure 2B). A second group of genes comprises proteasome subunits. Interestingly among the commonly down-regulated genes, metabolic elements and components of signaling pathways can be found.

It is known that the level of proteasomal subunits can influence responsiveness to bortezomib treatment [21–23]. Hence, we compared changes in the expression levels of all proteasomal genes. Up-regulation of mRNAs encoding for several proteasomal subunits is a mark of the response to both inhibitors. This response was more pronounced in the case of bortezomib, whereas the down-regulation of the immunoproteasome subunits PSMB8, PSMB9 and PSMB10 was comparable or even more evident in 2cPE treated cells.

The GO enrichment analysis for 2cPE and bortezomib regulated genes (Table 2) showed that the two drugs can elicit common but also distinct responses. Over-representations of processes such as protein folding, response to unfolded protein and response to organic substance characterize the genetic programs activated by 2cPE. Instead after bortezomib treatment, proteasome complex and regulation of E3 ligase activity are the most represented categories. Comparative analysis of the GO terms enrichment confirmed that the response to 2cPE treatment is strongly characterized by the up-regulation of chaperones, whereas the response to bortezomib is highly represented by UPS components (Supplementary Table S1).

Adaptive responses are engaged in B-CLL cells after 2cPE treatment

The microarray studies suggest that a substantial part of genes up-regulated in response to 2cPE are elements of adaptive programs aimed to sustain cell survival. These programs include the accumulation of new proteasomal units, to overcome its obstruction, the up-regulation of chaperones, to counteract misfolding and the potentiation of the anti-oxidant capabilities. In addition, 2cPE triggers also the down-regulation of some signaling pathways. To validate our studies we performed qRT-PCR analysis on four different genes, archetypes of the adaptive responses engaged by 2cPE. Three selected genes were up-regulated: *GCLM*, *HMOX1*, *SQSTM1/p62*, whereas the fourth gene, *LCK,* was down-regulated. Supplementary Table S2 shows the average fold induction and the correlation analysis, respect to the induction of apoptosis in the different B-CLL, for these genes.

GCLM (glutamate cysteine ligase modifier) encodes for the component of the glutamate cysteine ligase (GCL), the enzyme responsible for glutathione (GSH) synthesis.

Both subunits were increased after 2cPE treatment. The heme oxygenase-1 (*HMOX1*) encodes for an ubiquitous enzyme that supervises cytoprotective responses to toxic insults [24]. *SQSTM1/p62/sequestosome* encodes for a scaffold protein functioning as signaling hub in different pathways including autophagy [25]. Finally, *LCK* encodes for the T-cell-specific member of the Src family of tyrosine kinase, which is also expressed in B-CLL [26]. The qRT-PCR analysis corroborated the regulation of these genes in response to 2cPE treatment (Supplementary Figure S1).

We next confirmed these data in human chronic B-cell leukemia, MEC-1 cells. The 2cPE pro-drug and its unconjugated version, 2c induce comparable levels of cell death (Figure 3A), thus indicating that this cell line

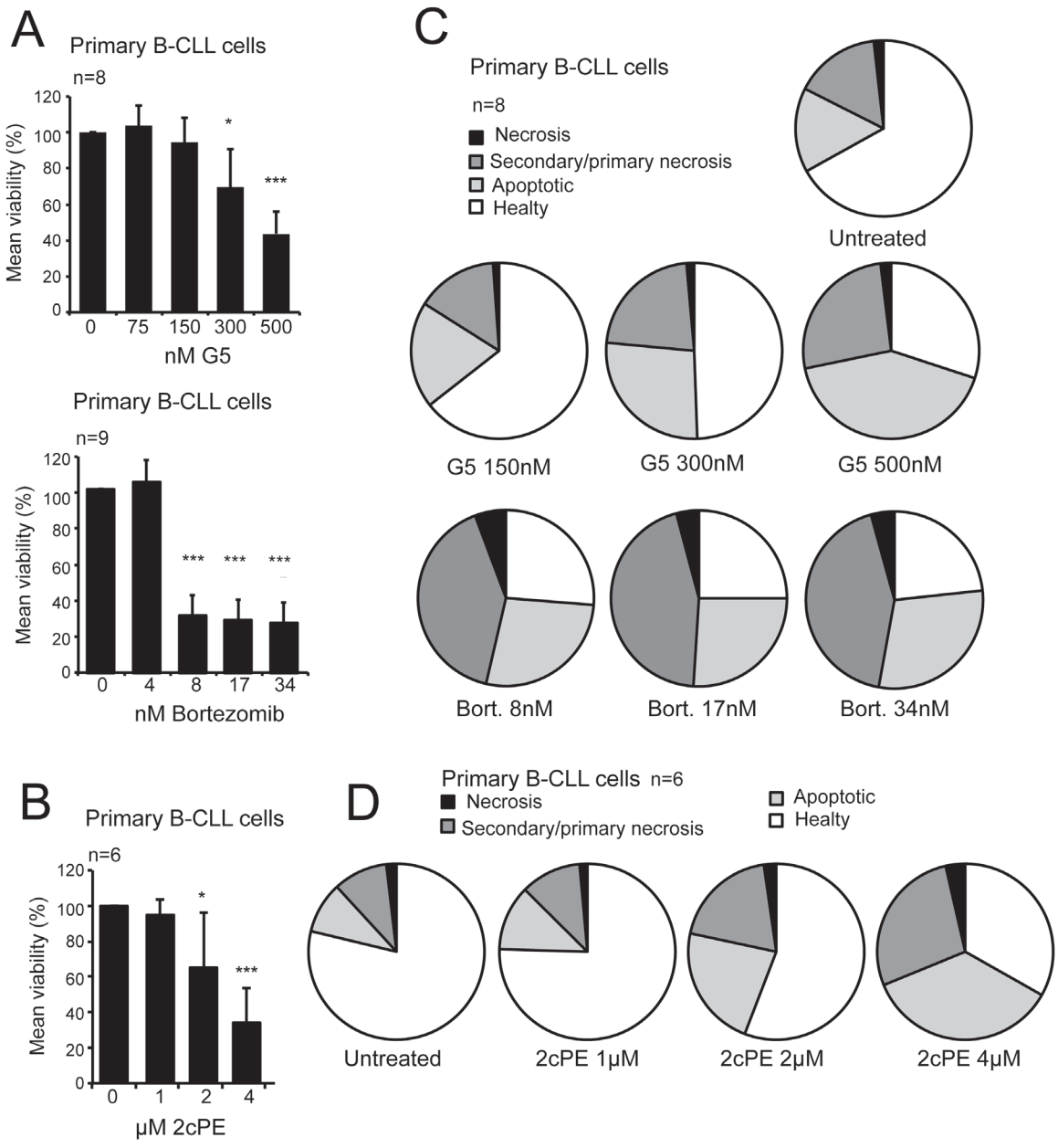

Figure 1: Pro-apoptotic activity of bortezomib, the P-SII G5 and its pro-drug derivative 2cPE in primary B-CLL cells. A. Primary B-CLL cells viability following treatment with escalating doses of G5 or bortezomib for 24 hours as indicated. Cell viability was calculated as percentage of cells negative to PI and Annexin V staining after cytofluorimetric analysis. **B.** Flow cytometry analysis for apoptotic markers (Annexin V/PI) in order to define the type of cell death. Primary B-CLL cells were treated with the indicated concentrations of bortezomib or G5 for 24 hours. **C.** Primary B-CLL cells viability following treatment with escalating doses of 2cPE for 24 hours as indicated. Cell viability was calculated as the percentage of cells negative to PI and Annexin V staining after cytofluorimetric analysis. **D.** Flow cytometry analysis for apoptotic markers (Annexin V/PI) in order to define the type of cell death. Primary B-CLL cells were treated with the indicated concentrations of 2cPE for 24 hours. Columns, mean loss of viability + SD. *=p<0.05; **=p<0.01; ***p=<0.005.

Table 1: Clinical characteristics, apoptotic response, mutational status and genetic alterations of the included patients

code	Sex/age	IGHV	FISH	RAI stage	CD38	2cPE	Bortezomib
LL300	F/79	U	13q-	II	NEG	88	89
LLC122	M/66	U	11q-	0	POS	15	59
LLC195	M/69	U	11q-; 13q-	II	POS	2	86
LLC351	M/67	U	17q-; 13q-	I	POS	81	92
LLC270	M/73	U	11q-	II	POS	17	65
LLC4	F/73	M	*	I	NEG	82	81
LLC305	M/56	M	Normal	0	NEG	75	54
LLC366	F/69	*	13q-; 12+; p53 mut	0	POS	45	77
LLC37	F/79	M	13q-	II	NEG	8	38
LLC43	M/83	M	12+	I	POS	68	82
						Apoptosis at 24 hours (%)	

Note: The gender of the patients, the IgHV mutational status (U=unmutated, M= mutated), CD38 expression (POS = positive for CD38 expression; NEG = negative CD38 expression), the cytogenetic alterations observed and the % of apoptosis after 24 of treatment with the indicated drugs for each patient sample are shown.
* indicates that the status of a specific characteristic for a patient is unknown.

secretes the esterase PLA2G7 [20]. 2c and 2cPE induced cell death was apoptotic, as confirmed by the caspase-dependent proteolytic cleavage of the death substrate GAS2 (Figure 3B) [27]. In MEC-1 cells, similarly to primary B-CLL cells, 2cPE treatment up-regulates the expression of *HMOX1*, *GSLM* as well as of *SQSTM1* and down-regulates *LCK* mRNA levels (Figure 3C).

HMOX1, *GCLM* and *SQSTM1* are components of the cytoprotective response to oxidative stress and, likewise other genes induced after 2cPE treatment, they are under the control of the transcription factor NRF2 [28, 29]. Figure 3D proves that 2cPE treatment augmented NRF2 levels in MEC-1 cells.

Inhibition of the adaptive responses elicited by 2cPE and effects on cell death

Several of 2cPE differentially expressed genes (DEGs) boost adaptive responses devoted for sustaining cell survival. Hence, suppressing these adaptive responses should potentiate apoptosis in response to 2cPE. To verify this hypothesis we co-treated MEC-1 cells with 2cPE in combination with buthionine sulfoximine (BSO), a selective inhibitor of γ-glutamylcysteine synthetase, or with the geldanamycin derivative 17-AAG, an inhibitor of HSP90. BSO alone was unable to trigger cell death but at highest doses it potentiated the pro-death effect of 2cPE, as scored by both PI positivity and caspase activity (Figure 4A). When the ROS generator DMNQ was used, as positive control, the cooperative effect of BSO was more evident (Figure 4A). Treatment with 17-AGG alone induces apoptosis in approximately 30% of cells, independently from the applied dose. When MEC-1 cells pre-incubated with escalating doses of 17-AGG were co-treated with 2cPE, cell death as well as the intensity of caspase activation, were significantly augmented (Figure 4B). Similarly, also bortezomib induced cell death was augmented in the presence of the HSP90 inhibitor (Figure 4B).

Down-regulation of LCK expression might be an important event for the pro-apoptotic activity of 2cPE. Also in this case treatment with an LCK inhibitor (LCKi) might exhibit an additive effect with 2cPE. Figure 3C evidences that co-treatment with 2cPE and LCKi potentiates apoptosis and caspase activation in response to 2cPE.

Markers of responsiveness to 2cPE treatment

The apoptotic responsiveness of B-CLL cells from the different patients to 2cPE is heterogeneous (Table 1). Some cells are highly susceptible and others are resistant. Hence, we decided to use the pattern of all DEGs in all patients to discover markers of 2cPE responsiveness. The lists of DEGs were fused and used to extract the values of single patient differences (fold changes >1.5 <-1.5; *P* values <0.05). An unsupervised clustering analysis was performed and the results are presented as heat map (Figure 5). The apoptotic responsiveness of the different leukemic B-cells is displayed by a colour code. The

B

Commonly up-regulated genes

7,5 6,5 5,5 4,5 3,5 2,5 1,5

Gene symbol	Gene name	2cPE Fold ind.	2cPE P	Bortezomib Fold ind.	Bortezomib P	Biological processes
BAG3	BCL2-associated athanogene 3	4,2462	0,0262	2,1356	0,0086	response to unfolded protein
DNAJB1	DNAJ/HSP40 homolog, subfamily b, member 1	3,8534	0,0226	1,7294	0,0068	response to unfolded protein
DNAJB4	DNAJ/HSP40 homolog, subfamily b, member 4	4,4082	0,0186	1,6538	0,0042	response to unfolded protein
E2F6	E2F transcription factor 6	1,8695	0,0194	1,8537	0,0068	inhibition of transcription
GADD45A	Growth Arrest- and Dna Damage-Inducible gene gadd45, alpha	2,0034	0,0302	1,6606	0,0059	apoptotic process
GCLM	Glutamate-cysteine Ligase, Modifier subunit	5,0008	0,0142	1,9413	0,0043	cysteine metabolic process
HSPA1A	Heat-Shock 70-kD protein 1A	4,6621	0,0155	3,1499	0,0104	response to unfolded protein
HSPA1B	Heat-Shock 70-kD protein 1B	6,9492	0,0183	3,2281	0,0102	response to unfolded protein
HSPA6	Heat-Shock 70-kD protein 6	7,6563	0,0315	1,8104	0,0209	response to unfolded protein
HSPA8	Heat-Shock 70-kD protein 8	1,9407	0,0179	1,6203	0,0160	response to unfolded protein
HSPH1	Heat-Shock 105/110-kD protein	3,2081	0,0203	1,6869	0,0074	response to unfolded protein
KEAP1	Kelch-like ECH-Associated protein 1	1,5506	0,0114	1,5879	0,0064	response to oxidative stress
LRP8	Low Density Lipoprotein Receptor-Related protein 8	1,5270	0,0231	1,6167	0,0095	cholesterol e lipid metabolism
MAFG	V-maf Avian Musculoaponeurotic Fibrosarcoma Oncogene Family, Protein G	2,1370	0,0187	1,6000	0,0051	regulation of cell proliferation
MIR22HG	long non coding RNA	2,7014	0,0203	2,0390	0,0027	chemical stress responses
PSMC2	Proteasome 26S Subunit, ATPase, 2	1,5162	0,0262	2,1857	0,0038	proteasome complex
PSMD14	Proteasome 26S Subunit, Non-ATPase, 14	1,5110	0,0318	2,1162	0,0027	proteasome complex
SRXN1	Sulfiredoxin 1	2,8933	0,0117	1,7259	0,0142	response to oxidative stress
ZFAND2A	Zinc Finger An1 Domain-Containing Protein 2A	2,2129	0,0373	1,7024	0,0106	proteasome complex

Commonly down-regulated genes

Gene symbol	Gene name	2cPE Fold ind.	2cPE P	Bortezomib Fold ind.	Bortezomib P	Biological processes
ADA	Adenosine Deaminase	-1,6760	0,0318	-1,6127	0,0477	metabolic process
AKAP5	A-Kinase Anchor Protein 5	-1,6535	0,0245	-1,6217	0,0116	energy reserve metabolic process
BTLA	B- and T-Lymphocyte Attenuator	-1,6378	0,0492	-1,5515	0,0052	lymphocyte costimulation
DUSP4	Dual-Specificity Phosphatase 4	-2,1808	0,0059	-1,9980	0,0213	inactivation of MAPK activity
ENC1	Ectodermal-Neural Cortex 1	-1,7000	0,0170	-1,5824	0,0146	actin cytoskeleton
FAM111B	Family with Sequence Similarity 111, Member B	-1,7306	0,0200	-1,6207	0,0094	metabolic process
GAPT	GRB2-Binding Adaptor Protein, Transmembrane	-1,7190	0,0283	-1,6868	0,0079	B cell activation
IL2RA	Interleukin 2 Receptor, Alpha	-1,7765	0,0228	-1,6484	0,0189	lymphocyte homeostasis
LILRB2	Leukocyte Immunoglobulin-like Receptor, Subfamily B, Member 2	-1,6349	0,0296	-1,6981	0,0318	positive regulation of tolerance
MS4A7	Membrane-Spanning 4-Domains, Subfamily A, Member 7	-1,6022	0,0291	-1,9534	0,0400	unknown
PVRIG	Poliovirus Receptor Related Immunoglobulin Domain Containing	-2,3021	0,0262	-2,0139	0,0041	unknown
PYCARD	Pyd And Card Domain-containing Protein	-1,6480	0,0224	-1,5048	0,0223	immunw response
RGCC	Regulator of Cell Cycle	-1,5693	0,0190	-1,5511	0,0256	Cell cycle
RNASE6	Ribonuclease, Rnase A Family, 6	-1,9681	0,0205	-1,6640	0,0142	RNA catabolic process
SOWAHD	Sosondowah Ankyrin Repeat Domain Family Member D	-1,7865	0,0286	-1,5023	0,0158	unknown

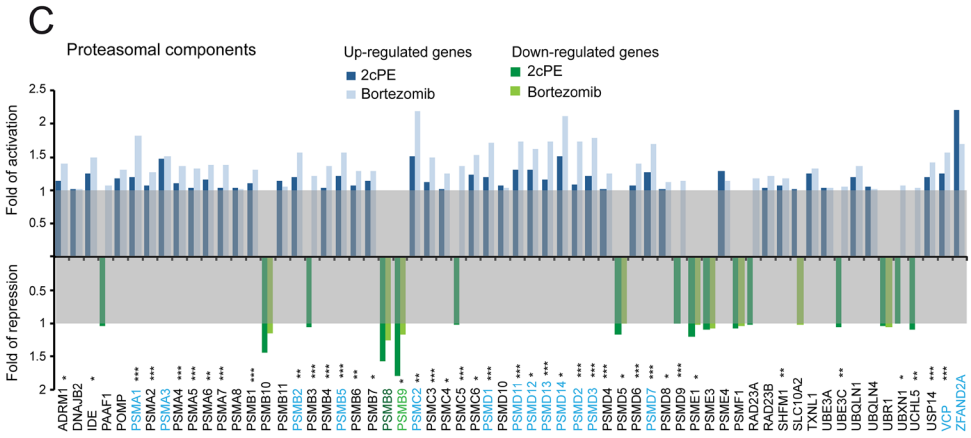

Figure 2: mRNA expression profiling of bortezomib and 2cPE treated B-CLL cells. A. Venn diagram of commonly down (green) and up-regulated (blue) genes (fold changes >1.5; *P* values <0.01) using the paired t-test, in leukemic B-cell from 10 different patients after 2cPE and bortezomib treatments. **B.** List in alphabetic order of the commonly up- and down-regulated genes in leukemic B-cells form the different patients in response to 2cPE and bortezomib treatments (mRNA fold changes >1.5; <-1.5). In the heat map positive values are displayed in blue and negative in dark green. A colour code was selected to illustrate the fold changes. **C.** mRNA fold changes of the different proteasomal components after 2cPE and bortezomib treatments as indicated by the different colours.

Table 2: GO-Terms enrichment analysis

Gene enrichment analysis in 2cPE treated primary B-CLL cells						
GO-Term	**Count**	**%**	**p Value**	**Benjamini**	**FDR**	**Fold Enr**
GO:0006986~response to unfolded protein	13	8,33	1,66E-12	2,67E-09	2,78E-09	19,82
GO:0051789~response to protein stimulus	13	8,33	3,90E-07	1,96E-07	4,08E-07	13,15
GO:0050865~regulation of cell activation	14	8,97	7,16E-09	3,84E-06	1,20E-05	8,66
GO:0010033~response to organic substance	25	16,02	3,11E-08	1,25E-05	5,21E-05	3,75
GO:0006457~protein folding	13	8,33	7,73E-08	1,75E-05	0,00013	7,94
GO:0042981~regulation of apoptosis	25	16,02	2,38E-07	4,80E-05	0,0004	3,37
Gene enrichment analysis in Bortezomib treated primary B-CLL cells						
GO-Term	**Count**	**%**	**p Value**	**Benjamini**	**FDR**	**Fold Enr**
GO:0000502~proteasome complex	14	15,73	4,31E-18	5,26E-16	4,97E-15	42,52
GO:0051351~positive regulation of ligase activity	15	16,85	1,35E-18	1,16E-15	2,09E-15	37,56
GO:0043161~proteasomal protein catabolic process	15	16,85	1,91E-16	1,91E-14	3,44E-13	26,88

hierarchical clustering evidences a strong correlation between the magnitude of changes in DEGs and the induction of cell death. In the case of 2cPE treatment, with the exclusion of patient LLC37, all B-CLL cells responsive to 2cPE in terms of apoptosis, cluster together and show elevated fluctuations of DEGs. On the other side, B-CLL cells, which are resistant to 2cPE treatment evidence fewer transcriptional changes and cluster together. The only exception concerns leukemic cells of patient LLC37, which are resistant to 2cPE treatment but cluster together with responsive cells. Interestingly, LLC37 cells are also partially resistant to bortezomib.

Resistance to 2cPE induced apoptosis in B-CLL cells from patients LLC122, LLC195 and LLC270

The resistance to 2cPE-induced apoptosis, observed in some leukemia B-cells (LLC122, LLC195 and LLC270) is tightly correlated to much lower variations in the transcriptome. This failure could arise from an incapability to process the pro-drug 2cPE in the extracellular environment, as observed in certain cancer cells [20]. mRNA expression levels analysis of PLAG7, the secreted esterase responsible for 2cPE pro-drug maturation, excludes this hypothesis (Supplementary Figure S2).

Alternatively, resistance to 2cPE could arise from a common mRNA signature, as generated during disease progression, through the accumulation of peculiar genetic alterations. This signature should predict drug-responsiveness. To verify this possibility, we performed hierarchical gene clustering analysis, of gene expression profiles of untreated B-CLL cells from all patients. Figure 6A shows that, the B-CLL cells of the three patients resistant to 2cPE treatment cluster together. Next, a standard t-test was performed to rank DEGs between 2cPE unresponsive (*n*3) and the responsive leukemia cells (*n*7) (Figure 6B). The *ATM* gene provided the best score (*P* value 2.9306E-005; fold change -1.87). In accordance, all three patients-derived B-CLL cells display the 11q deletion, which affects the *ATM* locus [30]. Other two genes, *NPAT* and *CUL5* lie in the same chromosome region and they also scored a significant reduction in terms of expression in the non-responsive patients (*P* value 0.0035; fold change -1.69 and *P* value 0.0020; fold change -1.64, respectively).

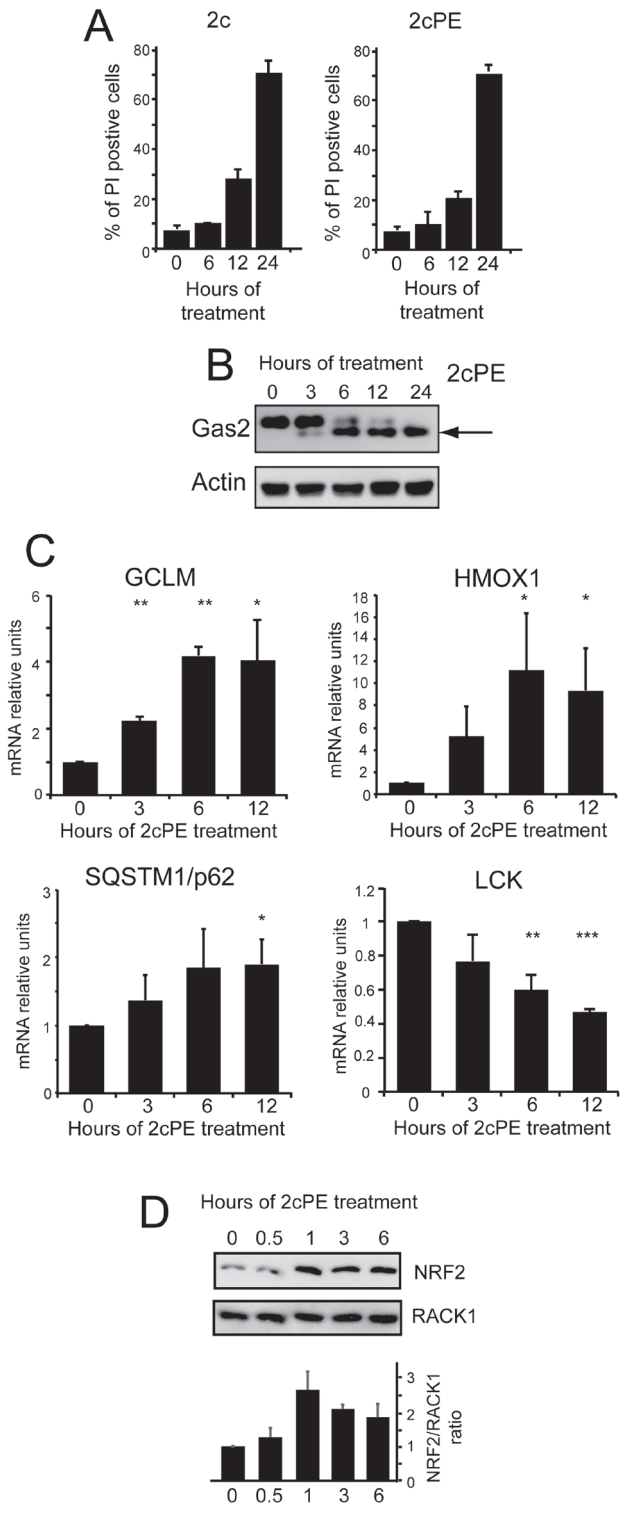

Figure 3: Adaptive responses elicited by 2cPE in MEC-1 cells. A. Induction of cell death in MEC-1 cells after treatment for the indicated times with 2c (2μM) or 2cPE (4μM). Cell viability was calculated as percentage of cells positive to PI staining using cytofluorimetric analysis. **B.** Caspase-dependent processing of the death substrate Gas2 in MEC-1 cells treated for the indicated times with 4μM of 2cPE. Cellular lysates were generated and subjected to immunoblot analysis. Antibodies anti-Gas2 and anti-actin (as loading control) were used. **C.** Time-course analysis of HOMX, GCLM, SQSTM and LCK mRNA expression levels. MEC-1 cells were treated 4μM of 2cPE for the indicated times and the mRNA levels were monitored by qRT-PCR. All reactions were done in triplicate. **D.** Immunoblot and densitometric analysis of NRF2 levels in MEC-1 cells treated for the indicated times with 4μM of 2cPE. Cellular lysates were generated and subjected to immunoblot analysis using the indicated antibodies. Data were from 2 experiments. Columns, mean loss of viability + SD. *=p<0.05; **=p<0.01; ***p=<0.005.

Since ATM is an important signaling molecule, we decided to study whether this kinase is activated in response to 2cPE. Figure 7A demonstrates that the ATM pathway is activated in response to 2cPE, as proved by the phosphorylation of the ATM substrates KAP1, Smc1, Chk2 and p53. The 2cPE-mediated activation of ATM prompted us to evaluate the induction of DNA double-strand breaks. Different concentrations of etoposide were used to induce DSBs and ATM activation. 4μM of 2cPE and 2.5/5 μM of etoposide elicited ATM activation at comparable intensities, as scored by KAP1 phosphorylation (Figure 7B). A robust increase of γH2AX positivity (a marker of DSBs) can be appreciated in cells treated with 2.5 or 5 μM of etoposide. By contrast, only a modest but significant increase in γH2AX positivity was triggered by 2cPE treatment (Figure 7C). We confirmed these data by a time-course analysis. Again a modest, compared to etoposide, but significant increase in γH2AX was detectable in 2cPE treated cells at 6 hour (Figure 7D).

Next we investigated the contribution of ATM in 2cPE-induced gene expression changes. Inhibition of the ATM kinase using the specific inhibitor KU-55933 did not influenced the 2cPE-mediated up-regulation of *GCLM, HOMX, SQSTM1* and the down-regulation

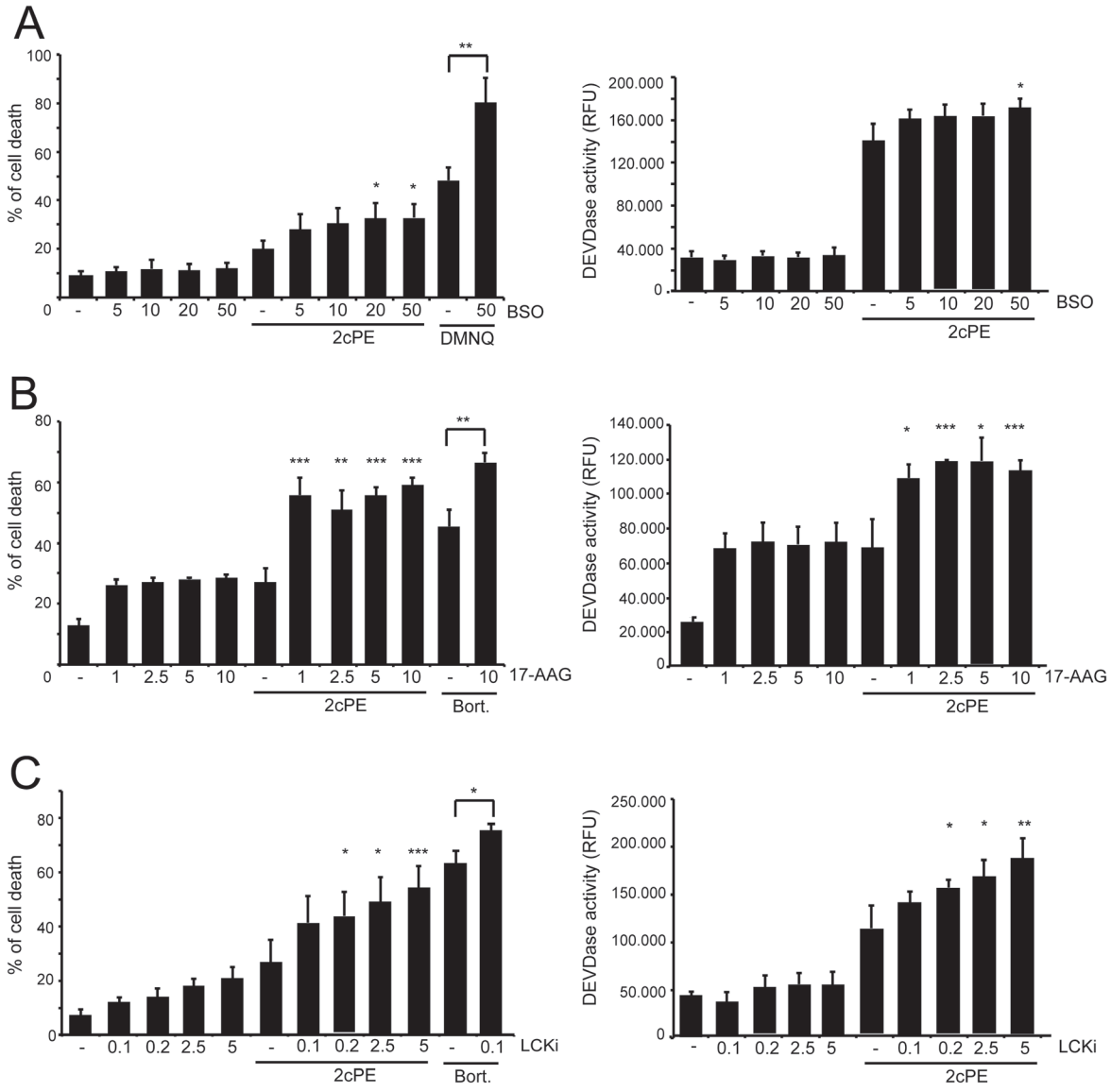

Figure 4: Interfering with the different adaptive responses elicited by 2cPE augmented the apoptotic response. A. MEC-1 cells were pre-treated with the indicated concentrations (μM) of BSO, for 24 h. Next, 2cPE (1μM), DMNQ (20μM) were added for further 24 h. **B.** MEC-1 cells were pre-treated with the indicated concentrations (μM) of 17-AAG for 1 h. Next, 2cPE (1μM), bortezomib (0.5 μM) were added for further 24 h. **C.** MEC-1 cells were pre-treated with the indicated concentrations (μM) of LCKi for 16 h. Next, 2cPE (1μM), bortezomib (0.5 μM) were added for further 24 h. Cell death was scored by PI staining using cytofluorimetric analysis and caspase activity was measured in parallel. Columns, mean (n = 3); bars, SD. *=p<0.05; **=p<0.01; ***p=<0.005.

of *LCK* (Figure 7E). Surprisingly, when the effect on cell survival was evaluated, the ATM inhibitor strongly potentiated apoptosis in response to 2cPE (Figure 8A). To confirm this result we used ataxia telangiectasia (AT)-derived lymphoblastoid cell lines (AT-LCLs) WT or lacking ATM protein expression, due to the homozygous mutation AT-52RM [31]. Figure 8B illustrates that cells lacking ATM expression are more sensitive to death induced by 2cPE treatment. Finally, we also generated MEC-1 cells with down-regulated ATM expression after lentiviral infections with a specific shRNA (Figure 8C). MEC-1 cells with down-regulated ATM were more susceptible to apoptosis after 2cPE treatment (Figure 8D).

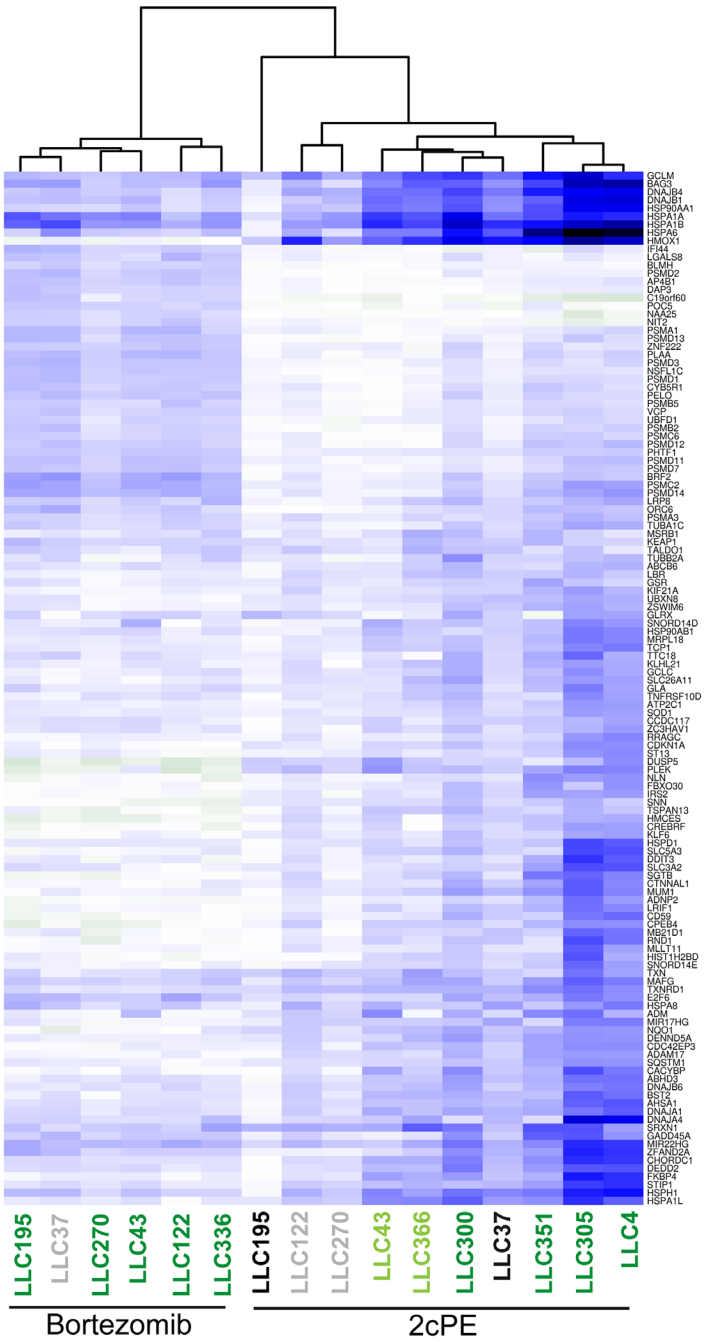

Figure 5: Resistance to 2cPE induced apoptosis correlates with the magnitude of changes in DEGs. DEGs induced by 2cPE or bortezomib treatments in B-CLL cells were hierarchically clustered as described in the material and methods. In the heat map up-regulated genes are displayed in blue and down-regulated genes in dark green. A colour code was used to represent the apoptotic responsiveness to 2cPE and bortezomib of the different B-CLL cells. Apoptosis >75% (dark green); apoptosis between 46-74% (light green) apoptosis <20% (grey) apoptosis <10% (black).

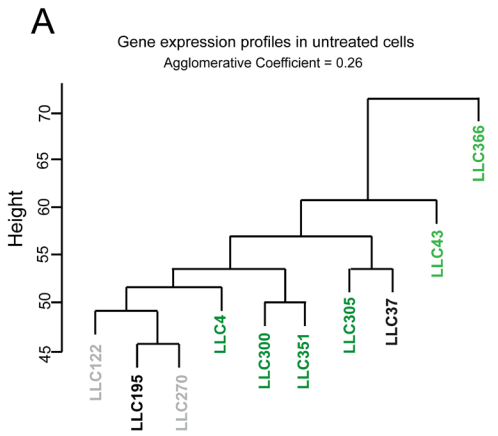

B

Symbol	Average resistant	Average responsive	Difference (FC)	p value
ATM	5,557007	6,461726	-1,87218	2,93E-05
ZNF667	4,640185	3,183585	2,744606	0,000258
CHST11	8,010218	7,157189	1,806289	0,000296
EHBP1L1	7,345079	6,585199	1,693349	0,000886
HIBCH	7,173304	6,460273	1,639245	0,001421
AHNAK	8,774350	7,763406	2,015229	0,001809
CUL5	7,124498	7,838978	-1,64089	0,002021
H1FX	8,152085	6,383874	3,406312	0,002371
SEMA4A	7,125484	5,685719	2,712767	0,002398
TAGLN2	9,437318	8,527226	1,879165	0,002464

Figure 6: ATM and the resistance to 2cPE. A. Hierarchical clustering of gene expression profiles of untreated B-CLL cells from the different patients. A colour code was used to represent the apoptotic responsiveness to 2cPE and bortezomib of the different B-CLL cells. Apoptosis >75% (dark green); apoptosis between 46-74% (light green) apoptosis <20% (grey) apoptosis <10% (black). **B.** 10 top DEGs in untreated B-CLL cells from patients LLC122, LLC195 and LLC270 compared to the untreated leukemia cells, responsive to 2cPE, from all other patients. DEGs were ranked for *P* value.

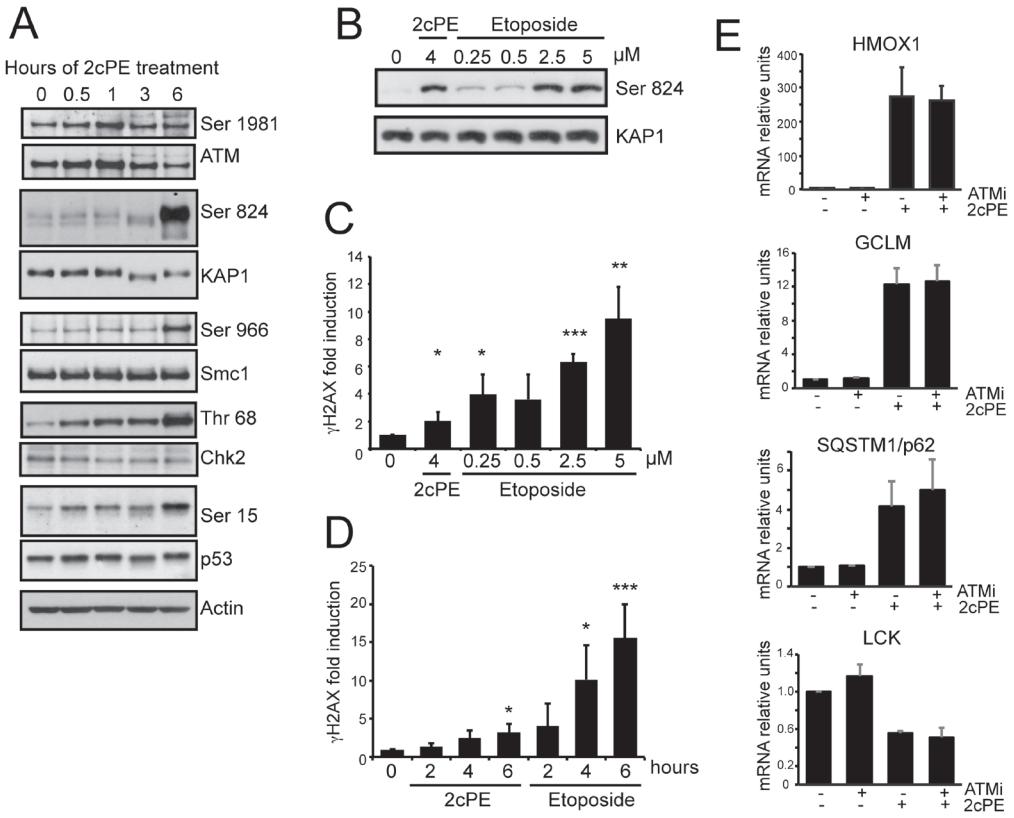

Figure 7: 2cPE activates ATM signaling. A. Activation of the ATM signaling pathway in response to 2cPE treatment. Cellular lysates were generated at the indicated time points and subjected to immunoblot analysis. The detected proteins and their phosphorylated forms are indicated. Actin was used as loading control. **B.** Immunoblot analysis comparing ATM activation in response to etoposide and 2cPE. KAP1 phosphorylation was used as read-out for ATM activation. MEC-1 cells were treated for 6 h with the indicated concentrations of the two drugs. **C.** Quantitative cytofluorimetric analysis of γH2AX positivity as marker of DNA damage induction. MEC-1 cells were treated for 6 hours with the indicated concentrations of the two drugs. **D.** Time-course of γH2AX positivity by quantitative cytofluorimetric analysis. MEC-1 cells were treated for the indicated hours with 4μM of 2cPE or 2.5μM of etoposide. **E.** Time-course analysis of HOMX, GCLM, SQSTM and LCK mRNA expression levels in MEC-1 cells treated with 4μM of 2cPE in the presence of the ATM inhibitor KU-55933. Cells were pre-treated for 1 hour with KU-55933 (10μM), next, 2cPE was added for further 6 h. Columns, mean (n = 3); bars, SD. *=p<0.05; **=p<0.01; ***p=<0.005.

DISCUSSION

Although bortezomib has proved inefficacy for the treatment of CLL patients [8], the UPS represents a promising therapeutic target and new UPS inhibitors are under evaluation [32–34]. In this manuscript we have demonstrated that 2cPE triggers apoptosis in B-CLL cells and activates multiple transcriptional programs.

The vast majority of DEGs associated to 2cPE and bortezomib treatments encode for elements of stress response pathways, aimed to sustain cell survival. Interfering with such adaptive pathways potentiates the pro-death effect of 2cPE. This discovery could help to improve the anti-neoplastic efficiency of these molecules, by applying selective co-treatments.

Interestingly 2cPE is a stronger inducer of proteotoxic stress compared to bortezomib. Proteotoxic stress is emerging as an attracting druggable response. Malignant cells exhibit higher levels of proteotoxic stress, as a consequence of their higher proliferative and mutational status [35–38]. This peculiarity renders cancer cells more dependent on the UPS and more vulnerable

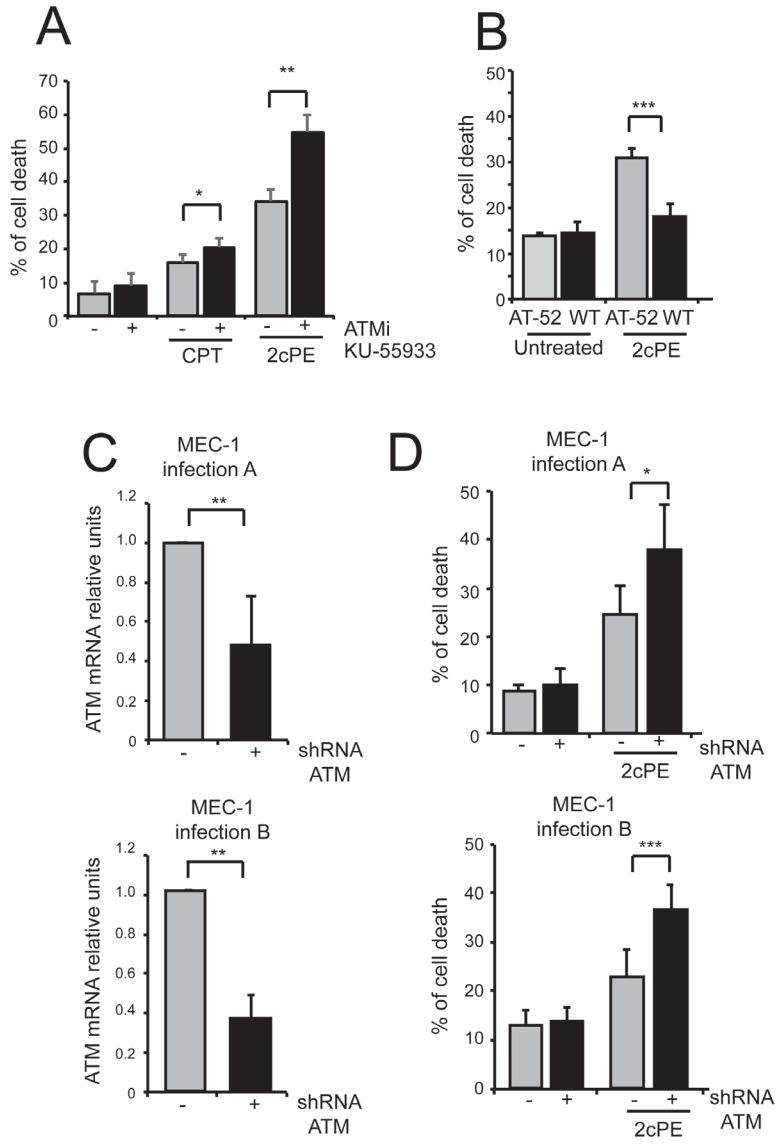

Figure 8: ATM inhibition strengthens apoptosis induced by 2cPE. A. MEC-1 cells were pre-treated for 1 hour with KU-55933 (10μM). Next, 2cPE (2μM) or camptothecin (CTP) (50μM) were added for further 20 h. Cell death was calculated as percentage of cells positive to PI staining using cytofluorimetric analysis. **B.** LCL cells WT or AT-52 mutated were treated for 22 h with 2μM of 2cPE. Cell death was scored by PI staining using cytofluorimetric analysis. **C.** ATM mRNA levels in MEC-1 cells expressing the shRNA against ATM or the control, as generated by two distinct lentiviral infections. **D.** MEC-1 cells with down-regulated ATM expression generated after two distinct infections (A and B) and control cells were treated with 2cPE (0.5μM) for 6 h. Cell death was calculated as percentage of cells positive to PI staining using cytofluorimetric analysis. Columns, mean (n = 4); bars, SD. *=p<0.05; **=p<0.01; ***p=<0.005.

to its inhibitors or to inducers of proteotoxic stress [39, 40]. We propose that 2cPE and similar compounds are efficient anti-neoplastic drugs *in vivo*, because they elicit a vicious cycle, by triggering proteotoxic stress in cancer cells, which already exhibit high level of such stress. By contrast, 2cPE-induced proteotoxic stress is manageable in normal cells, thus explaining the absence of general toxicity *in vivo* [40–42]. It is possible that 2cPE and similar compounds, in addition of targeting the catalytic cysteine of isopeptidases, react with and consume the glutathione pool, thus provoking oxidative-stress. In fact, NRF2 is activated and the GSH regenerating system is up-regulated in response to 2cPE. Moreover, pre-treatment of G5 with N-acetylcysteine completely abrogates its apoptotic activity (data not shown).

Because of the heterogeneity of this disease [43], some leukemia cells are resistant to 2cPE treatment. Gene expression profile analysis indicates two different conditions of resistance. In the first case, cells display overt changes in DEGs associated to 2cPE (patient LLC37). In the second case, which comprises leukemia cells from patients LLC122, LLC195 and LLC270, DEGs changes are dramatically reduced.

The components of the apoptotic machinery in LLC37 cells, (BCL2 family members and caspases) do not evidence alterations in their expression (data not shown). Hence, currently we cannot explain the origin of such resistance. Importantly, LLC37 cells were analogously resistant to bortezomib.

In leukemia cells from patients LLC122, LLC195 and LLC270, resistance is not due to deficit in pro-drug maturation, as recently observed in other cancer cells [20]. Hierarchical gene clustering analysis of the different patient-derived B-CLL cells and the presence of the 11q deletion suggested that ATM could be a candidate for such resistant phenotype. The ATM kinase has a well-defined role in sensing DNA double-strand breaks (DSB) and transducing downstream signals that activate the DNA repair and the cell cycle checkpoint machinery [44]. Notably, the ATM signaling pathway was stimulated by 2cPE.

ATM is also activated by oxidative stress, through a mechanism distinct to that of activation by DNA breaks [45]. The activation of the anti-oxidants response and the feeble appearance of DSBs in 2cPE treated cells, suggest that a perturbed redox balance might be responsible for ATM activation [46]. In an unexpected manner, ATM inhibition reinforced apoptosis in 2cPE treated cells. Hence, ATM cannot be responsible for the apoptotic resistance to 2cPE. Although we do not have an explanation for such resistance, our results disclose a new opportunity for testing 2cPE in cancer cells that have accumulated mutations in ATM, in p53, or in both genes [47, 48].

In conclusion we have demonstrated that 2cPE triggers pleiotropic cellular stresses. At first glance induction of multiple stresses does not seem to be attractive for the selective elimination of neoplastic cells, however several recent reports about the effectiveness in animal models of this class of compounds [12, 14, 15, 20] justify further studies to improve their anti-neoplastic activities.

MATERIALS AND METHODS

Patients, cell separation and culture conditions

The ethic approval for our study was obtained from ethic committee of "Regione Veneto": (Prot.n. 2662P). We obtained peripheral blood from 10 patients that satisfied standard morphological and immunophenotypic criteria for CLL according to the guidelines of the International Workshop on Chronic Lymphocytic Leukemia IWCLL [49]. No patient was previously treated with bortezomib or other proteasome inhibitors. Peripheral blood mononuclear cells (PBMCs) were isolated as previously described [50]. All samples utilized had a $CD19^+$ B-cell content greater than 95%. Purified cells were cultured in RPMI-1640 medium supplemented with 10% heated inactivated fetal calf serum (FCS; Invitrogen, Paisley, UK). Human chronic B-cell leukemia, MEC-1 cells and EBV-immortalized lymphoblastoid cell lines (LCLs) WT and AT52RM and compound heterozygous mutations 7626 C→T/8365 del A, were grown under similar conditions. Mediums were supplied with heated inactivated fetal calf serum (FCS; Sigma Aldrich), penicillin (100 U/mL), glutamine (2 mmol/L), and streptomycin (100 μg/mL).

Reagents and antibodies

Chemicals used were: bortezomib (LC Laboratories), 2,3-dimethoxy-1,4-naphthoquinone (DMNQ), Propidium Iodide (Sigma Aldrich), buthionine sulfoximine (BSO), 7-cyclopentyl-5-(4-phenoxyphenly)-7H-pyrrolo[2,3-d]pyrimidin-4-amine LCK inhibitor (LCKi), 17-(Allylamino)-17-demethoxygeldanamycin (17-AAG) (Cayman Chemicals), ATM inhibitor (KU-55933) (Abcam Biochemicals), 2c ((*E*)-3,5-Bis[(p-nitrophenyl)methylidene]-4-hydroxycyclohexanone), 2cPE ((*E*)-3,5-Bis[(p-nitrophenyl)methylidene]-4-oxocyclohexyl polyethyleneglycol succinate). Primary antibodies used were: anti-phospho-Ser139 H2A.X, anti-pKAP-1/TIF1β Ser824 and anti-KAP1/TIF1β (Cell Signaling), anti-actin (a2066 Sigma) anti-NRF2 (Santa Cruz Biotechnology).

RNA expression array and data analysis

Total RNA was isolated using RNeasy Mini kit (Qiagen). RNA samples concentration and purity (assessed as 260/280 nm and 260/230 nm ratios) were evaluated by NanoDrop ND-1000 spectrophotometer (NanoDrop Technologies; Wilmington, DE), while RNA integrity was assessed by using the Agilent 2100 Bioanalyzer (Agilent Technologies; Waldbrunn, Germany). For gene expression profiling (GEP) cDNA

synthesis and biotin-labeled target synthesis were performed using the GeneAtlas 3′ IVT Express Kit according to the protocol supplied by Affymetrix. The HG-U219 Array Strips (Affymetrix; Santa Clara, CA) hybridization, staining, and scanning were performed by using the GeneAtlas Platform. All the GEP data have been deposited in the NCBI's Gene Expression (GEO) public repository http://www.ncbi.nlm.nih.gov/geo/query/acc.cgi?token=kbapyckufpcdxwh&acc=GSE74514. Data analysis was performed using the paired t-test as previously described [51]. *P* values were adjusted for multiple testing using the False Discovery Rate method. Differentially expressed genes (DEGs) were selected based on fold change >1.5 and <-1.5 fold and *P* values <0.05. The analysis of Gene Ontology terms was performed using the DAVID server. DEGs in response to 2cPE or bortezomib were clustered using hierarchical clustering by computing the Euclidean distance and applying the complete linkage method. For the hierarchical clustering of the gene expression profiles of B-CLL cells from different patients before drug-treatment the average linkage method was used.

RNA extraction and qRT-PCR analysis

RNA was extracted using Tri-Reagent (Molecular Research Center) and retrotranscribed by using 100U of Moloney murine leukemia virus reverse transcriptase (Invitrogen). The primer sequences used are available upon request. Quantitative reverse transcription-PCR (qRT-PCR) analyses were performed using Bio-Rad CFX96 and SYBR Green technology. HPRT and GAPDH were used as normalizer genes. All reactions were done in triplicate. Data were from al least 3 experiments ± SD.

Caspase activation assays and cytofluorimetric analysis

Analysis of caspase-3 activation was performed using Caspase-3 fluorescent assay kit (Cayman chemical). For quantification of cell death, cells were re-suspended in 500 μL of PBS and stained with propidium iodide (PI). Fluorescence was determined with a FACScan™ (Beckman Dickinson). To detect H2AX phosphorylation cells were fixed in paraformaldehyde 3% for 20' at room temperature, permeabilized with 0.1% TritonX-100 and incubated with the primary antibody anti-pH2AX for 1hr. After washes, cells were incubated with the secondary antibody anti-rabbit Alexa Fluo-488 (Invitrogen) for 30 min. Results were from al least 3 experiments ± SD.

Western blotting and lentiviral infections

Proteins obtained after an SDS denaturating lysis and sonication were transferred to nitrocellulose membrane and incubated with the specific primary antibodies. Secondary antibodies were peroxidase-conjugated goat anti-rabbit or anti-mouse (Sigma). Blots were developed with Super Signal West Dura (Pierce). For stable ATM down-regulation, the vector-based shRNA interference pLenti6/BLOCK-iT-DEST (Invitrogen) was used as previously described [52]. Culture supernatant obtained from transfected recipient 293 cells, containing viral particles, was recovered and used to infect MEC-1 cells.

CONFLICTS OF INTEREST

The authors declare no conflicts of interest

FINANCIAL SUPPORT

This work was supported by FIRB (Progetto RBAP11S8C3_002) and by AIRC (Associazione Italiana per la Ricerca sul Cancro) to C.B, L.T. and G.S.

REFERENCES

1. Billard C, Merhi F, Bauvois B. Mechanistic insights into the antileukemic activity of hyperforin. Curr Cancer Drug Targets. 2013; 13:1-10.
2. Fakler M, Loeder S, Vogler M, Schneider K, Jeremias I, Debatin KM, Fulda S. Small molecule XIAP inhibitors cooperate with TRAIL to induce apoptosis in childhood acute leukemia cells and overcome Bcl-2-mediated resistance. Blood. 2009; 113:1710-22. doi: 10.1182/blood-2007-09-114314.
3. Smit LA, Hallaert DY, Spijker R, de Goeij B, Jaspers A, Kater AP, van Oers MH, van Noesel CJ, Eldering E. Differential Noxa/Mcl-1 balance in peripheral versus lymph node chronic lymphocytic leukemia cells correlates with survival capacity. Blood. 2007; 109:1660-8.
4. Pepper C, Lin TT, Pratt G, Hewamana S, Brennan P, Hiller L, Hills R, Ward R, Starczynski J, Austen B, Hooper L, Stankovic T, Fegan C. Mcl-1 expression has in vitro and in vivo significance in chronic lymphocytic leukemia and is associated with other poor prognostic markers. Blood. 2008; 112:3807-17. doi: 10.1182/blood-2008-05-157131.
5. Fulda S. Exploiting inhibitor of apoptosis proteins as therapeutic targets in hematological malignancies. Leukemia. 2012; 26:1155-65. doi: 10.1038/leu.2012.4.
6. Kelley TW, Alkan S, Srkalovic G, Hsi ED. Treatment of human chronic lymphocytic leukemia cells with the proteasome inhibitor bortezomib promotes apoptosis. Leuk Res. 2004; 28:845-50.
7. Pahler JC, Ruiz S, Niemer I, Calvert LR, Andreeff M, Keating M, Faderl S, McConkey DJ. Effects of the proteasome inhibitor, bortezomib, on apoptosis in isolated lymphocytes obtained from patients with chronic lymphocytic leukemia. Clin Cancer Res. 2003; 9:4570-7.
8. Faderl S, Rai K, Gribben J, Byrd JC, Flinn IW, O'Brien S, Sheng S, Esseltine DL, Keating MJ. Phase II study of single-agent bortezomib for the treatment of patients with

fludarabine-refractory B-cell chronic lymphocytic leukemia. Cancer. 2006; 107:916-24.

9. Liu FT, Agrawal SG, Movasaghi Z, Wyatt PB, Rehman IU, Gribben JG, Newland AC, Jia L. Dietary flavonoids inhibit the anticancer effects of the proteasome inhibitor bortezomib. Blood. 2008; 112:3835-46. doi: 10.1182/blood-2008-04-150227.

10. Arastu-Kapur S, Anderl JL, Kraus M, Parlati F, Shenk KD, Lee SJ, Muchamuel T, Bennett MK, Driessen C, Ball AJ, Kirk CJ. Nonproteasomal targets of the proteasome inhibitors bortezomib and carfilzomib: a link to clinical adverse events. Clin Cancer Res. 2011; 17:2734-43. doi: 10.1158/1078-0432.CCR-10-1950.

11. Aleo E, Henderson CJ, Fontanini A, Solazzo B, Brancolini C. Identification of new compounds that trigger apoptosome-independent caspase activation and apoptosis. Cancer Res. 2006; 66:9235-44.

12. Coughlin K, Anchoori R, Iizuka Y, Meints J, MacNeill L, Vogel RI, Orlowski RZ, Lee MK, Roden RB, Bazzaro M. Small-molecule RA-9 inhibits proteasome-associated DUBs and ovarian cancer in vitro and in vivo via exacerbating unfolded protein responses. Clin Cancer Res. 2014; 20:3174-86. doi: 10.1158/1078-0432.CCR-13-2658.

13. Mullally JE, Fitzpatrick FA. Pharmacophore model for novel inhibitors of ubiquitin isopeptidases that induce p53-independent cell death. Mol Pharmacol. 2002; 62:351-8.

14. D'Arcy P, Brnjic S, Olofsson MH, Fryknas M, Lindsten K, De Cesare M, Perego P, Sadeghi B, Hassan M, Larsson R, Linder S. Inhibition of proteasome deubiquitinating activity as a new cancer therapy. Nat Med. 2011; 17:1636-40. doi: 10.1038/nm.2536.

15. Kapuria V, Peterson LF, Fang D, Bornmann WG, Talpaz M, Donato NJ. Deubiquitinase inhibition by small-molecule WP1130 triggers aggresome formation and tumor cell apoptosis. Cancer Res. 2010; 70:9265-76. doi: 10.1158/0008-5472.CAN-10-1530.

16. Selvendiran K, Kuppusamy ML, Bratasz A, Tong L, Rivera BK, Rink C, Sen CK, Kálai T, Hideg K, Kuppusamy P. Inhibition of vascular smooth-muscle cell proliferation and arterial restenosis by HO-3867, a novel synthetic curcuminoid, through up-regulation of PTEN expression. J Pharmacol Exp Ther. 2009; 329:959-66. doi: 10.1124/jpet.108.150367.

17. Fontanini A, Foti C, Potu H, Crivellato E, Maestro R, Bernardi P, Demarchi F, Brancolini C. The Isopeptidase Inhibitor G5 Triggers a Caspase-independent Necrotic Death in Cells Resistant to Apoptosis: A comparative study with the proteasome inhibitor bortezomib. J Biol Chem. 2009; 284:8369-81. doi: 10.1074/jbc.M806113200.

18. Tomasella A, Blangy A, Brancolini C. A receptor-interacting protein 1 (RIP1)-independent necrotic death under the control of protein phosphatase PP2A that involves the reorganization of actin cytoskeleton and the action of cofilin-1. J Biol Chem. 2014; 289:25699-710. doi: 10.1074/jbc.M114.575134.

19. Foti C, Florean C, Pezzutto A, Roncaglia P, Tomasella A, Gustincich S, Brancolini C. Characterization of caspase-dependent and caspase-independent deaths in glioblastoma cells treated with inhibitors of the ubiquitin-proteasome system. Mol Cancer Ther. 2009; 8:3140-50. doi: 10.1158/1535-7163.MCT-09-0431.

20. Cersosimo U, Sgorbissa A, Foti C, Drioli S, Angelica R, Tomasella A, Picco R, Semrau MS, Storici P, Benedetti F, Berti F, Brancolini C. Synthesis, characterization, and optimization for in vivo delivery of a nonselective isopeptidase inhibitor as new antineoplastic agent. J Med Chem. 2015; 58:1691-704. doi: 10.1021/jm501336h.

21. Oerlemans R, Franke NE, Assaraf YG, Cloos J, van Zantwijk I, Berkers CR, Scheffer GL, Debipersad K, Vojtekova K, Lemos C, van der Heijden JW, Ylstra B, Peters GJ, et al. Molecular basis of bortezomib resistance: proteasome subunit beta5 (PSMB5) gene mutation and overexpression of PSMB5 protein. Blood. 2008; 112:2489-99. doi: 10.1182/blood-2007-08-104950.

22. Zhu YX, Tiedemann R, Shi CX, Yin H, Schmidt JE, Bruins LA, Keats JJ, Braggio E, Sereduk C, Mousses S, Stewart AK. RNAi screen of the druggable genome identifies modulators of proteasome inhibitor sensitivity in myeloma including CDK5. Blood. 2011; 117:3847-57. doi: 10.1182/blood-2010-08-304022.

23. Busse A, Kraus M, Na IK, Rietz A, Scheibenbogen C, Driessen C, Blau IW, Thiel E, Keilholz U. Sensitivity of tumor cells to proteasome inhibitors is associated with expression levels and composition of proteasome subunits. Cancer. 2008; 112:659-70. doi: 10.1002/cncr.23224.

24. Gozzelino R, Jeney V, Soares MP. Mechanisms of cell protection by heme oxygenase-1. Annu Rev Pharmacol Toxicol. 2010; 50:323-54. doi: 10.1146/annurev.pharmtox.010909.105600.

25. Nezis IP, Stenmark H. p62 at the interface of autophagy, oxidative stress signaling, and cancer. Antioxid Redox Signal. 2012; 17:786-93. doi: 10.1089/ars.2011.4394.

26. Majolini MB, D'Elios MM, Galieni P, Boncristiano M, Lauria F, Del Prete G, Telford JL, Baldari CT. Expression of the T-cell-specific tyrosine kinase Lck in normal B-1 cells and in chronic lymphocytic leukemia B cells. Blood. 1998; 91:3390-6.

27. Sgorbissa A, Benetti R, Marzinotto S, Schneider C, Brancolini C. Caspase-3 and caspase-7 but not caspase-6 cleave Gas2 in vitro: implications for microfilament reorganization during apoptosis. J Cell Sci. 1999; 112:4475-82.

28. Ye P, Mimura J, Okada T, Sato H, Liu T, Maruyama A, Ohyama C, Itoh K. Nrf2- and ATF4-dependent upregulation of xCT modulates the sensitivity of T24 bladder carcinoma cells to proteasome inhibition. Mol Cell Biol. 2014; 34:3421-34. doi: 10.1128/MCB.00221-14.

29. Son YO, Pratheeshkumar P, Roy RV, Hitron JA, Wang L, Divya SP, Xu M, Luo J, Chen G, Zhang Z, Shi X. Anti-oncogenic and oncogenic properties of Nrf2 in arsenic-induced carcinogenesis. J Biol Chem. 2015; 290:27090-100. doi: 10.1074/jbc.M115.675371.

30. Stankovic T, Skowronska A. The role of ATM mutations and 11q deletions in disease progression in chronic lymphocytic leukemia. Leuk Lymphoma. 2014; 55:1227-39. doi: 10.3109/10428194.2013.829919.

31. Takagi M, Delia D, Chessa L, Iwata S, Shigeta T, Kanke Y, Goi K, Asada M, Eguchi M, Kodama C, Mizutani S. Defective control of apoptosis, radiosensitivity, and spindle checkpoint in ataxia telangiectasia. Cancer Res. 1998; 58:4923-9.

32. Gupta SV, Hertlein E, Lu Y, Sass EJ, Lapalombella R, Chen TL, Davis ME, Woyach JA, Lehman A, Jarjoura D, Byrd JC, Lucas DM. The proteasome inhibitor carfilzomib functions independently of p53 to induce cytotoxicity and an atypical NF-kappaB response in chronic lymphocytic leukemia cells. Clin Cancer Res. 2013; 19:2406-19. doi: 10.1158/1078-0432.CCR-12-2754.

33. Crawford LJ, Irvine AE. Targeting the ubiquitin proteasome system in haematological malignancies. Blood Rev. 2013; 27:297-304. doi: 10.1016/j.blre.2013.10.002.

34. Mistry H, Hsieh G, Buhrlage SJ, Huang M, Park E, Cuny GD, Galinsky I, Stone RM, Gray NS, D'Andrea AD, Parmar K. Small-molecule inhibitors of USP1 target ID1 degradation in leukemic cells. Mol Cancer Ther. 2013; 12:2651-62. doi: 10.1158/1535-7163.MCT-13-0103-T.

35. Davis AL, Qiao S, Lesson JL, Rojo de la Vega M, Park SL, Seanez CM, Gokhale V, Cabello CM, Wondrak GT. The quinone methide aurin is a heat shock response inducer that causes proteotoxic stress and Noxa-dependent apoptosis in malignant melanoma cells. J Biol Chem. 2015; 290:1623-38. doi: 10.1074/jbc.M114.592626.

36. Tan K, Fujimoto M, Takii R, Takaki E, Hayashida N, Nakai A. Mitochondrial SSBP1 protects cells from proteotoxic stresses by potentiating stress-induced HSF1 transcriptional activity. Nat Commun. 2015; 6:6580. doi: 10.1038/ncomms7580.

37. De Raedt T, Walton Z, Yecies JL, Li D, Chen Y, Malone CF, Maertens O, Jeong SM, Bronson RT, Lebleu V, Kalluri R, Normant E, Haigis MC et al. Exploiting cancer cell vulnerabilities to develop a combination therapy for ras-driven tumors. Cancer Cell. 2011; 20:400-13. doi: 10.1016/j.ccr.2011.08.014.

38. Bazzaro M, Lee MK, Zoso A, Stirling WL, Santillan A, Shih Ie M, Roden RB. Ubiquitin-proteasome system stress sensitizes ovarian cancer to proteasome inhibitor-induced apoptosis. Cancer Res. 2006; 66:3754-63.

39. Bailey CK, Budina-Kolomets A, Murphy ME, Nefedova Y. Efficacy of the HSP70 inhibitor PET-16 in multiple myeloma. Cancer Biol Ther. 2015; 16:1422-6. doi: 10.1080/15384047.2015.1071743.

40. Chitta K, Paulus A, Akhtar S, Blake MK, Caulfield TR, Novak AJ, Ansell SM, Advani P, Ailawadhi S, Sher T, Linder S, Chanan-Khan A. Targeted inhibition of the deubiquitinating enzymes, USP14 and UCHL5, induces proteotoxic stress and apoptosis in Waldenstrom macroglobulinaemia tumour cells. Br J Haematol. 2015; 169:377-90. doi: 10.1111/bjh.13304. Epub 2015 Feb 17.

41. Raj L, Ide T, Gurkar AU, Foley M, Schenone M, Li X, Tolliday NJ, Golub TR, Carr SA, Shamji AF, Stern AM, Mandinova A, Schreiber SL, et al. Selective killing of cancer cells by a small molecule targeting the stress response to ROS. Nature. 2011; 475:231-4. doi: 10.1038/nature10167.

42. Dai C, Dai S, Cao J. Proteotoxic stress of cancer: implication of the heat-shock response in oncogenesis. J Cell Physiol. 2012; 227:2982-7. doi: 10.1002/jcp.24017.

43. Hallek M. Chronic lymphocytic leukemia: 2015 Update on diagnosis, risk stratification, and treatment. Am J Hematol. 2015; 90:446-60. doi: 10.1002/ajh.23979.

44. Shiloh Y, Ziv Y. The ATM protein kinase: regulating the cellular response to genotoxic stress, and more. Nat Rev Mol Cell Biol. 2013; 14:197-210.

45. Guo Z, Deshpande R, Paull TT. ATM activation in the presence of oxidative stress. Cell Cycle. 2010; 9:4805-11.

46. Cosentino C, Grieco D, Costanzo V. ATM activates the pentose phosphate pathway promoting anti-oxidant defence and DNA repair. EMBO J. 2011; 30:546-55. doi: 10.1038/emboj.2010.330.

47. Negrini S, Gorgoulis VG, Halazonetis TD. Genomic instability—an evolving hallmark of cancer. Nat Rev Mol Cell Biol. 2010; 11:220-8. doi: 10.1038/nrm2858.

48. Zhou B, Zuo Y, Li B, Wang H, Liu H, Wang X, Qiu X, Hu Y, Wen S, Du J, Bu X. Deubiquitinase inhibition of 19S regulatory particles by 4-arylidene curcumin analog AC17 causes NF-kappaB inhibition and p53 reactivation in human lung cancer cells. Mol Cancer Ther. 2013; 12:1381-92. doi: 10.1158/1535-7163.MCT-12-1057.

49. Hallek M, Cheson BD, Catovsky D, Caligaris-Cappio F, Dighiero G, Dohner H, Hillmen P, Keating MJ, Montserrat E, Rai KR, Kipps TJ. Guidelines for the diagnosis and treatment of chronic lymphocytic leukemia: a report from the International Workshop on Chronic Lymphocytic Leukemia updating the National Cancer Institute-Working Group 1996 guidelines. Blood. 2008;111:5446-56. doi: 10.1182/blood-2007-06-093906. Epub 2008 Jan 23.

50. Frezzato F, Trimarco V, Martini V, Gattazzo C, Ave E, Visentin A, Cabrelle A, Olivieri V, Zambello R, Facco M, Zonta F, Cristiani A, Brunati AM, et al. Leukaemic cells from chronic lymphocytic leukaemia patients undergo apoptosis following microtubule depolymerization and Lyn inhibition by nocodazole. Br J Haematol. 2014;165:659-72. doi: 10.1111/bjh.12815.

51. Picco R, Tomasella A, Fogolari F, Brancolini C. Transcriptomic analysis unveils correlations between regulative apoptotic caspases and genes of cholesterol homeostasis in human brain. PLoS One. 2014;9:e110610. doi: 10.1371/journal.pone.0110610.

52. Carlessi L, De Filippis L, Lecis D, Vescovi A, Delia D. DNA-damage response, survival and differentiation in vitro of a human neural stem cell line in relation to ATM expression. Cell Death Differ. 2009;16:795-806. doi: 10.1038/cdd.2009.10.

Ciotti et al. *Cell Death and Disease* (2018)9:184
DOI 10.1038/s41419-017-0259-1

Cell Death & Disease

ARTICLE Open Access

The binding landscape of a partially-selective isopeptidase inhibitor with potent pro-death activity, based on the bis (arylidene)cyclohexanone scaffold

Sonia Ciotti[1], Riccardo Sgarra[2], Andrea Sgorbissa[1], Carlotta Penzo[2], Andrea Tomasella[1], Federico Casarsa[3], Fabio Benedetti[3], Federico Berti[3], Guidalberto Manfioletti[2] and Claudio Brancolini[1]

Abstract

Diaryldienone derivatives with accessible β-carbons show strong anti-neoplastic properties, related to their ability to make covalent adducts with free thiols by Michael addition, and low toxicity in vivo. Accumulation of poly-ubiquitylated proteins, activation of the unfolded protein response (UPR) and induction of cell death are universal hallmarks of their activities. These compounds have been characterized as inhibitors of isopeptidases, a family of cysteine-proteases, which de-conjugate ubiquitin and ubiquitin-like proteins from their targets. However, it is unclear whether they can also react with additional proteins. In this work, we utilized the biotin-conjugated diaryldienone-derivative named 2c, as a bait to purify novel cellular targets of these small molecules. Proteomic analyses have unveiled that, in addition to isopeptidases, these inhibitors can form stable covalent adducts with different intracellular proteins, thus potentially impacting on multiple functions of the cells, from cytoskeletal organization to metabolism. These widespread activities can explain the ability of diaryldienone derivatives to efficiently trigger different cell death pathways.

Introduction

During the past decades the identification of new small molecule therapeutics has provided some improvements for clinical treatments in patients with various tumors. However, for certain cancers and particularly solid tumors, exhibiting extreme drug resistance, the demand of new agents is still urgent. A class of small organic molecules, which derive from diaryldienone and contain cross-conjugated α,β-unsaturated ketones with accessible β-carbons, have evidenced anti-neoplastic properties and low toxicity in different preclinical studies in vivo[1–6]. The β carbon atoms of α,β-unsaturated ketones are available to alkylate various cellular nucleophiles[6–9]. These small molecules have been proposed as non-selective inhibitors of isopeptidases, a family of enzymes that are involved in the de-conjugation of ubiquitin and ubiquitin-like proteins from different targets[1,10]. Indeed, cells treated with these molecules accumulate poly-ubiquitylated proteins in the presence of unperturbed proteasomal catalytic activity[1,2,5,10,11]. Since several isopeptidases are cysteine-proteases, they are prone to react with the α,β-unsaturated ketones, thus leading to enzyme inactivation. Importantly, these compounds cannot efficiently inhibit the activity of other cysteine proteases, such as caspases or cathepsins, thus indicating a certain degree of specificity[9].

In vitro they can inhibit the activity of recombinant isopeptidases[8,12] and the presence of different groups, in addition to the pharmacophore, can modulate the

Correspondence: Claudio Brancolini (claudio.brancolini@uniud.it)
[1]Department of Medicine, Università degli Studi di Udine, P.le Kolbe 4, 33100 Udine, Italy
[2]Department of Life Sciences, Università degli Studi di Trieste, Via L. Giorgieri 5, 34127 Trieste, Italy
Full list of author information is available at the end of the article
Edited by G Melino

SPRINGER NATURE CDDpress

promiscuity of these compounds[9,13]. Hence, we refer to them as partially-selective isopeptidase inhibitors (P-SIIs).

In cells treated with these P-SIIs, accumulation of poly-ubiquitylated proteins is evident, in partial analogy to bortezomib treatment[2,14]. Bortezomid/Carfilzomib are inhibitors of the proteasomal catalytic chamber approved for the use in clinic[9]. For this reason P-SIIs are usually considered as alternative proteasome inhibitors. However, when the cellular responses to the two inhibitors are compared by gene expression profile studies, the signatures are not entirely superimposable. For example, 2c, a P-SII previously identified and characterized[8], exhibits broader effects in terms of activation of adaptive responses. The response to oxidative stress and protein misfolding are more pronounced in 2c compared to bortezomib treated cells[14].

The identification of the cellular targets of compounds with therapeutic potential is an important step to improve their activities and to understand potential side effects. Chemical proteomics is an innovative approach to unmask the cellular targets of small molecule therapeutics. In chemical proteomics, affinity chromatography is combined with proteomic techniques such as mass spectrometry for the unbiased identification of protein targets[15]. To identify the cellular target of P-SIIs and to clarify their selectivity, we isolated cellular proteins bound by 2c and analysed them by mass spectrometry. Our approach employed a 2c-biotin conjugate as a probe to identify in vivo the cellular targets of P-SIIs.

Results

Generation of the 2c-biotinylated probe

In order to better characterize the mechanisms through which, diaryldienone-derivatives P-SIIs trigger cell death and to define their cellular targets, we generated a biotinylated probe of 2c (Fig. 1). 2c is a P-SII that we have recently synthetized and optimized for in vivo delivery[8]. We initially compared the ability of 2c-biotin, with respect to the original compound, of triggering cell death. MEC-1 chronic lymphocytic leukemia cells were treated for different times with the two compounds and the appearance of cell death was evaluated by cytofluorimetric analysis. Cell death was similarly induced by 2c and its biotinylated version (Fig. 1b). Next, we verified that the death response occurred through the activation

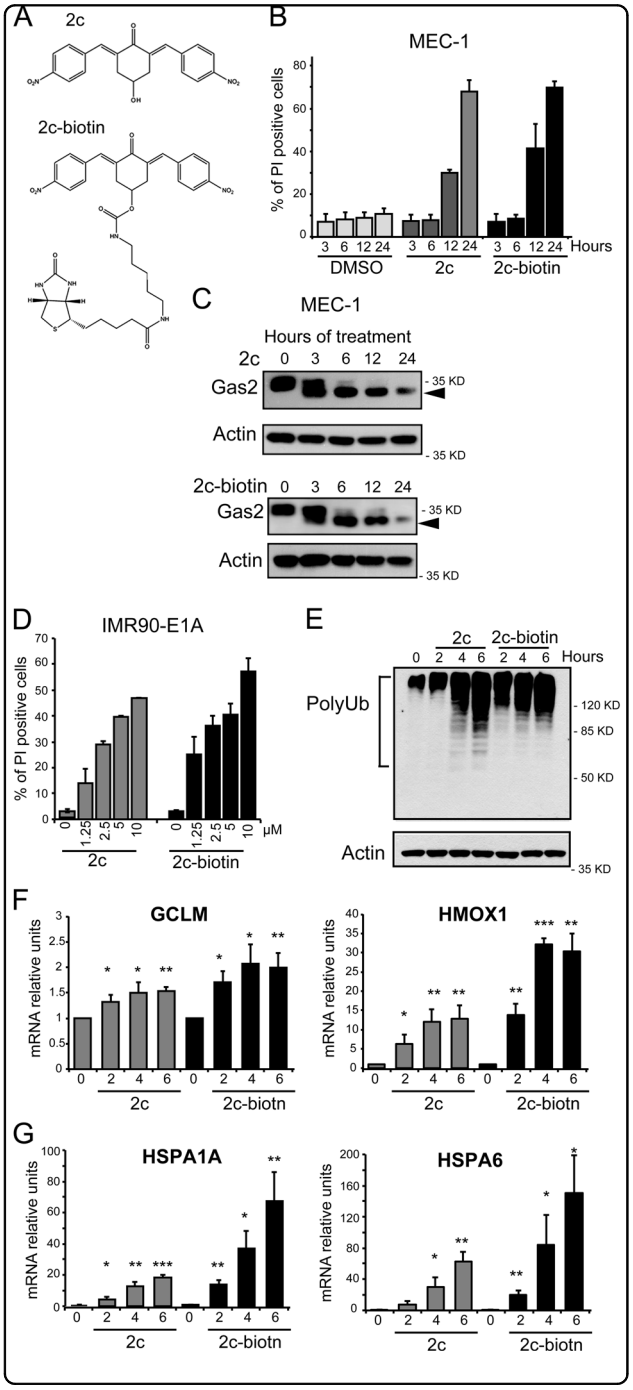

Fig. 1 Generation and characterization of biotin-conjugated 2c. a Structure of 2c and of the 2c-biotin conjugate. **b** MEC-1 cells were treated for the indicated times with 2 μM 2c, 2c-biotin, or DMSO alone as control. After 24 h cells were stained wit PI fixed and processed for cytofluorimetric analysis. Mean ± SD; $n = 3$. **c** Cellular lysates of MEC-1 cells treated with 2 μM 2c or of 2c-biotin for the indicated times were subjected to immunoblotting using the anti-Gas2 antibody. Actin immuno-detection was used as loading control. Arrowhead points to the caspase-cleaved product. **d** IMR90-E1A cells were treated with the indicated concentrations of 2c, 2c-biotin, or DMSO as control. After 24 h cells were stained wit PI fixed and processed for cytofluorimetric analysis. Mean ± SD; $n = 3$. **e** Cellular lysates of IMR90-E1A cells treated with 10 μM 2c or 2c-biotin for the indicated times were subjected to immunoblotting using the anti-ubiquitin antibody. Actin was used as loading control. **f** qRT-PCR analysis of mRNA expression levels for GLCM and HMOX1 in cells treated for the indicated hours with 10 μM 2c or 2c-biotin. Mean ± SD; $n = 3$. **g** qRT-PCR analysis of mRNA expression levels of HSPA1A and HSPA6 in cells treated for the indicated hours with 10 μM 2c or 2c-biotin. Mean ± SD; $n = 3$

of apoptosis. Caspase-dependent processing of GAS2 was detected as early as after 3 h of treatment and was also comparable for the two compounds (Fig. 1c)[16]. Finally, we also compared the pro-death activities of 2c and of 2c-biotin in a different cell line. IMR90-E1A cells evidence a similar dose-dependent response, when challenged with the two compounds (Fig. 1d). In summary, biotinylation of 2c does not perturb its ability to trigger cell death.

Biotinylation does not alter the biological properties of 2c

Cell death induced by 2c and similar compounds is characterized by: (i) the accumulation of poly-ubiquitylated proteins, (ii) the induction of oxidative stress response and (iii) of the unfolded protein response (UPR)[1,8,14,17]. To verify that the presence of the biotin tag does not influence the activation of these cellular responses, we initially investigated the accumulation of polyubiquitylated proteins. Figure 1e illustrates that both 2c and 2c-biotin elicit the accumulation of poly-ubiquitylated proteins. Data suggest that the original compound is slightly more efficient in blocking proteasomal deubiquitylase activities. To evaluate the up-regulations of the oxidative stress signaling, qRT-PCR analysis was performed to measure the relative mRNA levels of heme oxygenase HMOX1 and of GCLM, the regulative subunit of the first rate-limiting enzyme in glutathione biosynthesis[14]. The expression of both genes was upregulated in response to both 2c and 2c-biotin. In this instance, the mRNA levels of both genes were higher in cells treated with the biotinylated 2c (Fig. 1f). Finally, we also investigated the upregulation of the UPR (Unfolded Protein Response). We previously observed that treatment with 2c triggers the upregulation of several chaperons, including HSPA1A and HSPA6[14]. Figure 1g illustrates that the mRNA levels of HSPA1A and HSPA6 were both increased in IMR90-E1A cells treated with 2c or its biotinylated analog. However, this upregulation was stronger in the case of 2c-biotin. In summary, our studies indicate that 2c and 2c-biotin elicit similar adaptive cellular responses, even though some specificity can be appreciated.

Nuclear accumulation of 2c-biotin

2c and similar compounds, containing electrophilic α,β-unsaturated carbonyl units as Michael acceptors, show very high and selective affinity for thiol residues, in particular for cysteines. Impairment of the α, β-unsaturated carbonyl reactivity in these compounds results in a strong decrease of their pro-death potency[6,8,18]. Accordingly, when 2c or 2c-biotin were pre-incubated with N-acetyl cysteine (NAC) their pro-death activity was suppressed (Fig. 2a). Hence, we used NAC as a tool to evaluate the specificity of 2c-biotin activities in vivo.

Initially, cells were treated with biotin alone, 2c-biotin, or 2c-biotin pre-incubated with NAC. After 6 h cells were fixed and processed for fluorescence analysis using streptavidin-tetramethylrhodamine (TRITC). Confocal images were acquired and then analysed for fluorescence intensity. Fluorescence was dramatically augmented when cells were treated with 2c-biotin and this fluorescence was suppressed when the compound was pre-incubated with NAC (Fig. 2b).

Next we performed a time-course analysis to visualize variations of the subcellular localization of 2c-biotin with time. 2c-biotin positivity was detectable as soon as 5 min after treatment and fluorescence was evident in the nucleus and also in the cytoplasm (Fig. 2c). After 10 min the intensity of fluorescence was further increased. At later time-points (6 h) some signs of cellular stress, such as reduced cell spreading, were evident. At this time nuclear localization of 2c-biotin was even stronger, whereas in the cytoplasm it accumulates in a perinuclear area (see arrows and the higher magnification).

Pre-treatment with NAC completely abolishes the fluorescent signals. This behavior suggests that covalent binding of 2c to cellular thiols is necessary for its intracellular accumulation or that the NAC-2c complex is not transported through the plasma membrane. thus confirming that covalent binding of 2c to cellular thiols is necessary for its intracellular accumulation (Fig. 2d). Finally, analysis of mitotic cells suggests that 2c does not interact with chromatin, being chromosomes in metaphase negative for 2c-biotin signals (Fig. 2e).

Intracellular targets of the PS-II 2c

In order to identify PS-IIs intracellular targets, IMR90-E1A cells were treated with 2c-biotin and, after lysis, cellular extracts were incubated with streptavidin beads. NAC was added to verify that binding of the targets was due to the Michael acceptor activity of the probe. To evaluate the binding to isopeptidases, we performed immunoblot analysis on proteins purified after 2c-biotin mediated pull-down. For enrichment comparison, each pull-down was incubated in parallel with antibodies against unrelated proteins.

We initially evaluated the enrichments of USP1 and of actin, used as negative control, with respect to their inputs. USP1 signal was highly enriched in a NAC-dependent manner after 2c-biotin purification (Fig. 3a). In the case of actin, only a weak signal was observed in the 2c pull-down. Next, we analysed the binding of 2c-biotin to USP33 and to the serine-threonine kinase AKT, for comparison (Fig. 3b). USP33, similarly to USP1, was enriched after 2c-biotin pull-down in a NAC dependent manner. Surprisingly, also AKT, after incubation with 2c-biotin was enriched. Hence, we repeated the experiment with USP1 using a different control, the chaperon GRP78.

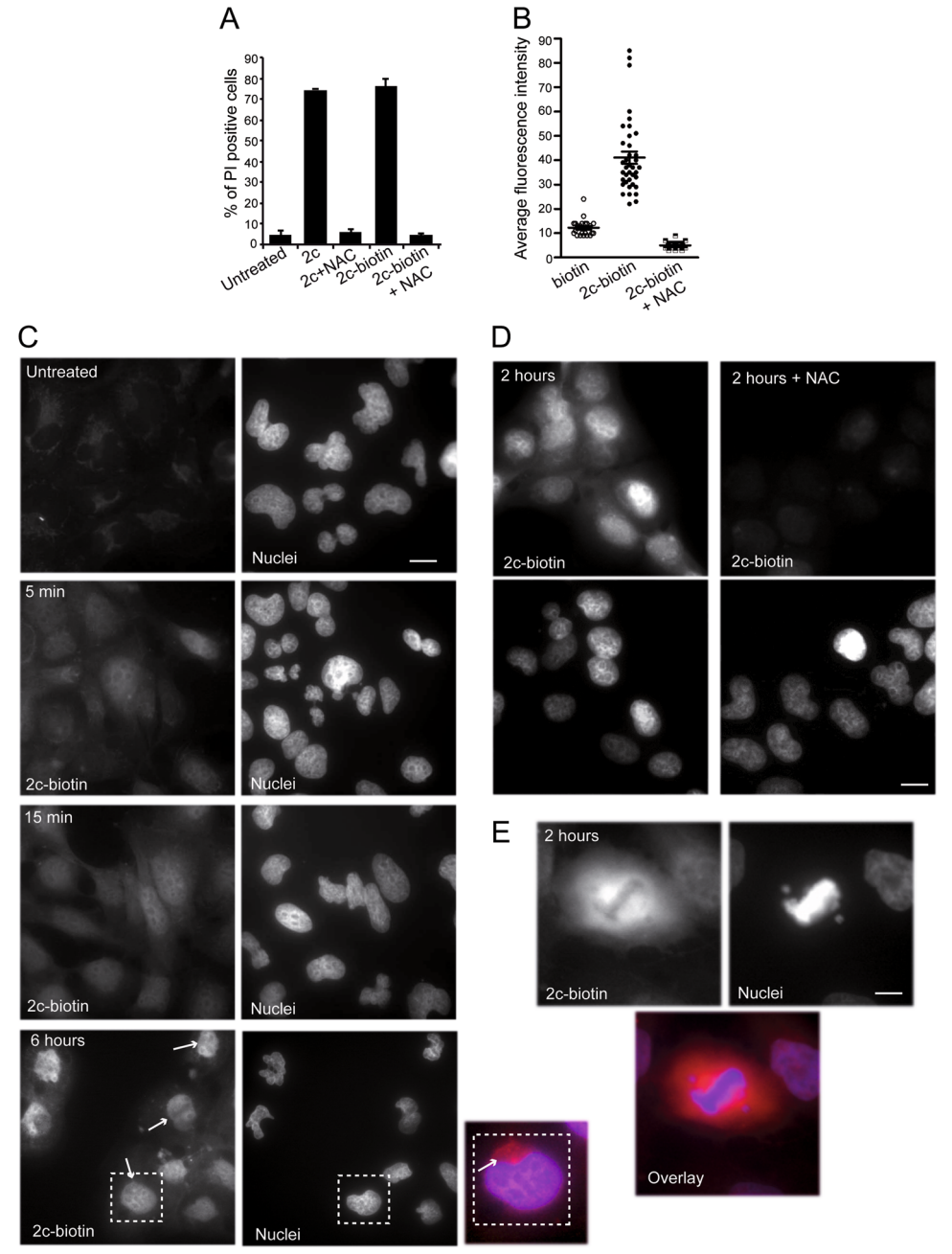

Fig. 2 Dynamics of 2c-biotin uptake and accumulation in cells. a IMR90-E1A cells were treated for 24 h as indicated. Cell death was scored as PI positivity by cytofluorimetric analysis. 2c and 2c-biotin were used at 10 μM. NAC was 2 mM. Mean ± SD; $n = 3$. **b** IMR90-E1A cells grown on coverslips were treated for 6 h as indicated. Cells were fixed and analysed with confocal microscope using the same parameters of acquisition. 2c-biotin was revealed using streptavidin-TRITC. Quantitative analysis of the fluorescence intensity was performed using the Metamorph software. **c** IMR90-E1A cells were treated with 2c-biotin [2 μM] for the indicated times. After fixation cells were incubated with streptavidin-TRITC. Nuclei were visualized using Hoechst 33,342. Arrows point to cytosolic accumulation of 2c-biotin. The dotted square indicates the enlarged area. Images were obtained with an epifluorescence microscopy. Bar 30 μm. **d** IMR90-E1A cells were treated with 2c-biotin [2 μM] for 2 h. When used in pre-treatment, NAC was 2 mM. After fixation cells were incubated with streptavidin-TRITC. Nuclei were visualized using Hoechst 33,342. Images were obtained with an epifluorescence microscopy. Bar 30 μm. **e** IMR90-E1A cells were treated with 2c-biotin [2 μM] for 2 h. After fixation cells were incubated with streptavidin-TRITC. Nuclei were visualized using Hoechst 33,342. Images were obtained with an epifluorescence microscopy. A mitotic cell is shown. Bar 50 μm. Images are shown in pseudocolors

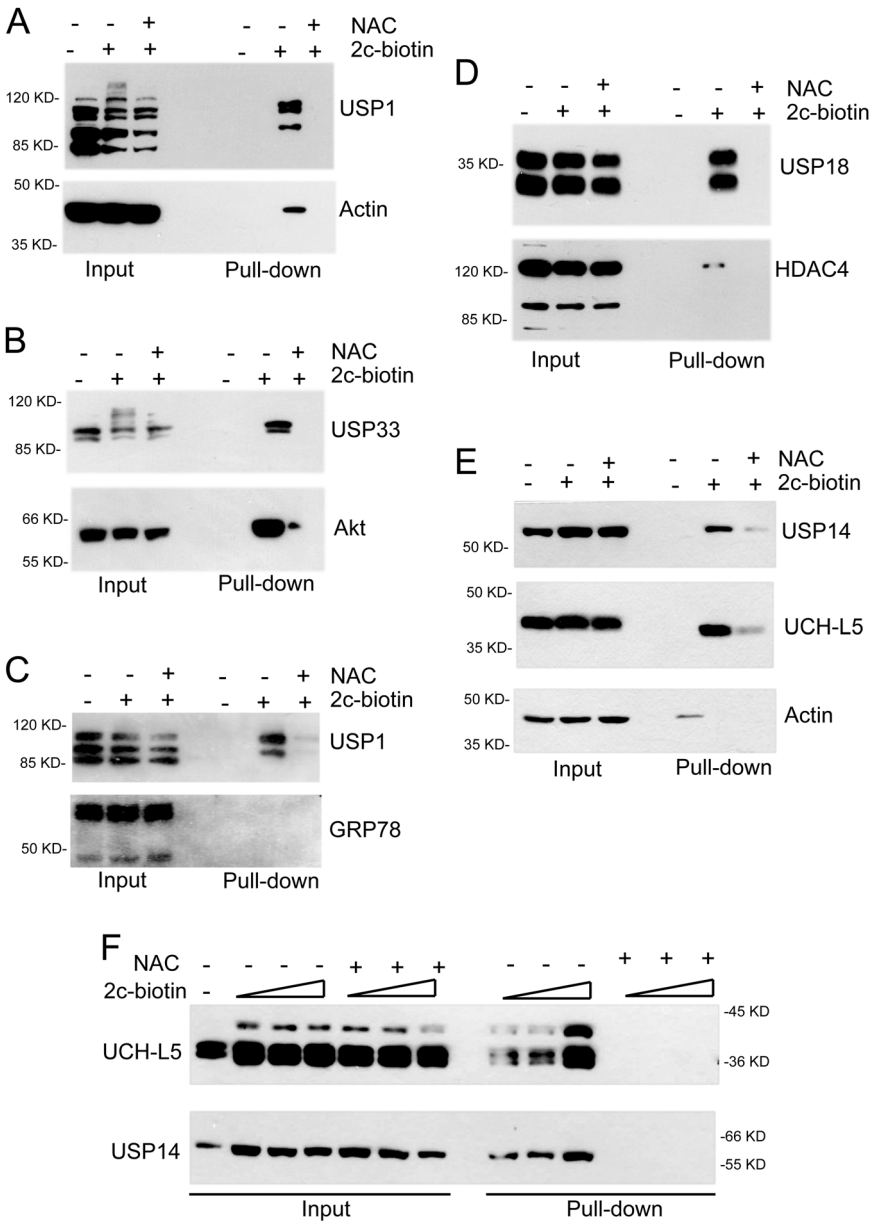

Fig. 3 Identification of target isopeptidases by biotin pull-down experiments. a/b/c/d/e IMR90-E1A cells were treated for 2 h with 10 μM 2c-biotin or left untreated. 2c-botin was pre-incubated with 5 mM of NAC, as a negative control. Cellular proteins were purified by 2c-biotin pull-down using streptavidin-agarose beads. Protein complexes were separated by SDS/PAGE and immunoblotted using the indicated antibodies. Inputs are included for enrichment comparison. In the case of USP18 cells were pre-treated for 24 h with interferon-α. **f** IMR90-E1A cells were treated for 2 h with the indicated concentrations of 2c-biotin or left untreated. As a control, 2c-biotin was pre-incubated with 5 mM NAC. Cellular proteins were purified by 2c-biotin pull-down. Protein complexes were separated by SDS/PAGE and immunoblotted using the anti-USP14 or the anti-UCH-L5 antibodies. Inputs are included for enrichment comparison

USP1 was again enriched, whereas GRP78 was almost undetectable in the 2c-biotin pull-down (Fig. 3c). Since previous studies showed that 2c inhibits the deISGlase activity of USP18, we also evaluated the 2c pull-down for USP18[8]. Here as control we used HDAC4. Binding to USP18 was evident whereas binding of HDAC4 was very weak (Fig. 3d).

Finally, we compared the binding of 2c to UCH-L5 and USP14, the two cysteine-deubiquitylases of the proteasome. Their inhibition should represent the key contribution to the accumulation of poly-ubiquitylated proteins[9,13]. The pull-down of both DUBs was enriched compared to Actin (Fig. 3e). Previous studies, using different assays, indicated that compounds similar to 2c

exhibit higher inhibition of USP14 activity compared to UCH-L5. Hence, we compared in more detail the binding of 2c-biotin to the two DUBs using different concentrations of the inhibitor. Figure 3f confirms that in vivo 2c-biotin binds with comparable intensity USP14 and UCH-L5.

In summary, we demonstrated that the compound 2c shows a certain affinity for isopeptidases. The spectrum of enzymes recognized by 2c seems to be quite wide, thus confirming its partial selectivity. However, USP1/USP33 showed a higher affinity when compared to USP18/UCH-L5/USP14. As expected, unrelated control proteins such as Actin, HDAC4 and GRP78 showed a weak reaction with 2c-biotin. Surprisingly, AKT can be covalently modified by 2c-biotin.

Proteomic profiling of 2c adducts in transformed cells

The above study suggests that, in addition to isopeptidases, 2c might target additional proteins such as AKT. To characterize the binding landscape of 2c, we applied a chemical proteomic strategy. IMR90-E1A cells were treated with 10 µM 2c-biotin for 2 h and lysed. Biotinylated proteins were then isolated using avidin column chromatography. As a control, the same experiment was performed in the presence of NAC. After SDS-PAGE separation and blue coomassie staining, lanes were divided in five parts, excised and trypsin digested. The resulting peptides were analyzed by liquid chromatography coupled to tandem mass spectrometry (LC–MS/MS) and 25 proteins were successfully identified.

Table 1 summarizes the results of such analysis. The identified proteins fall into five different functional classes including; metabolism (33%), proteostasis (33%), cytoskeleton (19%), signaling (10%) and oxidative stress (5%) (Fig. 4a). As expected some proteins were detected after the NAC treatment as well. They could represent contaminants such as Tubulin and Actin. Hence, we excluded them from the analysis. Pyruvate kinase and Eukaryotic initiation factor 4A-1 were the two proteins detected with the highest scores. To clarify whether the 2c-biotin modified proteins, identified by mass-spectrometry, reflect their relative abundance, we interrogated the protein abundance database PaxDb (http://pax-db.org.)[19]. We also compared the abundance of the isopeptidases USP1, USP14, USP18 USP33 and UCH-L5. Different cell lines and different datasets were scrutinized[20–24]. Figure 4b shows the result of this analysis. As expected, among the isopeptidases, the proteasome components UCH-L5 and USP14 show higher abundance. Surprisingly, USP14 in certain cell lines is much more abundant than UCH-L5. USP1, USP18 and USP33 are quite rare proteins. USP18, being interferon-inducible was almost undetectable.

Although there is some variability among cell lines and datasets, overall the newly identified 2c-biotin targets represent high abundant proteins (GAPDH, ENO1, and PKM) frequently ranking within the 5% more abundant proteins. The only exception in the investigated cell lines was myosin light chain 6B MYL6B.

Interestingly, among the 2c targets we identified Cofilin-1. This protein is of particular interest since Cofilin-1 is involved in mediating cytoskeletal changes and cell death in response to a 2c analogous[25].

Cofilin-1 phosphorylated at serine 3 interacts with 2c-biotin

To corroborate the proteomic data, we performed 2c-biotin pull-down experiments. We focused the analysis on Cofilin-1, for the above-mentioned reasons. Surprisingly, 2c-biotin pull-down experiments did not evidence any interaction with Cofilin-1 (Fig. 5a). Importantly, Cofilin-1 activities are regulated by phosphorylation of serine 3. Therefore, we performed pull-down experiments using an antibody recognizing Cofilin-1 when phosphorylated at serine 3. Figure 5a indicates that 2c-biotin preferentially reacts with the phosphorylated pool of Cofilin-1.

Cofilin-1 has 4 cysteines at positions 39, 80, 139, and 147 (Fig. 5b). Figure 5d highlights that two cysteine residues (Cys139, Cys147) are located on the surface and are thus potentially available for the reaction with 2c. The other two residues are partially (Cys39) and completely buried (Cys80).

Discussion

Diaryldienone-derivatives comprise an interesting and heterogeneous family of molecules, which selectively elicit apoptosis in neoplastic cells. Marks of their activities are induction of the UPR, oxidative stress, and the accumulation of poly-ubiquitylated proteins. These multiple cellular responses have been attributed to their ability to function as Michael acceptors against the catalytic cysteine of isopeptidases. Several groups have demonstrated the ability of these molecules to impact on the activity of these enzymes[1–8,10,26]. However, the presence of additional targets has been underestimated.

To clarify this point and to better understand the behavior of these molecules, we generated a biotinylated version of 2c, a diaryldienone-derivative. Our studies demonstrate that addition of biotin does not perturb the activity of 2c. Induction of cell death, activation of caspases, accumulation of poly-ubiquitylated proteins, induction of the anti-redox and of the UPR response were comparable between the original 2c and its biotinylated version. Studies in vivo indicated that the compound is rapidly up-taken by the cells. It shows a diffuse localization and accumulates in the nuclei. Absence of punctate staining points against an uptake through vesicle-

Table 1 Candidate 2c-biotin targets identified by mass-spectrometry

Database/Gene	Protein	2c-biotin		2c-biot/NAC	
		P.S.	P.N.	P.S	P.N.
TBA1B	Tubulin alpha-1A/1B chain	313	6	95	2
KPYM/PKM	Pyruvate kinase PKM	184	4	nd	nd
BAD96752.1	Beta actin variant	180	5	163	4
RL40	Ubiquitin-60S ribosomal protein L40	140	3	94	1
IF4A1/EIF4A1	Eukaryotic initiation factor 4A-I	128	2	nd	nd
AAF36537.1/EEF1A1	glucocorticoid receptor AF-1 specific elongation factor, partial	113	3	nd	nd
TBB5	Tubulin beta chain	107	2	nd	nd
HS90B	Heat shock protein HSP 90-beta	87	2	nd	nd
COF1	Cofilin-1	83	2	nd	nd
IF5A1/EIF5A1	Eukaryotic translation initiation factor 5A-1	81	1	nd	nd
AAA36787.1	ubiquitin precursor, partial	78	1	nd	nd
PRDX1	Peroxiredoxin-1	76	1	nd	nd
MYL6B	Myosin light chain 6B	66	1	nd	nd
CYB5B	Cytochrome b5 type B	65	1	nd	nd
EAW53693.1/RACK1	guanine nucleotide binding prot., beta polypeptide 2-like 1, isoform CRA_b	65	1	nd	nd
ALDOA	Fructose-bisphosphate aldolase A	61	1	nd	nd
MPCP/SLC25A3	Phosphate carrier protein, mitochondrial	56	1	nd	nd
ENOA/ENO1	Alpha-enolase	55	1	nd	nd
NDKA/NME1	Nucleoside diphosphate kinase A	51	1	nd	nd
ANXA2	Annexin A2	51	1	nd	nd
HSP7C/HSAP8	Heat shock cognate 71 kDa protein	50	1	nd	nd
RL11/RPL11	60S ribosomal protein L11	48	1	nd	nd
G3P/GAPDH	Glyceraldehyde-3-phosphate dehydrogenase	46	1	nd	nd
TPM1	Tropomyosin alpha-1 chain	45	1	nd	nd
RS27A	Ubiquitin-40S ribosomal protein S27a	nd	nd	47	1

P.S. indicates the Mascot protein identification score. Only proteins having one or more peptides with a score higher than 44 (identity or extensive homology, $P < 0.05$) were included in the protein list. P.N. indicates the number of peptides identified and assigned to each single protein. ND (non detectable). Pull-down experiments were performed also in the presence of NAC. Proteins that were isolated in the presence of NAC are indicated in gray and considered as contaminant.

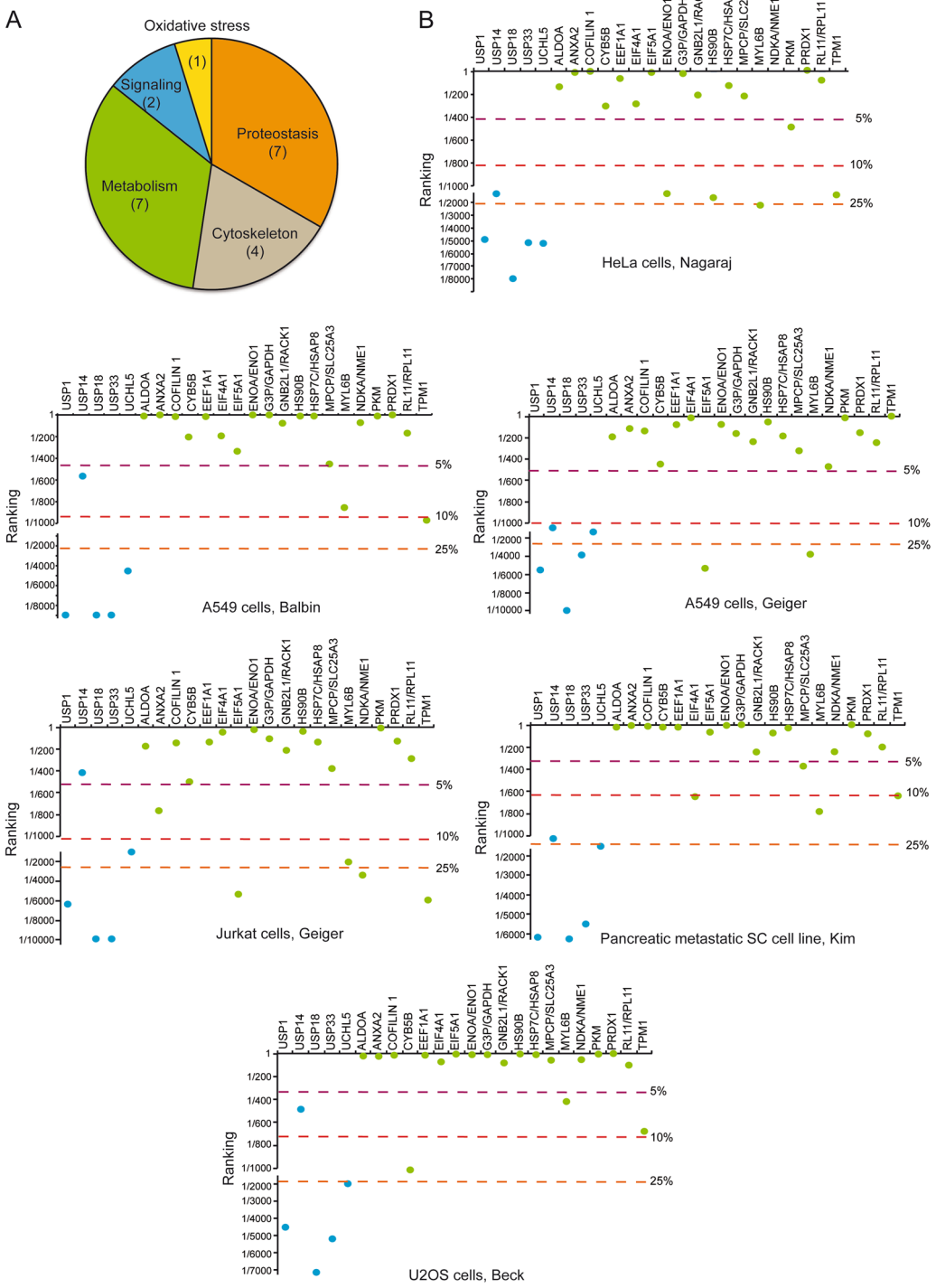

Fig. 4 Candidate 2c-biotin targets identified by mass-spectrometry. a Identified proteins can be grouped into categories: metabolism, proteostasis, cytoskeleton, oxidative stress, and signaling. Numbers of proteins of each category are indicated. **b** Relative abundance of the isopeptidases evaluated for 2c-biotin binding by immunoblots (blue dots) in comparison with proteins identified by mass-spectrometry (green dots). Data are presented as ranking. Data were obtained from http://pax-db.org. The selected cell lines and the original datasets are indicated

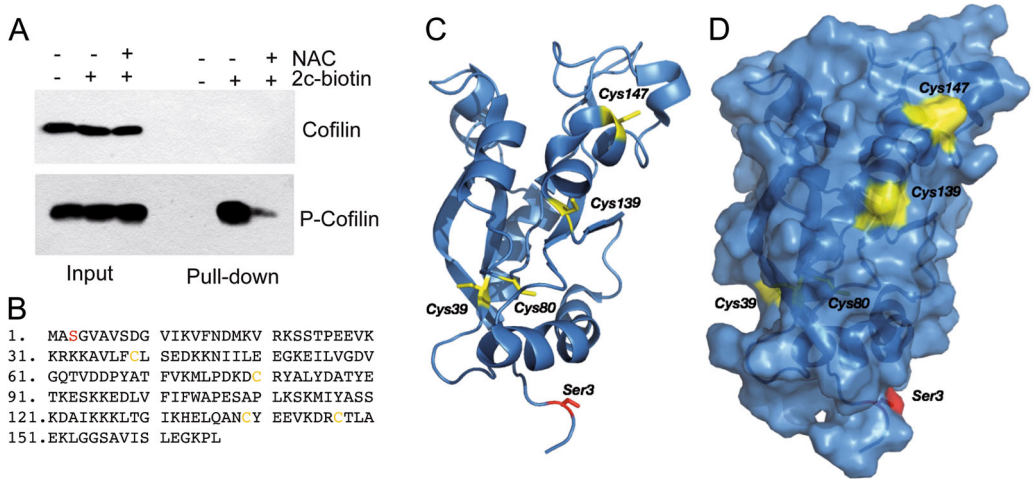

Fig. 5 Only the phosphorylated version of Cofilin-1 reacts with 2c. a IMR90-E1A cells were treated for 2 h with 10 μM 2c-biotin or left untreated. As a control, 2c-botin was pre-incubated with 5 mM NAC. Cellular proteins were purified by 2c-biotin pull-down, next immunoblotting were performed using the indicated antibodies. Inputs are for enrichment comparison. **b** Primary sequence of human Cofilin-1. Cysteine residues are highlighted in yellow and serine 3 in red. **c** Cartoon structure of Cofilin-1 (PDB: 1Q8G) showing the phosphorylation site (Ser3) in red and the four cysteine residues in yellow. **d** Protein surface superimposed to the cartoon representation, with the same color code. The distance between Ser3 and the available cysteines is 26 Å (Cys139) and 34 Å (Cys147). Images were obtained with the PyMOL Molecular Graphics System, Schrödinger, LLC

mediated trafficking. These data are in agreement with previous hypotheses based on studies with a structurally related compound[18].

Biotin pull-down experiments demonstrated that 2c covalently binds several isopeptidases, in a NAC-dependent manner and with higher affinity compared to different control proteins. Although these studies need further validation using different essays, we observed a higher binding affinity for USP1 and USP33 compared to USP14, USP18, or UCH-L5. We cannot exclude that these differences stem from a different in vivo accessibility of the enzymes, due to the existence of multi-protein complexes.

Surprisingly, the serine/threonine kinase AKT was bound with high affinity by 2c-biotin. AKT is an important signaling enzyme, regulating survival and proliferation, whose activity is affected by G5, a 2c-like compound[25]. AKT kinase activity depends on two critical residues; threonine 308 and serine 437. Treatment with G5 promotes a transient phosphorylation of threonine 308, followed by its dephosphorylation. By contrast, serine 473 is dephosphorylated at earlier time-points. While dephosphorylation of threonine 308 is PP2A-dependent, serine 473 dephosphorylation is largely independent[25]. Interestingly, cysteine residues 310 and 296 found in the T-loop region are critical for AKT activity and can be subjects of bioreductive alkylation by pyranonaphthoquinone lactones[27,28]. Hence, AKT contains 2c-addictable cysteines critical for its activity. Further study will be necessary to understand whether the reaction with 2c or similar compounds impairs AKT enzymatic activity.

The mass-spec analysis confirmed that additional cellular proteins are modified by 2c-biotin. These proteins can be grouped in five major functional classes (metabolism, proteostasis, cytoskeleton, signaling, and oxidative stress).

Previous studies indicated that these compounds can be relatively promiscuous. Actin can be addicted by 15-Deoxy-$\Delta^{12,13}$-prostaglandin J_2 that contains the same unsaturated ketone pharmacophore of 2c[29]. The bis (benzylidene)piperidone RA190 reacts with cysteine 88 of the proteasome ubiquitin receptor hRpn13 and MCB-613 (4-ethyl-2,6-bis-pyridin-3-ylmethylene-cyclohexanone), a molecule structurally similar to 2c, can stimulate steroid receptor co-activators (SRCs) transcriptional activity[7,30].

Surprisingly, isopeptidases were not identified by this analysis. It should be noted that, among the identified 2c targets, high abundance proteins are the foremost represented. In principle, these high abundance targets could compete with high affinity but low abundant targets, such as USP1 and USP33.

2c and similar molecules trigger profound changes of cytoskeleton and cell morphology. Time-lapse experiments demonstrated that, before the appearance of apoptosis, stress fibers disassemble and cells lose adhesion[31]. An important contribution to these cytoskeletal changes is provided by Cofilin-1. Cofilin-1 dephosphorylation triggers F-actin disassembling and 2c can favor this dephosphorylation[25]. Importantly, 2c-biotin

preferentially modifies the phosphorylated pool of Cofilin-1. This observation suggests that 2c could impact F-actin dynamic directly, by hijacking Cofilin-1 functions. Cofilin dimers/oligomers exhibit bundling activities and dimerization occurs via the formation of intermolecular disulfide bridges involving Cys (39) and, probably, Cys (147) of adjacent Cofilin units. Indeed, these cysteines can react with cucurbitacins, triterpenoid natural compounds[32]. Smilarly, by reacting with the cysteines of Cofilin, 2c might impair dimerization and thus impact directly on F-actin severing[33–35]. Cysteine residues (Cys139, Cys147) are located on the surface and are thus potentially available for the reaction with 2c. Interestingly, the distance between Ser3 and these cysteines is 26 Å (Cys139) and 34 Å (Cys147).

In summary, our studies demonstrate that diaryldienone-derivatives can be addicted to several cellular proteins in addition to isopeptidases. The combination of different targets can elicit multiple stresses, which are not manageable in neoplastic cells, thus explaining their efficient anti-tumor activity observed in vivo.

Materials and methods

Reagents and antibodies

Chemicals used were: bortezomib (LC Laboratories), Propidium Iodide and N-acetylcysteine (Sigma Aldrich). Primary antibodies used were: anti-Gas2[36] anti-actin (Sigma/Aldrich) anti-USP1[37] anti-USP33 (Millipore) anti-AKT (Cell Signaling) anti-UCH-L5 (Abcam), anti-USP18[38] anti-HDAC4[39] anti-MEF2D (BD Bioscience), anti-GRP78, anti-USP14, anti-Cofilin-1, anti-pCofilin-1 (Santa Cruz Biotechnologies).

Synthesis of the biotinylated version of 2c

Briefly, the biotinylated derivative of 2c was obtained by the insertion of a cadaverine linker between biotin and 2c. To this end, biotin was first used to acylate one of the amino groups of cadaverine, and then the resulting adduct was linked to 2c via a carbamate linkage obtained by reaction with 2c-OSu. Products and intermediates were characterized by Electrospray Ionization mass spectrometry (ESI-MS) performed on an Esquire 4000 (Bruker Daltonics) spectrometer and by ^{1}H and ^{13}C NMR (Varian, 500 MHz). Full details are reported in the supplementary materials.

Culture conditions, fluorescence microscopy, and cell death analysis

MEC-1 cells were grown in RPMI medium whereas IMR90-E1A cells were cultured in DMEM. Mediums were supplemented with heated inactivated fetal calf serum (Sigma Aldrich), penicillin (100 U/mL), glutamine (2 mmol/L), and streptomycin (100 µg/mL). Fluorescence microscopy was performed as previously described[1]. Briefly, cells were fixed in 3% paraformaldehyde, permeabilized with 1% Triton-X100 and incubated with TRITC streptavidin (Molecular probes). For the quantification of cell death, cells were re-suspended in 500 µL of PBS and stained with propidium iodide (PI). Fluorescence was determined with a FACScan™ (Beckman Dickinson). IFN-α2a (1000 units/mL; Jena Bioscience) was used as previously described[40].

2c-Biotin pull-down and immunoblotting

For pull-down experiments 4.5×10^5 IMR90-E1A cells were treated with 10 µM 2c-biotin for 2 h. When used, N-acetylcysteine (NAC) was 5 mM. Cell lysis was performed in lysis buffer (PBS, 2%SDS, 5 mM DTT). Proteins obtained after an SDS denaturating lysis and sonication, were incubated with streptavidin-agarose beads (GE Healthcare). After several washes in lysis buffer, they were eluted after boiling in sample buffer. Next SDS/PAGE electrophoresis was performed and proteins were transferred to nitrocellulose membrane and incubated with the specific primary antibodies. Secondary antibodies were peroxidase-conjugated goat anti-rabbit or anti-mouse (Sigma/Aldrich). Blots were developed with Super Signal West Dura (Pierce).

RNA extraction and qRT-PCR analysis

RNA was extracted using Tri-Reagent (Molecular Research Center) and retrotranscribed by using 100U of Moloney murine leukemia virus reverse transcriptase (Invitrogen). The primer sequences used are available upon request. Quantitative reverse transcription-PCR (qRT-PCR) analyses were performed using Bio-Rad CFX96 and SYBR Green technology. HPRT and GAPDH were used as normalizer genes. All reactions were done in triplicate. Data were from al least three experiments ±SD.

Proteomic analysis

2c–biotin pull down samples were separated by SDS—PAGE and the gel stained by Coomassie blue. The lanes corresponding to 2c—biotin and 2c—biotin plus NAC were excised and divided into five parts. Proteins were in gel digested and identified by LC-MS/MS analysis essentially as previously described using a 1200 Series Nano HPLC (Agilent)[41]. Only proteins having one or more peptides with a score higher than 44 (identity or extensive homology, $P < 0.05$) were included in the protein list. Keratins and Streptavidin were excluded from the identified proteins. Protein have been listed according to the Mascot protein score[42,43].

Acknowledgements

This work was supported by grant from Regione Friuli-Venezia Giulia POR FESR 2014-2020 "ATENA" and AIRC (Associazione Italiana per la Ricerca sul Cancro) CB

Author details
[1]Department of Medicine, Università degli Studi di Udine, P.le Kolbe 4, 33100 Udine, Italy. [2]Department of Life Sciences, Università degli Studi di Trieste, Via L. Giorgieri 5, 34127 Trieste, Italy. [3]Dipartimento di Scienze Chimiche e Farmaceutiche, Universita degli Studi di Trieste, Via Giorgieri 1, 34127 Trieste, Italy

Conflict of interest
The authors declare that they have no conflict of interest.

Supplementary Information accompanies this paper at https://doi.org/10.1038/s41419-017-0259-1.

Received: 13 October 2017 Revised: 7 December 2017 Accepted: 22 December 2017
Published online: 07 February 2018

References

1. Aleo, E., Henderson, C. J., Fontanini, A., Solazzo, B. & Brancolini, C. Identification of new compounds that trigger apoptosome-independent caspase activation and apoptosis. *Cancer Res.* **66**, 9235–9244 (2006).
2. D'Arcy, P. et al. Inhibition of proteasome deubiquitinating activity as a new cancer therapy. *Nat. Med.* **17**, 1636–1640 (2011).
3. Coughlin, K. et al. Small-molecule RA-9 inhibits proteasome-associated DUBs and ovarian cancer in vitro and in vivo via exacerbating unfolded protein responses. *Clin. Cancer Res.* **20**, 3174–3186 (2014).
4. Issaenko, O. A. & Amerik, A. Y. Chalcone-based small-molecule inhibitors attenuate malignant phenotype via targeting deubiquitinating enzymes. *Cell Cycle* **11**, 1804–1817 (2012).
5. Shukla, N. et al. Proteasome addiction defined in ewing sarcoma is effectively targeted by a novel class of 19S proteasome inhibitors. *Cancer Res.* **76**, 4525–4534 (2016).
6. Karki, S. S. et al. 3,5-Bis(3-alkylaminomethyl-4-hydroxybenzylidene)-4-piperidones: a novel class of potent tumor-selective cytotoxins. *J. Med. Chem.* **59**, 763–769 (2016).
7. Anchoori, R. K. et al. A bis-benzylidine piperidone targeting proteasome ubiquitin receptor RPN13/ADRM1 as a therapy for cancer. *Cancer Cell* **24**, 791–805 (2013).
8. Cersosimo, U. et al. Synthesis, characterization, and optimization for in vivo delivery of a nonselective isopeptidase inhibitor as new antineoplastic agent. *J. Med. Chem.* **58**, 1691–1704 (2015).
9. Selvaraju, K. et al. Inhibition of proteasome deubiquitinase activity: a strategy to overcome resistance to conventional proteasome inhibitors? *Drug. Resist. Updates* **21-22**, 20–29 (2015).
10. Mullally, J. E. & Fitzpatrick, F. A. Pharmacophore model for novel inhibitors of ubiquitin isopeptidases that induce p53-independent cell death. *Mol. Pharmacol.* **62**, 351–358 (2002).
11. Tian, Z. et al. A novel small molecule inhibitor of deubiquitylating enzyme USP14 and UCH-L5 induces apoptosis in multiple myeloma and overcomes bortezomib resistance. *Blood* **123**, 706–716 (2014).
12. Nicholson, B. et al. Characterization of ubiquitin and ubiquitin-like-protein isopeptidase activities. *Protein Sci.* **17**, 1035–1043 (2008).
13. Wang, X. et al. The proteasome deubiquitinase inhibitor VLX1570 shows selectivity for ubiquitin-specific protease-14 and induces apoptosis of multiple myeloma cells. *Sci. Rep.* **6**, 26979, https://doi.org/10.1038/srep26979 (2016).
14. Tomasella, A. et al. The isopeptidase inhibitor 2cPE triggers proteotoxic stress and ATM activation in chronic lymphocytic leukemia cells. *Oncotarget* **7**, 45429–45443 (2016).
15. Karasawa, T., Wang, Q., David, L. L. & Steyger, P. S. CLIMP-63 is a gentamicin-binding protein that is involved in drug-induced cytotoxicity. *Cell Death Dis.* **1**, e102 (2010).
16. Brancolini, C., Benedetti, M. & Schneider, C. Microfilament reorganization during apoptosis: the role of Gas2, a possible substrate for ICE-like proteases. *Embo J.* **14**, 5179–5190 (1995).
17. Oh, B. M. et al. Cystatin SN inhibits auranofin-induced cell death by autophagic induction and ROS regulation via glutathione reductase activity in colorectal cancer. *Cell Death Dis.* **8**, e3053, https://doi.org/10.1038/cddis.2017.446 (2017).
18. Wang, X. et al. The 19S Deubiquitinase inhibitor b-AP15 is enriched in cells and elicits rapid commitment to cell death. *Mol. Pharmacol.* **85**, 932–945 (2014).
19. Wang, M. et al. PaxDb, a database of protein abundance averages across all three domains of life. *Mol. Cell Proteom.* **11**, 492–500 (2012).
20. Nagaraj, N. et al. Deep proteome and transcriptome mapping of a human cancer cell line. *Mol. Syst. Biol.* **7**, 548 (2011).
21. Balbin, O. A. et al. Reconstructing targetable pathways in lung cancer by integrating diverse omics data. *Nat. Commun.* **4**, 2617 (2013).
22. Geiger, T., Wehner, A., Schaab, C., Cox, J. & Mann, M. Comparative proteomic analysis of eleven common cell lines reveals ubiquitous but varying expression of most proteins. *Mol. Cell Proteom.* **11**, M111.014050 (2012).
23. Kim, M. S. et al. Heterogeneity of pancreatic cancer metastases in a single patient revealed by quantitative proteomics. *Mol. Cell Proteom.* **1311**, 2803–2811 (2014).
24. Schmidt, A. et al. Absolute quantification of microbial proteomes at different states by directed mass spectrometry. *Mol. Syst. Biol.* **7**, 510 (2011).
25. Tomasella, A., Blangy, A. & Brancolini, C. A receptor-interacting protein 1 (RIP1)-independent necrotic death under the control of protein phosphatase PP2A that involves the reorganization of actin cytoskeleton and the action of cofilin-1. *J. Biol. Chem.* **289**, 25699–25710 (2014).
26. Wang, S. et al. Inhibition of the deubiquitinase USP5 leads to c-Maf protein degradation and myeloma cell apoptosis. *Cell Death Dis.* **8**, e3058 (2017).
27. Salaski, E. J. et al. Pyranonaphthoquinone lactones: a new class of AKT selective kinase inhibitors alkylate a regulatory loop cysteine. *J. Med. Chem.* **52**, 2181–2184 (2009).
28. Toral-Barza, L. et al. Discovery of lactoquinomycin and related pyranonaphthoquinones as potent and allosteric inhibitors of AKT/PKB: mechanistic involvement of AKT catalytic activation loop cysteines. *Mol. Cancer Ther.* **6**, 3028–3828 (2007).
29. Aldini, G. et al. Identification of actin as a 15-deoxy-Delta12,14-prostaglandin J2 target in neuroblastoma cells: mass spectrometric, computational, and functional approaches to investigate the effect on cytoskeletal derangement. *Biochemistry* **46**, 2707–2718 (2007).
30. Wang, L. et al. Characterization of a steroid receptor coactivator small molecule stimulator that overstimulates cancer cells and leads to cell stress and death. *Cancer Cell* **28**, 240–252 (2015).
31. Fontanini, A. et al. The isopeptidase inhibitor G5 triggers a caspase-independent necrotic death in cells resistant to apoptosis: a comparative study with the proteasome inhibitor bortezomib. *J. Biol. Chem.* **284**, 8369–8381 (2009).
32. Gabrielsen, M. et al. Cucurbitacin covalent bonding to cysteine thiols: the filamentous-actin severing protein Cofilin1 as an exemplary target. *Cell Commun. Signal.* **11**, 58 (2014).
33. Bernstein, B. W. & Bamburg, J. R. ADF/cofilin: a functional node in cell biology. *Trends Cell Biol.* **20**, 187–195 (2010).
34. Pfannstiel, J. et al. Human cofilin forms oligomers exhibiting actin bundling activity. *J. Biol. Chem.* **276**, 49476–49484 (2001).
35. Cameron, J. M. et al. Polarized cell motility induces hydrogen peroxide to inhibit cofilin via cysteine oxidation. *Curr. Biol.* **25**, 1520–1525 (2015).
36. Brancolini, C. & Bottega, S. Schneider C. Gas2, a growth arrest-specific protein, is a component of the microfilament network system. *J. Cell Biol.* **117**, 1251–1261 (1992).
37. Cataldo, F. et al. CAPNS1 regulates USP1 stability and maintenance of genome integrity. *Mol. Cell. Biol.* **33**, 2485–2496 (2013).
38. Potu, H., Sgorbissa, A. & Brancolini, C. Identification of USP18 as an important regulator of the susceptibility to IFN-alpha and drug-induced apoptosis. *Cancer Res.* **70**, 655–665 (2010).
39. Di Giorgio, E. et al. The co-existence of transcriptional activator and transcriptional repressor MEF2 complexes influences tumor aggressiveness. *PLoS Genet.* **13**, e1006752 (2017).
40. Sgorbissa, A., Tomasella, A., Potu, H., Manini, I. & Brancolini, C. Type I IFNs signaling and apoptosis resistance in glioblastoma cells. *Apoptosis* **16**, 1229–1244 (2011).
41. Sgarra, R. et al. Interaction proteomics of the HMGA chromatin architectural factors. *Proteomics* **8**, 4721–4732 (2008).
42. Pope, B. J., Zierler-Gould, K. M., Kühne, R., Weeds, A. G. & Ball, L. J. Solution structure of human cofilin: actin binding, pH sensitivity, and relationship to actin-depolymerizing factor. *J. Biol. Chem.* **279**, 4840–4848 (2004).
43. Mizuno, K. Signaling mechanisms and functional roles of cofilin phosphorylation and dephosphorylation. *Cell. Signal.* **25**, 457–469 (2013).